THESIS

MICHIGAN STATE UNIVERSITY LIBRARIES
3 1293 01055 4396

This is to certify that the

dissertation entitled

Nuclear Models for Beta
and Double Beta Decay

presented by

Liang Zhao

has been accepted towards fulfillment
of the requirements for

Ph.D. degree in Physics

Major professor

Date April 21, 1992

*MSU is an Affirmative Action/Equal Opportunity Institution*

LIBRARY
Michigan State
University

**PLACE IN RETURN BOX** to remove this checkout from your record.
**TO AVOID FINES** return on or before date due.

| DATE DUE | DATE DUE | DATE DUE |
|---|---|---|
| | | |
| | | |
| | | |
| | | |
| | | |
| | | |
| | | |

MSU Is An Affirmative Action/Equal Opportunity Institution
c:\circ\datedue.pm3-p.1

# NUCLEAR MODELS FOR BETA AND DOUBLE-BETA DECAYS

By

LIANG ZHAO

A DISSERTATION

Submitted to
Michigan State University
in partial fulfillment of the requirements
for the Degree of

DOCTOR OF PHILOSOPHY

Department of Physics and Astronomy

1992

699-6930

# ABSTRACT

# NUCLEAR MODELS FOR BETA AND DOUBLE-BETA DECAYS

By

Liang Zhao

The $2\nu\beta\beta$ decay matrix element of $^{48}$Ca is studied with a large-basis shell-model calculation. The theoretical and experimental $\beta^-$ and $\beta^+$ spectra and their relation to $2\nu\beta\beta$ are discussed. A new empirical effective interaction is found to give the best agreement to $\beta^-$ and $\beta^+$ spectra with the effective Gamow-Teller operator $\tilde{\sigma}t$=$0.77\sigma t$. Our shell-model prediction of $T_{1/2}$=$1.9\times10^{19}$ yr differs by a factor of two from present experimental limit of $T_{1/2} > 3.6\times10^{19}$ yr.

The validity and accuracy of the pnQRPA as a model to study $\beta^+$ and $\beta\beta$ decay are examined by making a comparison of the pnQRPA and the full-basis shell-model calculations for the fp shell nuclei. Our comparison includes the total decay matrix elements, the relevant strength distributions and coherent one-body transition densities. The coherent one-body density is introduced in order to study the single-particle state contributions to the total Gamow-Teller strength. Discrepancies between the two models are found. The pnQRPA overestimates the total $\beta^+$ and $\beta\beta$ matrix elements. There are large disagreements in the shape of the spectra as well as in the coherent one-body transition densities between the pnQRPA and shell-model results. Empirical improvements for the pnQRPA are discussed.

The correlated BCS wave function is introduced by first-order perturbation theory, in which the four quasiparticle correlations are taken into account. The extended

BCS equation is derived. The applications of the extended BCS have shown some improvements compared to the standard BCS theory.

An extended pnQRPA equation is developed based on the extended BCS theory and applied to study $\beta^+$ and $\beta\beta$ decay. The calculations show that the disagreements between the pnQRPA and the shell model in the total B(GT$^+$) strengths and $\beta\beta$ decay matrix elements have been reduced, but those in the shape of the spectra have not yet been improved.

Other possible improvements for the pnQRPA are discussed. A second pnQRPA equation is developed by including two and four quasiparticle excitations in the phonon creation operator. An extended second pnQRPA equation is obtained by combination of the second pnQRPA and extended pnQRPA equations. They should provide more accurate methods for studying the transition of the one- and two-body charge exchange modes.

# ACKNOWLEDGMENTS

First of all, I would like to express deepest thanks to my advisor B. Alex Brown for his guidance and patience during five years of my graduate study. He has taught me what nuclear physics is and how to do good research. I will appreciate this for the rest of my life.

I wish to thank my guidance committee members, Prof. George F. Bertsch, Prof. Aaron Galonsky, Prof. Wayne W. Repko and Prof. Susan M. Simkin. I have a special acknowledgement for Prof. Aurel Bulgac and Prof. Pawel Danielewicz with whom I had many helpful discussions. I thank Dr. Andy Sustich for the help and friendship I received. I am also grateful to Dr. Don Cha for his helpful suggestions for part of my thesis.

I appreciate Prof. Kovacs for the help I received in my pursuit of graduate study at Michigan State University. Thanks are also due to my friends, Renyong Fan, Dr. Minzhuan Gong, Nengjiu Ju, Jianan Liu, Andre Maul, Dr. David Mikolas, Zhijun Sun, Yang Wang, Qing Yang, Weiqing Zhong, Fan Zhu and many others for their help and friendship.

I would like to express my gratitude to my family members, my parents, Prof. Minlun Zhao and Prof. Shujing Shen, for their constant encouragement and for their always stressing the importance of education, and my brother Dr. Jian Zhao and his wife Dr. Xiaofeng Li for their discussions, advice, help and support, especially in this five years. Thanks are due to my mother-in-law, Dr. Pingling Liu, my aunt Dr. Shuzhao Shen and her husband Prof. Dashou Sheng.

Finally, I heartily thank my wife, Dr. Rong Xu, for her love and also for her financial support in finishing my thesis.

# Contents

**LIST OF TABLES** vi

**LIST OF FIGURES** ix

**1 Introduction** 1

1.1 Beta and Double-Beta Decays . . . . . . . . . . . . . . . . . . . . . . 1

1.2 Shell Model Theory . . . . . . . . . . . . . . . . . . . . . . . . . . . 2

1.3 pnQRPA Theory . . . . . . . . . . . . . . . . . . . . . . . . . . . . 8

1.4 Beyond RPA . . . . . . . . . . . . . . . . . . . . . . . . . . . . . . 12

1.5 Thesis Organization . . . . . . . . . . . . . . . . . . . . . . . . . . 13

**2 Shell-model Calculation for Two-neutrino Double-beta Decay of $^{48}$Ca** 16

2.1 Introduction . . . . . . . . . . . . . . . . . . . . . . . . . . . . . . 16

2.2 Model Spaces and Effective Interactions . . . . . . . . . . . . . . . . 19

2.3 Calculations and Discussions . . . . . . . . . . . . . . . . . . . . . 20

2.4 Summary . . . . . . . . . . . . . . . . . . . . . . . . . . . . . . . . 32

**3 Comparison between pnQRPA and Shell Model I: $\beta^+$ Decay** 33

3.1 Introduction . . . . . . . . . . . . . . . . . . . . . . . . . . . . 33
3.2 Formalism . . . . . . . . . . . . . . . . . . . . . . . . . . . . 35
  3.2.1 pnQRPA equations . . . . . . . . . . . . . . . . . . . . . 35
  3.2.2 BCS equations . . . . . . . . . . . . . . . . . . . . . . . 38
  3.2.3 $B$(GT) in shell-model calculations . . . . . . . . . . . . . . 39
  3.2.4 The coherent one-body transition density . . . . . . . . . . . 40
3.3 Calculations and Discussions . . . . . . . . . . . . . . . . . . . 41
  3.3.1 Comparison of pnQRPA and shell model . . . . . . . . . . . . 41
  3.3.2 Empirical improvements of pnQRPA . . . . . . . . . . . . . . 46
3.4 Summary and Conclusions . . . . . . . . . . . . . . . . . . . . . 49

**4 Comparison between pnQRPA and Shell Model II: $2\nu\beta\beta$ Decay 52**

4.1 Introduction . . . . . . . . . . . . . . . . . . . . . . . . . . . . 52
4.2 Formalism of $2\nu\beta\beta$ Decay . . . . . . . . . . . . . . . . . . . 54
4.3 Results and Discussions . . . . . . . . . . . . . . . . . . . . . . 56
4.4 Summary and Conclusions . . . . . . . . . . . . . . . . . . . . . 69

**5 BCS Theory and Extension 71**

5.1 Introduction . . . . . . . . . . . . . . . . . . . . . . . . . . . . 71
5.2 BCS Theory for Proton-Neutron System . . . . . . . . . . . . . . . 73
  5.2.1 Nuclear Hamiltonian in quasiparticle space . . . . . . . . . . 73
  5.2.2 BCS equations ( independent quasiparticle ) . . . . . . . . . . 76
  5.2.3 BCS energy spectrum . . . . . . . . . . . . . . . . . . . . 80

5.3 Extended BCS Theory . . . . . . . . . . . . . . . . . . . . . . . . . . 81
5.3.1 Interactions between quasiparticles . . . . . . . . . . . . . . . 81
5.3.2 Correlated BCS wave function . . . . . . . . . . . . . . . . . . 83
5.3.3 Construction of two-quasiproton two-quasineutron excitations in the J-scheme . . . . . . . . . . . . . . . . . . . . . . . . . 84
5.3.4 Formalism of extended BCS theory . . . . . . . . . . . . . . . 87
5.4 Application . . . . . . . . . . . . . . . . . . . . . . . . . . . . . . . 90
5.5 Summary . . . . . . . . . . . . . . . . . . . . . . . . . . . . . . . . 92

**6 Extended pnQRPA Theory and Applications 93**

6.1 Introduction . . . . . . . . . . . . . . . . . . . . . . . . . . . . . . . 93
6.2 Extended pnQRPA Equations . . . . . . . . . . . . . . . . . . . . . 94
6.3 Application and Discussions . . . . . . . . . . . . . . . . . . . . . . 97
6.4 Summary and Conclusions . . . . . . . . . . . . . . . . . . . . . . . 102

**7 Further Improvements and Considerations 104**

7.1 Introduction . . . . . . . . . . . . . . . . . . . . . . . . . . . . . . . 104
7.2 Second pnQRPA Equations . . . . . . . . . . . . . . . . . . . . . . . 105
7.3 Extended Second pnQRPA Equations . . . . . . . . . . . . . . . . . 109
7.4 Summary . . . . . . . . . . . . . . . . . . . . . . . . . . . . . . . . 109

**8 Summary and Conclusions 111**

**A QRPA equations 115**

B Relation between QRPA and pnQRPA Equations 117

C Second QRPA Equations 119

D Coherent One-Body Transition Density 122

E BCS and Extended BCS in Uncoupled Representation 124

F Spurious States in the BCS and extended BCS. 127

LIST OF REFERENCES 131

# List of Tables

2.1 Summary of the $B(\mathrm{GT}^-)$ and $B(\mathrm{GT}^+)$ values obtained from the experiments and compared to the theoretical calculations with the MSOBEP and the MH interactions. . . . . . . . . . . . . . . . . . . . . . . . . 24

2.2 Comparison of the nuclear matrix elements $B(cls)$ and $M^{2\nu}_{\mathrm{GT}}$, the average excited energy $< E_m >$ and half life $T_{1/2}$. The shell-model space configurations are described by $f^{8-n}_{7/2}(p_{3/2}f_{5/2}p_{1/2})^n$ with n=0 to n$_{max}$ for the fp shell referring to the initial(i), intermediate(m) and final(f) states. . . . . . . . . . . . . . . . . . . . . . . . . . . . . . . 28

2.3 The first ten $B(\mathrm{GT}^-)$, $B(\mathrm{GT}^+)$ and $\mathrm{M}^{m}_{GT}$ values obtained with the MSOBEP interaction . . . . . . . . . . . . . . . . . . . . . . . . 29

2.4 Comparison of $\mathrm{M}^{2\nu}_{\mathrm{GT}}$ in different truncations. The shell-model space configurations are described by $f^{8-n}_{7/2}(p_{3/2}f_{5/2}p_{1/2})^n$ for the fp shell and $d^{6-n}_{5/2}(s_{1/2}d_{3/2})^n$ for the sd shell referring to the initial(i), intermediate(m) and final(f) states with n=0 to n$_{max}$. The full-basis means n$_{max}$=8 in the fp shell or n$_{max}$=6 in the sd shell. The MSOBEP interaction was used for $^{48}$Ca and $^{46}$Ca and the interaction [Wil 84] was used for $^{22}$O. . . . . . . . . . . . . . . . . . . . . . . . . . . . 31

3.1 $^{46}$Ti: Proton and neutron: single particle energies $\varepsilon_i$ (MeV), gap parameters $\Delta_i$ (MeV) and occupation probabilities $v_i^2$ from BCS and the shell-model $E_i$(SM) and $v_i^2$(SM) . The Fermi energies obtained from the BCS calculation are $-12.968$ MeV and $-10.868$ MeV for proton and neutron, respectively. . . . . . . . . . . . . . . . . . . . . . . . . . 41

3.2 Comparison of the coherent one-body transition density (COBTD) obtained in the pnQRPA, modified pnQRPA and shell-model calculations of $^{46}$Ti. . . . . . . . . . . . . . . . . . . . . . . . . . . . . . . . . . . 45

3.3 Comparison of the coherent transition matrix elements (CTME) obtained in the pnQRPA, modified pnQRPA and shell-model calculations of $^{46}$Ti. Labels (A), (B), (C), (D) and (E) are given by Table 3.2 . . . 46

4.1 $^{46}$Ca: Neutron single particle energies $\varepsilon_i$ (MeV), gap parameters $\Delta_i$ (MeV) and occupation probabilities $v_i^2$ and quasineutron energies $E_i$ (MeV) from BCS, the shell-model $E_i$(SM), $v_i^2$(SM) defined in Chapter 3. The neutron Fermi energy is $-8.712$ MeV. . . . . . . . . . . . . . . . 65

5.1 $^{46}$Ti: The occupation probabilities $< |a_{jm}^\dagger a_{jm}| > /(2j+1)$ for protons and neutrons obtained from the BCS, extended BCS (EBCS) and shell-model calculations, respectively. . . . . . . . . . . . . . . . . . . . . . . . . 91

5.2 The extended BCS parameters, $u_i^2$, $v_i^2$, gap parameters $\Delta_i$ (MeV) and quasiparticle energies $E_i$ (MeV) for $^{46}$Ti . . . . . . . . . . . . . . . . . 91

6.1 Comparison of the coherent one-body transition density (COBTD) obtained for the pnQRPA, extended pnQRPA and shell model calculations of $^{46}$Ti. The labels represent (A): COBTD in the pnQRPA ; (B): COBTD in the extended pnQRPA ; (C): COBTD in the shell model. 98

6.2 Comparison of the coherent transition matrix elements (CTME) obtained in the pnQRPA, extended pnQRPA and shell model calculations of $^{46}$Ti. Labels (A), (B) and (C) are given by Table 6.1 . . . . . . . . 102

# List of Figures

1.1 (a) The single-particle energies of a harmonic-oscillator potential. N is the oscillator quantum number. (b) The single-particle energies of a Woods-Saxon potential. (c) The single-particle energies of a Woods-Saxon potential plus spin-orbit coupling. Each state is labeled by $(nlj)$. (d) The numbers $\sum(2j+1)$. . . . . . . . . . . . . . . . . . . . . . . . . 4

1.2 Schematic representation of the simple shell-model configurations (a) $^{48}$Ca ground state (closed shell). (b) $^{49}$Ca ground state. (c) $^{48}$Ca excitation state. (d) $^{49}$Ca excitation state. . . . . . . . . . . . . . . . . 6

1.3 Schematic representation of the TDA and RPA configurations for $^{48}$Ca (a) TDA ground state (closed shell). (b) RPA ground state. (c) TDA excitation state. (d) RPA excitation state. . . . . . . . . . . . . . . . . 10

1.4 Schematic representation of the pnTDA configurations for $^{48}$Ca (a) pnTDA ground state (close shell). (b) pnTDA excitation state. . . . . . 11

2.1 Mass spectrum for A=48 nuclei. The double-beta decay is a possible decay mode for the $^{48}$Ca ground state. See text about the single $\beta^-$ decay of $^{48}$Ca. . . . . . . . . . . . . . . . . . . . . . . . . . . . . . 18

2.2 $M_{\rm GT}(E_m)$ as a function of $E_m$. The first $M_{\rm GT}(E_m)$ is fixed at $E_1$=2.52 MeV. In (a), the solid line is obtained from the MSOBEP interaction, and dashed line from the MH interaction. The truncation for both curves is (D: $n \leq 4$ for $^{48}$Ca and $^{48}$Ti, $n \leq 5$ for $^{48}$Sc). (b) shows the results for the MSOBEP interaction at different levels of truncation for ($^{48}$Ca, $^{48}$Sc, $^{48}$Ti): A ($n=0$, $n \leq 1$, $n=0$); B ($n \leq 1$, $n \leq 2$, $n \leq 1$) and C ($n \leq 2$, $n \leq 3$, $n \leq 2$). . . . . . . . . . . . . . . . . . . . . . . . . . . 22

2.3 The $B(\mathrm{GT}^-)$ spectra for $^{48}\mathrm{Ca} \rightarrow {}^{48}\mathrm{Sc}$. The spectrum with FWHM = 100 keV obtained with the MSOBEP interaction is shown in (a). The spectra with FWHM = 400 keV obtained with the MSOBEP (solid line) and MH interaction (dashed line ) are shown in (b). The effective operator defined in Eq.(2.1) is employed in our calculations. The experimental $B(\mathrm{GT}^-)$ from [And 85] and B.D. Anderson (private communication) is presented in (c). The hatched area indicates the uncertainty resulting from subtracting the Fermi strength in the $0^+$(T=4) state at 6.8 MeV. . . . . . . . . . . . . . . . . . . . . . . . . . . . 25

2.4 The $B(\mathrm{GT}^+)$ values for $^{48}\mathrm{Ti} \rightarrow {}^{48}\mathrm{Sc}$. The experimental values from [Alf 91] are compared to the results obtained with the MSOBEP and MH interactions. The effective operator defined in Eq. (2.1) is employed in our calculations. . . . . . . . . . . . . . . . . . . . . . . . . . 26

3.1 Summed Gamow-Teller strength for $^{46}\mathrm{Ti} \rightarrow {}^{46}\mathrm{Sc}$. The solid line is the shell-model result while the dashed line is the pnQRPA result. . . . . 42

3.2 Summed Gamow-Teller strength for $^{46}\mathrm{Ti} \rightarrow {}^{46}\mathrm{Sc}$ with various particle-particle strength $g_{pp}$ where $g_{ph} = 1$. . . . . . . . . . . . . . . . . . . . . 43

3.3 The pnQRPA result with the shell-model quasiparticle energies and/or occupation probabilities ( see Table 3.1 ). . . . . . . . . . . . . . . . . . 50

4.1 Mass spectrum for A=46 nuclei, where the double-beta decay is the only possible decay mode for the $^{46}$Ca. ground state . . . . . . . . . . 55

4.2 Summed Gamow-Teller strength $B(\mathrm{GT}^{-})$ of $^{46}\mathrm{Ca} \rightarrow ^{46}\mathrm{Sc}$. The dashed and solid lines are the pnQRPA and shell-model results, respectively . 58

4.3 Summed energy dependent $2\nu\beta\beta$ decay matrix element $M_{\mathrm{GT}}(E_m)$ as the function of the excitation energies, the solid line and dashed line are the shell-model and pnQRPA results, respectively . . . . . . . . . 59

4.4 Summed closure $2\nu\beta\beta$ decay matrix element $B_{\mathrm{CLS}}(E_m)$ as the function of the excitation energies, the solid line and dashed line are the shell-model and pnQRPA results, respectively . . . . . . . . . . . . . . . 60

4.5 Summed closure matrix element $B_{\mathrm{CLS}}(E_m)$, the solid line is from the shell-model calculation, the dashed line is pnQRPA result with $g_{pp}$ = 0.0 and $g_{ph} = 1.0$ . . . . . . . . . . . . . . . . . . . . . . . . . . . 61

4.6 Summed closure matrix element $B_{\mathrm{CLS}}(E_m)$, the solid line is from the shell-model calculation, the dashed line is pnQRPA result with $g_{pp}$ = 0.5 and $g_{ph} = 1.0$ . . . . . . . . . . . . . . . . . . . . . . . . . . . 62

4.7 Summed closure matrix element $B_{\mathrm{CLS}}(E_m)$, the solid line is from the shell-model calculation, the dashed line is pnQRPA result with $g_{pp}$ = 1.28 and $g_{ph} = 1.0$. The pnQRPA reproduces shell-model total $B_{\mathrm{CLS}}$ value. . . . . . . . . . . . . . . . . . . . . . . . . . . . . . . . 63

4.8 Summed energy dependent matrix element $M_{\rm GT}(E_m)$, the solid line is from the shell-model calculation, the dashed line is pnQRPA result with $g_{pp} = 1.2$ and $g_{ph} = 1.0$. The pnQRPA reproduces shell-model total $M_{\rm GT}$ value. . . . . . . . . . . . . . . . . . . . . . . . . . . . 64

4.9 Summed closure matrix element $B_{\rm CLS}(E_m)$, the dashed line obtained by the pnQRPA with E, u,v from BCS and the dotted line with E from shell model and u,v from BCS, respectively. . . . . . . . . . . . . . . . 66

4.10 Summed closure matrix element $B_{\rm CLS}(E_m)$, the dashed line obtained by the pnQRPA with E, u,v from BCS and the dotted line with E from BCS and u,v from shell model, respectively. . . . . . . . . . . . . . . . 67

4.11 Summed closure matrix element $B_{\rm CLS}(E_m)$, the dashed line obtained by the pnQRPA with E, u,v from BCS and the dotted line with u,v and E from shell model, respectively. . . . . . . . . . . . . . . . . . . . 68

6.1 Summed Gamow-Teller strength for $^{46}$Ti $\rightarrow ^{46}$Sc. The solid line, the dashed line and the dotted line are obtained by the shell model, pnQRPA and extended pnQRPA, respectively. . . . . . . . . . . . . . . . 99

6.2 Summed energy dependent $2\nu\beta\beta$ decay matrix element $M_{\rm GT}(E_m)$ as the function of the excitation energies, the solid line, the dashed line and the dotted line are obtained by the shell model, pnQRPA and extended pnQRPA, respectively . . . . . . . . . . . . . . . . . . . . . . . 100

6.3 Summed closure $2\nu\beta\beta$ decay matrix element $B_{\rm CLS}(E_m)$ as the function of the excitation energies, the solid line, the dashed line and the dotted line are obtained by the shell model, pnQRPA and extended pnQRPA, respectively . . . . . . . . . . . . . . . . . . . . . . . . . . . . . . . 101

# Chapter 1

# Introduction

## 1.1 Beta and Double-Beta Decays

The beta ($\beta$) decay process was one of the first types of radioactivity to be observed and still provides new valuable insight into weak interaction and nuclear structure. In this process, the $\beta$ unstable nucleus can become more stable by converting a proton ( neutron ) within the nucleus into a neutron ( proton ). So the mass number of the nucleus, $A$, remains the same but the nuclear charge number, $Z$, changes by one unit. The $\beta^-$ decay involves emission an electron and an antineutrino, $(A, Z) \rightarrow (A, Z+1) + e^- + \bar{\nu}$, and $\beta^+$ decay involves a positron and a neutrino $(A, Z) \rightarrow (A, Z-1) + e^+ + \nu$. The $\beta$ decay mechanism is well described by the standard weak interaction theory. The beta transition probability $T(\beta)$ depends on two different nuclear matrix elements and can be written as

$$T(\beta) \propto G_{\mathrm{V}}^2 B(\mathrm{F}) + G_{\mathrm{A}}^2 B(\mathrm{GT}), \tag{1.1}$$

where $G_{\mathrm{V}}$ and $G_{\mathrm{A}}$ are the coupling constants associated with the vector part and the axial-vector part of charge-current, respectively. $B(\mathrm{F})$ is the Fermi transition strength related to the isospin operator. $B(\mathrm{GT})$ is the Gamow-Teller transition strength associated with the Pauli spin operator as well as the isospin operator.

Nuclear double-beta ($\beta\beta$) decay phenomena is a rare transition between two nuclei of the same mass number having a change of two units of nuclear charge. In cases of interest, ordinary single beta decay is forbidden because of energy conservation or because of very strong suppression due to a large angular momentum mismatch between the parent and daughter states. There are two modes of double-beta decay [Hax 84, Doi 85, Mut 88, Ver 86],

$$2\ \nu \text{ mode}: (A,Z) \rightarrow \quad (A,Z+2)+2e^- + 2\bar{\nu} \tag{1.2}$$

$$0\ \nu \text{ mode}: (A,Z) \rightarrow \quad (A,Z+2)+2e^-. \tag{1.3}$$

The first one is called two-neutrino ($2\nu$) $\beta\beta$ decay, which involves the emission of two antineutrinos and two electrons ($2\nu$ mode), it occurs in second order in the standard weak interaction theory. Another is called neutrinoless ($0\nu$) $\beta\beta$ decay, which involves the emission of two electrons and no neutrinos. This process violates the lepton number conservation and requires the neutrino to be a Majorana particle and have a nonzero mass and/or a nonstandard right-hand coupling. It occurs in some theories beyond the standard weak interaction model.

The $2\nu\beta\beta$ decay has been observed in recent experiments [Ell 87, Avi 91, Eji 91, Tur 91], but the $0\nu\beta\beta$ decay has not yet been observed.

There are two important nuclear models which can be applied to the study of the $\beta$ and $\beta\beta$ decays which occur in nuclei, the *shell model* and the *pnQRPA* model. We will briefly discuss them in the following sections.

## 1.2 Shell Model Theory

The nuclear shell-model theory was introduced by Mayer and Jensen 40 years ago [May 55]. The basic assumption is that each nucleon (proton and neutron) moves independently in a potential that represents the average interaction with the other nucleons in the nucleus. This potential is the combination of a central part and the spin-orbit coupling term. The energy levels obtained by solving the Schrödinger equation for a nucleon in the potential are given in Figure 1.1. The energy levels in the column (a) and (b) are obtained by using harmonic-oscillator and Wood-Saxon potentials, respectively, where the spin-orbit coupling term has not been included. $s, p, d, f$, etc stand for orbital momentum $l = 0, 1, 2, 3$, etc. The column (c) in Figure 1.1 illustrates the level splitting due to addition of spin-orbit coupling term. Each level in column (c) is called a single-particle state and is labeled as $(nlj)$ in this thesis, where $n$ is the radial quantum number and $j = l + s$.

The ground state in the *simple shell model* is assumed to be the configuration in which the energy levels are filled consecutively by the nucleons with the constraint of the Pauli principle. For example, the configuration of the $^{48}$Ca ground state is that the 28 neutrons have filled the single-particle states up to $1f_{7/2}$ shell, and the 20 protons have filled the single-particle states up to $1d_{3/2}$ shell. $^{48}$Ca is a closed shell nucleus. The schematic representation of $^{48}$Ca is shown in Figure 1.2 (a). For the ground state of $^{49}$Ca, the configuration in the simple shell model is that the valence neutron occupies the $2p_{3/2}$ state outside of the $^{48}$Ca closed shell as shown in Figure 1.2 (b). So the ground state spin should be $J^{\pi} = 3/2^{-}$. The success of this simple model is that there are many nuclei whose ground states properties agree with these assumptions.

In order to simplify our discussions for the excitations in the simple shell model, we only consider two single-particle states $1f_{7/2}$ and $2p_{3/2}$. Then the excitations of $^{48}$Ca can be constructed by removing one nucleon from $1f_{7/2}$ to $1p_{3/2}$ state, forming the one-particle-one-hole configurations. For $^{49}$Ca, the excitations are two-particle-

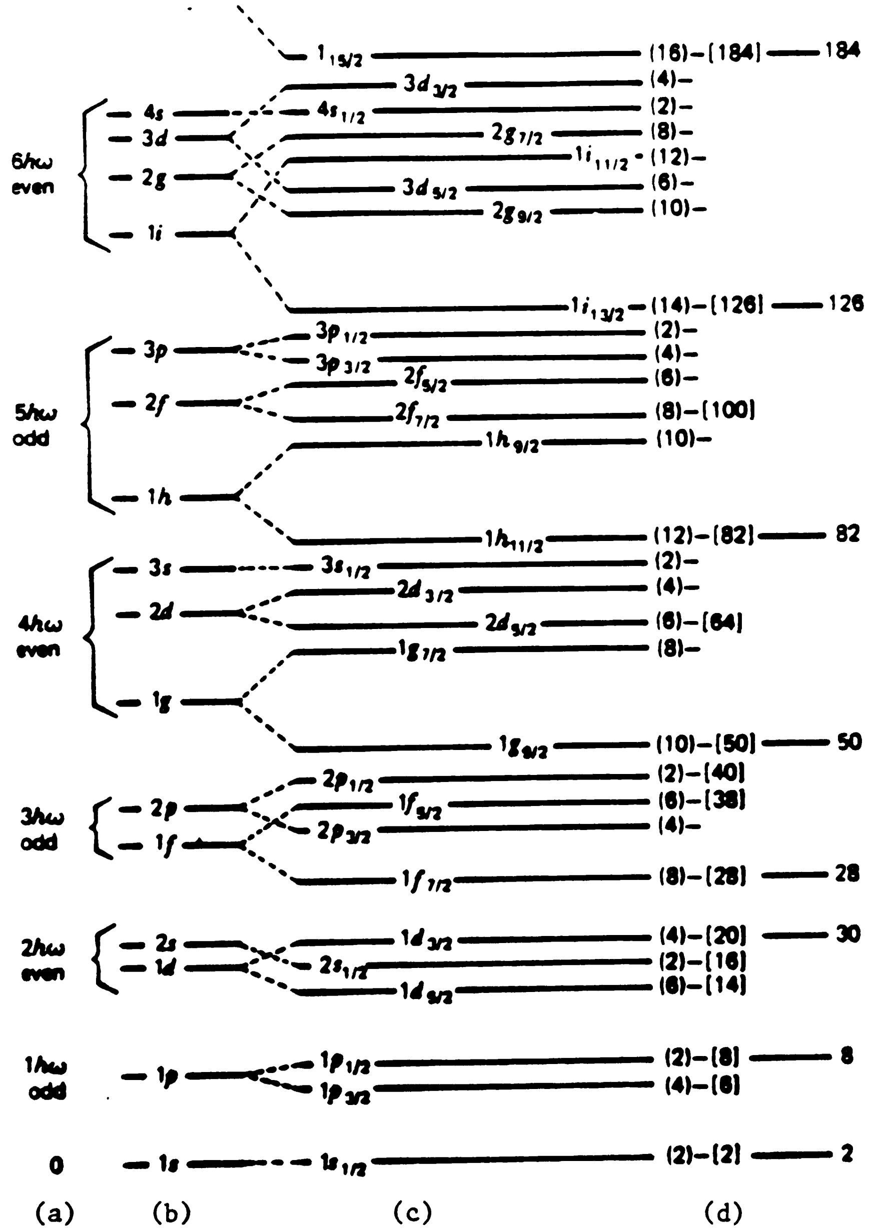
1i15/2 (16)-[184] 184
3d3/2 (4)-
4s 4s1/2 (2)-
3d 2g7/2 (8)-
6ħω even
2g 1i11/2 (12)-
3d5/2 (6)-
2g9/2 (10)-
1i
1i13/2 (14)-[126] 126
3p 3p1/2 (2)-
3p3/2 (4)-
2f5/2 (6)-
5ħω odd
2f 2f7/2 (8)-[100]
1h9/2 (10)-
1h
1h11/2 (12)-[82] 82
3s 3s1/2 (2)-
2d3/2 (4)-
4ħω even
2d 2d5/2 (6)-[64]
1g7/2 (8)-
1g
1g9/2 (10)-[50] 50
2p1/2 (2)-[40]
3ħω odd
2p 1f5/2 (6)-[38]
1f 2p3/2 (4)-
1f7/2 (8)-[28] 28
2ħω even
2s 1d3/2 (4)-[20] 30
1d 2s1/2 (2)-[16]
1d5/2 (6)-[14]
1ħω odd
1p 1p1/2 (2)-[8] 8
1p3/2 (4)-[6]
0 1s 1s1/2 (2)-[2] 2
(a) (b) (c) (d)

Figure 1.1: (a) The single-particle energies of a harmonic-oscillator potential. N is the oscillator quantum number. (b) The single-particle energies of a Woods-Saxon potential. (c) The single-particle energies of a Woods-Saxon potential plus spin-orbit coupling. Each state is labeled by $(nlj)$. (d) The numbers $\sum(2j+1)$.

one-hole configuration. The schematic illustrations of these excitation configurations are presented in Figure 1.2 (c) and (d).

In present shell-model theory, the nuclear structure properties are assumed to be determined by the valence nucleons which simultaneously occupy several different, partially filled, single-particle states within one or two given major shells. For light nuclei ( A$\leq$ 40), the major shells are the oscillator shells indicated by the $N$ labels on the left-hand side of Figure 1.1. For heavy nuclei (A$\geq$ 40), the major shells usually include the addition of one high $j$-state from the $(N+1)$ oscillator shell. This is called the ***large-basis shell-model calculation.*** Many multinucleon configurations are taken into account in this calculation. For example, the ground state configuration of $^{48}$Ca in the full fp shell ($1f_{7/2}, 2p_{3/2}, 1f_{5/2}$ and $2p_{1/2}$) is considered as the linear combination of all possible configurations in which eight neutrons simultaneously occupy all states in the fp shell. The label $|n_1n_2n_3n_4>$ used below indicates that $n_1$ neutrons occupy the $1f_{7/2}$, $n_2$ the $2p_{3/2}$, $n_3$ the $1f_{5/2}$, and $n_4$ the $2p_{1/2}$. The Pauli principle and sum $n_1 + n_2 + n_3 + n_4 = 8$ must be satisfied. Then the wave function of the $^{48}$Ca ground state is expanded as

$$\begin{aligned} |^{48}\mathrm{Ca}, 0^+ > &= a_1|8000> + a_2|6200> + a_3|5300> + a_4|4400> + \cdots + \\ & \quad a_{72}|0242> + a_{73}|0062>\ , \end{aligned} \tag{1.4}$$

with $\sum_i a_i^2 = 1$. There are 73 terms (partitions) in Eq. (1.4). Some terms are missing due to angular momentum coupling restriction [Etc 85]. Within this set of partitions, the number of independent states with $J = 0$ is 347, and the number of independent states with $M = 0$ is 12022. These numbers are referred to the $J$-dimension and $M$-dimension, respectively. In the simple shell model, all coefficients in Eq. (1.4) are zeros except $a_1 = 1$. The corresponding $J-$ and $M-$ dimensions are both equal to 1.

The large-basis shell-model calculation includes three steps: (1) setting up the

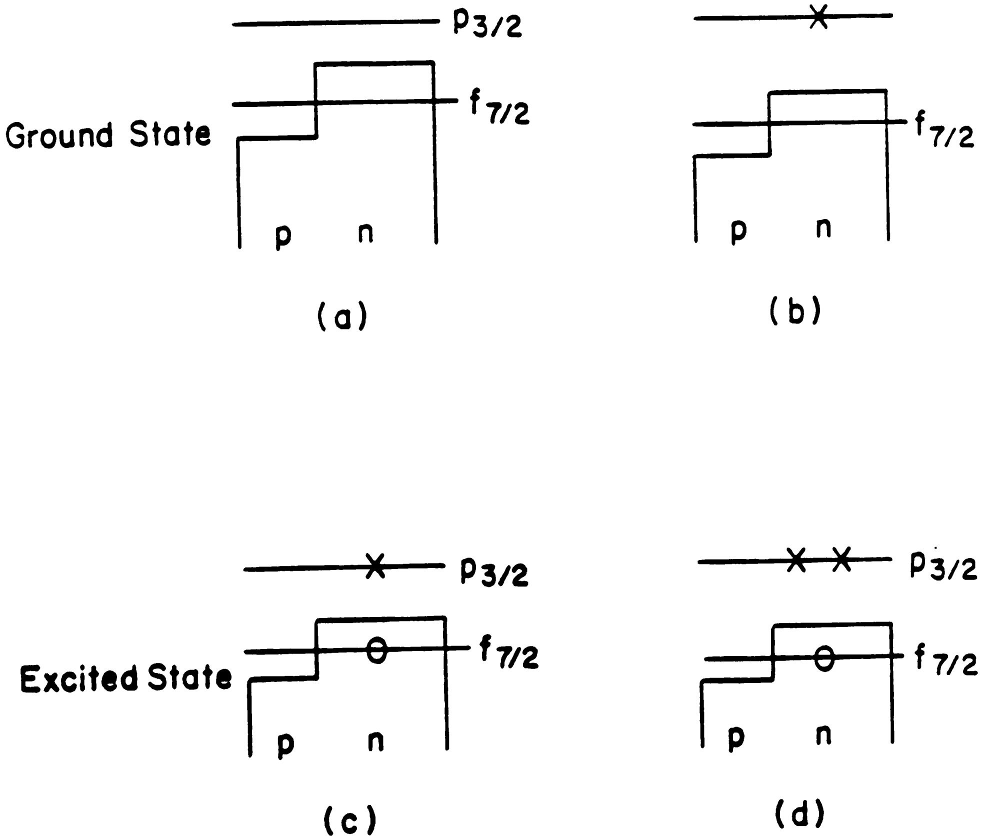
Ground State
Excited State
$p_{3/2}$
$f_{7/2}$
p
n
(a)
(b)
(c)
(d)

Figure 1.2: Schematic representation of the simple shell-model configurations (a) $^{48}$Ca ground state (closed shell). (b) $^{49}$Ca ground state. (c) $^{48}$Ca excitation state. (d) $^{49}$Ca excitation state.

single-particle basis, (2) construction of the Hamiltonian matrix, and (3) diagonalization of this matrix. However, carrying out the large-basis shell-model calculation requires extensive numerical computation, so better numerical methods and modern computer facilities are very important.

The phrase of the *full-basis shell-model calculation* will refer to a large-basis shell-model calculation in which all possible configurations in a major shell are included.

However, a limiting constraint on the large-basis shell-model calculations is that the dimension of the Hamiltonian matrix increases rapidly when the single-particle basis increases. For example, the dimension of $J^\pi = 0^+$ of the $^{48}$Ca ground state is one in the $1f_{7/2}$ shell, 14 in the full f shell ( $1f_{7/2}, 1f_{5/2}$ ), and 347 in the full fp shell ( $1f_{7/2}, 2p_{3/2}, 1f_{5/2}, 2p_{1/2}$ ). In medium and heavy nuclei ( $A \geq 50$ ), the dimensions are extremely large. For example, in $^{154}_{62}\mathrm{Sn}_{92}$, if we allow the 12 valence protons to occupy $1g_{7/2}, 2d_{5/2}, 2d_{3/2}, 3s_{1/2}, 1h_{11/2}$ states, and 10 valence neutrons to occupy $1h_{9/2}, 2f_{7/2}, 2f_{5/2}, 3p_{3/2}, 3p_{1/2}, 1i_{13}/2$ states. the dimension of $J^\pi = 0^+$ matrix is 41,654,193,516,917 [Iac 87]. This is of course completely beyond current computer capability. Thus present shell-model calculations for heavy nuclei are performed within very truncated model spaces. In the extreme limit, they may go back to the simple shell model. Because of the difficulties in carrying out the large-basis shell-model calculation, the RPA, the QRPA and the pnQRPA, which are discussed in the next section, are frequently employed to study the properties of medium and heavy nuclei.

Another important aspect in the shell model is the *effective interaction.* The first and reasonable guess is from the theoretical G-matrix calculations [Rin 80]. But more precise and reliable effective interactions are currently obtained from two methods. One of them is using an unconstrained Hamiltonian, in which all two-body matrix elements and single-particle energies are allowed to vary as free parameters in a fit to experimental data ( for example, see ref. [Wil 84]). Another is employing some well-understood nuclear potentials ( such as one pion or one boson exchange potentials ) and fitting the parameters in these models with the experimental data. Here the experimental data usually includes the binding energies and low-lying excitation energies ( for example, see [BAB 88, Ric 91] ). In this thesis, we will use the effective interaction from previous determination.

Most experimental data for light nuclei ( A$\leq$40 ) can be successfully explained and even predicted by the large-basis shell-model calculations [Bru 77, Law 80]. For example, the Gamow-Teller transition strengths of the full-basis shell-model calculations in the sd shell ($1d_{5/2}, 2s_{1/2}$ and $1d_{3/2}$) are in good agreement with those in the experiments [Bro 85, Bro 88].

## 1.3 pnQRPA Theory

In this section, we discuss the *proton-neutron Quasiparticle Random Phase Approximation* (pnQRPA), which is widely used for $\beta-$ and $\beta\beta-$ decay calculations in heaver nuclei. The method of the pnQRPA is totally different from that of the shell model. In order to understand this theory, it is useful to understand the following theories and their relations: the Tamm-Dancoff Approximation ( TDA ), the Random Phase Approximation ( RPA ) and the Quasiparticle Random Phase Approximation ( QRPA ). Their mathematical derivations can be found on the textbook of many-body problem such as [Row 70]. Here we only concentrate on the physical picture.

First, we qualitatively describe the TDA and RPA models for $^{48}$Ca. The TDA ground state is the $^{48}$Ca closed shell shown in Figure 1.3 (a), and the excited states are constructed by removing a neutron in $1f_{7/2}$ closed shell, creating another one in the empty states above $1f_{7/2}$ shell, and forming one-particle-one-hole ( 1p1h ) configurations, see Figure1.3 (c). Thus we find the TDA is the same as the simple shell model shown in Figure 1.2 (a) and (c). In the RPA, the ground state is not pure closed shell, but has mixtures of some types of 2p2h, 4p4h, $\cdots$, components as shown in Figure 1.3 (b). The excitations of the RPA can be obtained by removing one neutron from the $1f_{7/2}$ to other states above $1f_{7/2}$ like the TDA, and also can be constructed by removing a neutron above $f_{7/2}$ states and creating a neutron in $f_{7/2}$ state, see Figure 1.3 (d). The RPA theory cannot be simply linked to the simple shell model or large-basis shell model.

For the even-even nuclei away from closed shells, the experimental results have suggested that the ground state may be dominated by pairing correlations [Row 70, Rin 80]. The BCS ( Bardeen, Cooper and Schrieffer ) theory assumes all nucleons in the ground state to be paired. ( BCS theory is discussed in more detail in Chapter 5 ). In terms of the Bogoliubov quasiparticle, which is a linear combination of the particle and hole, the BCS ground state is a vacuum with respect to the quasiparticle. The Quasiparticle Tamm-Dancoff Approximation ( QTDA ) suggests that the excitations are obtained by creating two quasiparticles from the BCS ground state. Similar to the relation between the TDA and RPA, the QRPA assumes the ground state configuration is the quasiparticle vacuum plus mixtures of some types of four quasiparticle, eight quasiparticle, $\cdots$, components. Thus the excitations in the QRPA are performed by creating and destroying two quasiparticles from the QRPA ground state. In the TDA, RPA and QRPA, the excitations and ground states are with respect to the same nucleus.

Now we generalize the TDA to the pnTDA in order to study the charge-exchange processes. Starting at the $^{48}$Ca closed shell, as an example, the excitations in the

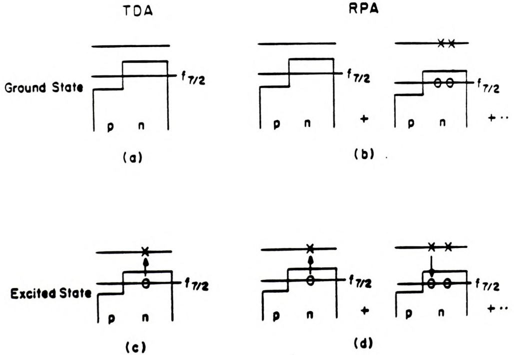
TDA
RPA
Ground State
Excited State
$f_{7/2}$
p
n
+
+ ..
(a)
(b)
(c)
(d)

Figure 1.3: Schematic representation of the TDA and RPA configurations for $^{48}$Ca (a) TDA ground state (closed shell). (b) RPA ground state. (c) TDA excitation state. (d) RPA excitation state.

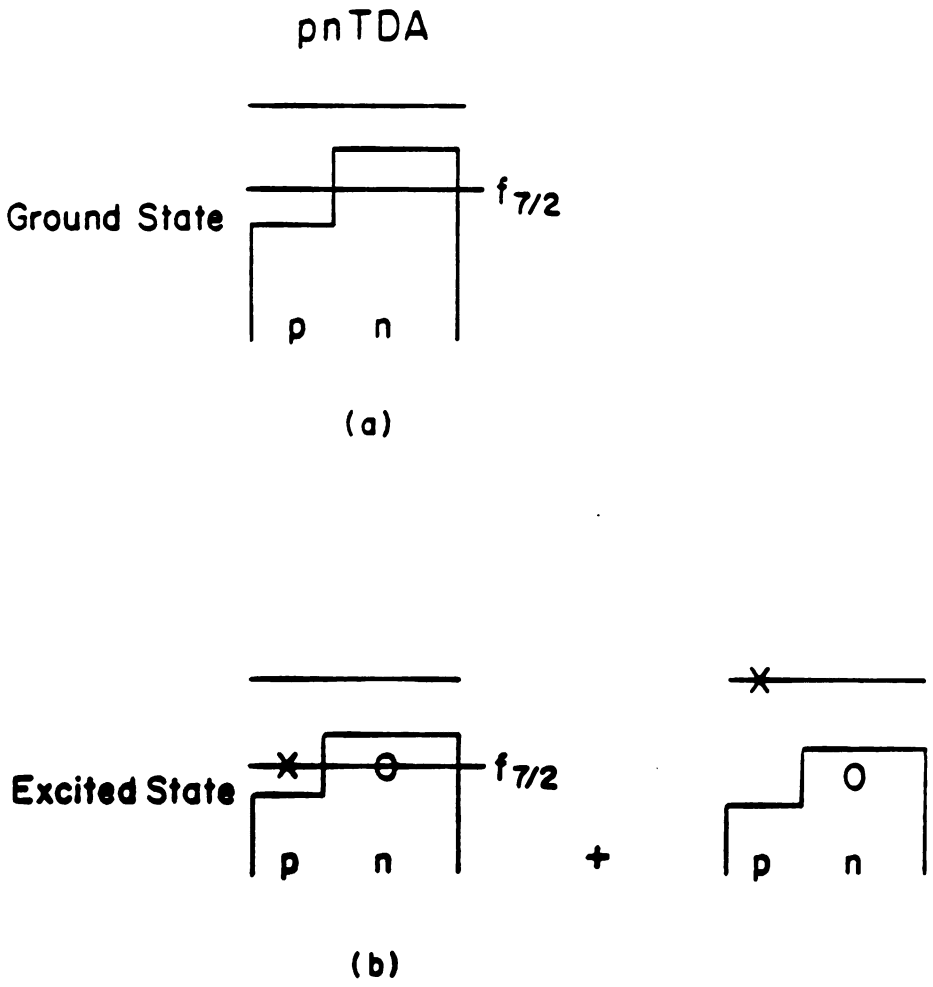
pnTDA
Ground State
f7/2
p
n
(a)
Excited State
f7/2
p
n
+
p
n
(b)

Figure 1.4: Schematic representation of the pnTDA configurations for $^{48}$Ca (a) pnTDA ground state (close shell). (b) pnTDA excitation state.

pnTDA are constructed by transferring a neutron from the $1f_{7/2}$ single-particle state to a proton which can occupy all empty proton states including the $1f_{7/2}$. So the configuration is the proton-particle neutron-hole shown in Figure 1.4. Then the transition matrix elements of the charge-exchange operator can be calculated in the pnTDA.

One can derive the pnQRPA model from the pnTDA, along the line TDA → RPA → QRPA. The basic idea is that the pnQRPA excitations, which contribute to the charge-exchange mode, are obtained by creating and destroying one quasiproton-quasineutron pair from the even-even nucleus ground state. The even-even nucleus ground state is assumed to be a quasiparticle vacuum ( BCS ) with the addition of mixtures of some types of four quasiparticle, eight quasiparticle, $\cdots$, components, where the quasiparticle could be the quasiproton or quasineutron. The transition strengths in the pnQRPA describe the charge-exchange processes.

The advantage of the TDA, RPA, QRPA, and pnQRPA is the small dimension involved. For example, the dimension of $J^\pi = 0^+$ matrix in the QRPA is 4 for the fp shell nuclei. The TDA, RPA, QRPA and pnQRPA are approximate models. The accuracies of these theories should be examined.

## 1.4 Beyond RPA

Improvement of the QRPA and pnQRPA may be an important goal in the field of nuclear structure theory as well as in the many-body problem. Since the derivation of the QRPA is similar to that of the RPA [Row 70, Rin 80], it is useful to review the development of the RPA theory. The physical picture of the RPA was discussed in section 1.3. The mathematical derivation of RPA equation can be achieved from the equation of motion method [Row 70, Rin 80], time-dependent Hartree-Fock theory [Row 70] and the Green's Function method [Fet 71, Bro 71]. We will concentrate here on the equation of motion method because it is the most appropriate for the extensions we will develop [Row 70, Rin 80].

In the equation of motion, the excitation states are constructed by acting a phonon creation operator $Q_\nu^\dagger$ on the ground state. This equation corresponds exactly to the full many-body Schrödinger equation if and only if the ground state in the equation of motion is the true ground state and the phonon creation operator exhausts the whole Hilbert space (i.e., 1p1h, 2p2h, 3p3h, and so on). For the RPA theory, there are two important assumptions. Only one-particle-one-hole (1p1h) creation and destruction operators are used in the phonon creation operator and the Hartree-Fock (HF) ground state is employed to calculate the matrix elements in the RPA equation. The HF ground state is obtained by the mean field.

Recently three ideas for improving RPA have been suggested [Dro 90]. One of them is the second RPA [Yan 83], in which the phonon creation operator is expanded up to 2p2h creation and destruction operators and the HF ground state is retained. Several numerical calculations have been made for giant resonances in the second RPA theory. However, the second RPA is still missing some types of correlations in the ground state [Tak 88]. Another idea is the extended RPA which uses an improved HF wave function to calculate the RPA matrix elements [Ada 88]. This improved HF wave function consists of the usual HF ground state plus 2p2h correlation corrections. The third idea combines these previous two and is called the extended second RPA [Tak 88]. It not only includes the 2p2h expansions in the phonon creation operator similar to the second RPA, but also uses an improved HF wave function as a ground state. Then the extended second RPA contains all the correction terms up to second-order perturbations in the two-body interaction. These second-order corrections are important for the more precisely measured magnetic moments and

$\beta$-decay matrix elements [Ari 87, Tak 84]. Improvements for the RPA suggest the generalization to the QRPA and pnQRPA which we will develop in Chapter 5, 6, 7.

## 1.5 Thesis Organization

The goals of this thesis consist of three aspects: (1) study of the $\beta$ and $\beta\beta$ decay of mass $A = 48$ nuclei with the large-basis shell-model calculations, (2) examinations of the validity and accuracy of the pnQRPA for $\beta^+$ and $\beta\beta$ processes, and (3) improvements and extensions of the pnQRPA model.

In Chapter 2, we study the $\beta^-$ and $\beta^+$ Gamow-Teller transition strength with the large-basis shell-model calculations for the nuclei $^{48}$Ca and $^{48}$Ti, respectively. The agreements between the theoretical results and the experimental data are examined. The half life of two-neutrino double-beta decay of $^{48}$Ca is calculated as well.

Since the pnQRPA is an approximate theory as we mentioned in section 1.3, we examine the validity and accuracy of the pnQRPA theory as a model for $\beta^+$ decay and double-beta $\beta\beta$ decay in Chapter 3 and Chapter 4, where the comparison of the pnQRPA and full-basis shell-model calculations ( exact model ) are made. We conclude that there are some correlations which are important in $\beta$ and $\beta\beta$ decay but are not included in the pnQRPA. Some empirical improvements for the pnQRPA have been suggested and tested.

In Chapter 5, the BCS theory for the proton-neutron system is reviewed. The correlated BCS wave function is introduced by incorporating the quasiparticle correlations with first-order perturbation theory. An extended BCS is derived and is applied to study the nuclear ground state properties.

In Chapter 6, we develop an extended pnQRPA equation with the correlated BCS ground state. The application of the extended pnQRPA is presented and compared to the pnQRPA and shell-model calculations. Some improvements over the pnQRPA are found.

In Chapter 7, we present the formalism for further possible improvements for the pnQRPA equation. The second pnQRPA and the extended second pnQRPA equations are derived. They should provide more accurate methods for studying the transition of the charge-exchange modes.

The summary and discussions are given in Chapter 8. We derive the QRPA equation in Appendix A and discuss the relation between the QRPA and pnQRPA in Appendix B. The second QRPA and coherent one-body transition density are given in Appendix C and D, respectively. In Appendix E, the BCS and the extended BCS theories are derived in angular momentum uncoupled space. In Appendix F, we discuss the spurious state in the BCS and the extended BCS theories.

# Chapter 2

# Shell-model Calculation for Two-neutrino Double-beta Decay of $^{48}$Ca

## 2.1 Introduction

The theory and experiment of double-beta ($\beta\beta$) decay have greatly attracted elemental particle and nuclear physicists for a long time. It is an important process for examining the character of the neutrino and for testing the theories beyond the standard weak interaction theory. On the other hand, the calculations for the $\beta\beta$ matrix elements provide a strong challenge to nuclear physicists, because $\beta\beta$ decays which are experimentally accessible occur in medium and heavy nuclei where we are still not clear how to precisely take into account the ground state correlations as well as calculate the excitations.

In order to analyse the experimental results to determine the character of the neutrino in $\beta\beta$ decay, precise calculations of the nuclear matrix elements are required. For example, the neutrino masses and the right-handed current coupling constants, which can be deduced from the experimental neutrinoless decay half-life, depend on the relevant nuclear matrix elements which have to be calculated theoretically [Hax 84, Doi 85, Mut 88],

However, in particular, the agreement between the experiment and theory for the standard $2\nu$ mode is one of the prerequisites for a reliable interpretation of the more exotic $0\nu$ mode. In this Chapter, we study the $2\nu\beta\beta$ decay of $^{48}$Ca which has the largest double-beta decay Q-value of any nucleus and where the large basis shell-model calculations are possible. The mass spectrum of A=48 is given in Figure 2.1.

In fact, the lowest states ( $6^+, 5^+$ and $4^+$ ) of $^{48}$Sc are located in the $^{48}$Ca's Q-value window [Alb 85], but these single $\beta$ decays are highly forbidden because of the angular momentum mismatch. Their half-lives are estimated to be about a factor of 10 times that of $2\nu\beta\beta$ decay [War 85].

There are serval difficulties with previous shell-model calculations for $2\nu\beta\beta$ decay of $^{48}$Ca. In cases where intermediate states in $^{48}$Sc were considered explicitly the fp shell-model space was highly truncated [Tsu 84, BAB 85, Sko 83, Ver 86], in other cases where the truncation was less severe the intermediate states were not calculated and the closure approximation was used instead [Hax 84, Ver 86, Zam 82]. Also the effective interactions used were not always well tested with regard to the nuclear spectra. In a more recent calculation [Oga 89], a new method was used to implicitly take into account the spectrum of the intermediate $1^+$ states exactly. However, we will emphasize below the importance of the testing the interactions with respect to the explicit intermediate spectrum. In the following, we calculate the nuclear matrix elements for $2\nu\beta\beta$ decay of $^{48}$Ca and the related $\beta^-$ and $\beta^+$ decay in the fp shell space with a much larger basis than previously used and with a new effective interaction than previously used.

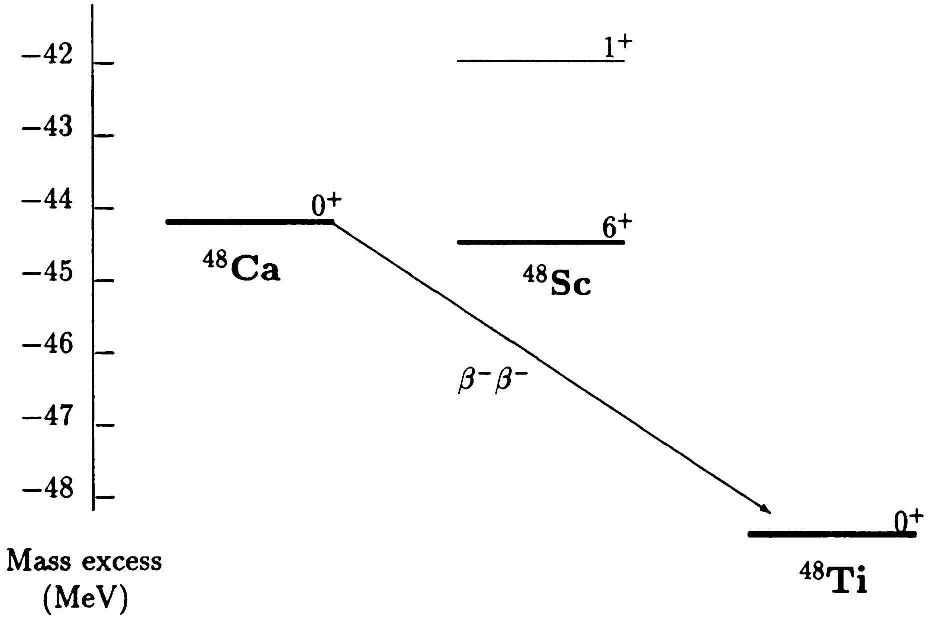
−42
−43
−44
−45
−46
−47
−48
Mass excess
(MeV)
0+
48Ca
1+
6+
48Sc
β−β−
0+
48Ti

Figure 2.1: Mass spectrum for A=48 nuclei. The double-beta decay is a possible decay mode for the $^{48}$Ca ground state. See text about the single $\beta^-$ decay of $^{48}$Ca.

## 2.2 Model Spaces and Effective Interactions

Because of the present computational limitations, a truncated shell-model basis is used in our calculations. The truncated space in the fp shell is defined by the set of partitions $f_{7/2}^{8-n}(p_{3/2}f_{5/2}p_{1/2})^n$. In this work, the partitions assumed for $^{48}$Ca($0^+$,T=4), $^{48}$Sc($1^+$,T=3) and $^{48}$Ti($0^+$,T=2) are $(n \leq 4), (n \leq 5)$ and $(n \leq 4)$, respectively. The $n \leq n_{\mathbf{max}}$ means that $n = 0, \cdots, n_{\mathbf{max}}$ are allowed. The corresponding J-scheme dimensions are 133, 5599 and 3613, respectively. This is an order of magnitude larger basis than has been used in previous calculations. Our calculations were carried out with the shell-model code OXBASH [Etc 85] on a VAX computer. The most complete fp shell calculation should be based on the full-basis space (n $\leq$ 8), but at present this is impossible because of the large dimensions involved. For example, the J-scheme dimension for the $^{48}$Ti ground state is 10872 in the full-basis space. It is at edge of our current computer capability. In later discussions, we will argue that our truncation is a good approximation with respect to the full-basis space.

The model space for the intermediate nucleus ($^{48}$Sc) should include all states which can be reached by a one-body operator from the initial and final nuclei. Thus for our initial ($^{48}$Ca) and final ($^{48}$Ti) states which have $n \leq 4$, we include $n \leq 5$ configurations in the intermediate system. Then the $B$(GT) from the $^{48}$Ti or $^{48}$Ca ground states satisfy the sum rule,

$$\sum B(\mathrm{GT}^-) - \sum B(\mathrm{GT}^+) = 3(N - Z), \qquad (2.1)$$

where $B(\mathrm{GT}) = (< f||\sigma t||i >)^2/(2J_i + 1)$.

The effective interactions used in this Chapter are called MH [Mut 84] and MSOBEP [Ric 91]. The MH interaction has a long history. McGrory et al. [McG 70] started with the renormalized Kuo-Brown interaction [Kuo 68] and changed several two-body matrix elements (TBME), which involved the $f_{7/2}$ and/or $p_{3/2}$ orbits. Later McGrory et al. [McG 81] added 50 keV to the $f_{7/2} - f_{5/2}$ diagonal TBME and introduced new single-particle energies. Based on Ref. [McG 81], Muto and Horie shifted the monopole of the inter-shell matrix elements $< f_{7/2}j|V|f_{5/2}j >^{T=0,J}$ ($j = p_{3/2}, p_{1/2}$ and $f_{7/2}$) matrix elements by $-0.3$ MeV [Mut 84].

MSOBEP is a new effective interaction based on a modified surface (MS) one-boson exchange potential (OBEP) [BAB 88]. *Modified* refers to the addition of monopole (infinitely long range) terms to the central part of the potential, and *surface* refers to an assumed density dependence which empirically is surface peaked. This MSOBEP potential has been successful in reproducing the sd-shell energy levels in terms of a few parameters associated with the strengths of the various OBEP channels. Richter et al. [Ric 91] have recently refit the parameters of this potential to 61 energy level data in the lower part of the fp shell, and this is the new interaction which we employ in the present work.

## 2.3 Calculations and Discussions

In this section, we will discuss the results for the double-beta decay matrix element of $^{48}$Ca. At first we introduce the effective Gamow-Teller operator based on previous beta decay and (p,n) reaction studies [Bro 88]

$$\tilde{\sigma} = 0.77\sigma. \tag{2.2}$$

This is used because experimental $B(\mathrm{GT})$ strengths are uniformly 30%~50% less than the shell-model calculations. The missing strength can be explained by a combination of the coupling to a $\Delta$-particle-N-hole configurations [Goo 81, Boh 81, Ari 87, Tow 87], and to the admixtures of 2p-2h configurations [Ber 82, Ari 87, Tow 87].

For purposes of discussion, we introduce the matrix element for $2\nu\beta\beta$ decay,

$$M_{\mathrm{GT}}(E_m) = \sum_{m=1}^{E_m} M_{\mathrm{GT}}^{m} = \sum_{m=1}^{E_m} \frac{< 0_f^+||\tilde{\sigma}t^-||1_m^+ >< 1_m^+||\tilde{\sigma}t^-||0_i^+ >}{E_m + E_0}, \tag{2.3}$$

which is a function of the $1^+$ excitation energy $E_m$ in $^{48}$Sc. $E_0 = T_0/2 + \Delta M$, where $T_0$ is the Q-value for $\beta\beta$ decay of $^{48}$Ca and $\Delta M$ is the mass difference between $^{48}$Sc and $^{48}$Ca, $T_0$=4.27 MeV and $\Delta$M=−0.277 MeV [Wap 85]. The total matrix element for $2\nu\beta\beta$ is given by $M_{\mathrm{GT}}^{2\nu} = M_{\mathrm{GT}}(E_m = \infty)$. The Fermi transition contribution vanishes when isospin is conserved. An estimate of its contribution with isospin-mixed wave functions indicates that it is small and can be neglected [BAB 85]. The half life is given by

$$\frac{1}{T_{1/2}} = G|M_{\mathrm{GT}}^{2\nu}|^2, \tag{2.4}$$

where G is related to fundamental constants and the phase space integral [Mut 88]. In fact, G depends somewhat on the GT strength distribution [Mut 88, Tsu 84] as well. Since the strength distribution of [Tsu 84] is close to ours, we use a value of $G = 1.10\times10^{-17}$ yr$^{-1}$(MeV)$^2$ deduced from the first row in Table 2.1 of Ref. [Tsu 84].

The closure approximation employed in the earlier calculations is defined by

$$B_{\mathrm{CLS}}(E_m) = \sum_{m=1}^{E_m} < 0_f^+||\tilde{\sigma}t^-||1_m^+ >< 1_m^+||\tilde{\sigma}t^-||0_i^+ > = \sum_{m,n} < 0_f^+||\tilde{\sigma_m}\cdot\tilde{\sigma}_n t_m^- t_n^-||0_i^+ >, \tag{2.5}$$

and

$$M_{\mathrm{GT}}^{2\nu}(cls) = \frac{B_{\mathrm{CLS}}}{< E_m > + E_0}. \tag{2.6}$$

where $B_{\mathrm{CLS}} = B_{\mathrm{CLS}}(E_m = \infty)$. In this approximation, $B_{\mathrm{CLS}}$ does not depend on the intermediate states. Estimates for the average energy $< E_m >$ of the $1^+$ states in $^{48}$Sc

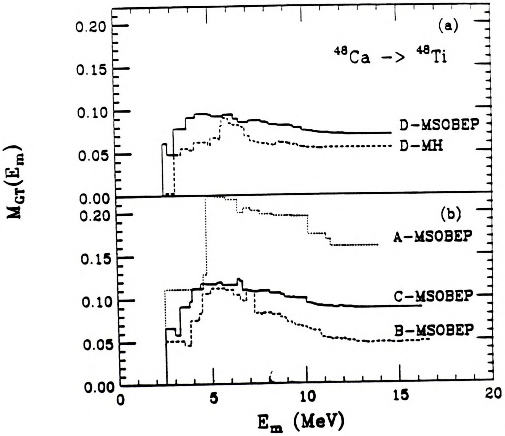

Figure 2.2: $M_{\rm GT}(E_m)$ as a function of $E_m$. The first $M_{\rm GT}(E_m)$ is fixed at $E_1$=2.52 MeV. In (a), the solid line is obtained from the MSOBEP interaction, and dashed line from the MH interaction. The truncation for both curves is (D: n$\leq$4 for $^{48}$Ca and $^{48}$Ti, n$\leq$ 5 for $^{48}$Sc). (b) shows the results for the MSOBEP interaction at different levels of truncation for ($^{48}$Ca, $^{48}$Sc, $^{48}$Ti): A (n=0, n$\leq$ 1, n=0); B (n$\leq$1, n$\leq$ 2, n$\leq$1) and C (n$\leq$2, n$\leq$ 3, n$\leq$2).

were made to obtain $M^{2\nu}_{\mathrm{GT}}(cls)$ [Hax 84]. These previous estimates can be compared with exact results, given by the comparison between $M^{2\nu}_{\mathrm{GT}}$ and $M^{2\nu}_{\mathrm{GT}}(cls)$

$$< E_m >= \frac{B_{\mathrm{CLS}}}{M^{2\nu}_{\mathrm{GT}}} - E_0. \tag{2.7}$$

The calculated matrix elements $M_{\mathrm{GT}}(E_m)$ as a function of $E_m$ for the MH and MSOBEP interactions are shown in Fig 2.2(a). There are about 300 eigenstates in each curve from 2.52 MeV $\sim$ 15 MeV. The $M_{\mathrm{GT}}(E_m)$ become negligibly small after about 12 MeV even though there are still many $1^+$ states (over 5000) above this energy in the calculation.

To understand the $\beta\beta$ matrix elements, we examine the $\beta^-$ and $\beta^+$ spectra. The theoretical $B(\mathrm{GT}^-)$ strengths vs $E_m$ are shown in Figure 2.3. The experimental distribution in Figure 2.3(c) represents the strength above the background line in Figure 1 of [And 85]. There is additional strength in the background between 4.5 and 14.5 MeV not shown in Figure 2(c) but indicated in the numerical comparisons made in Table 2.1. There may be more strength in the background above 14.5 MeV which we will comment on latter. The experimental spectrum in Figure 2.3(c) was obtained by the fitting the experimental cross section to a series of Gaussian peaks and then converting the cross section in each peak into a Gamow-Teller strength ( [And 85] and B.D. Anderson, private communication). Because the experimental measurement has a finite resolution, the theoretical $B(\mathrm{GT}^-)$ spectra are smoothed by a Gaussian. The $B(\mathrm{GT}^-)$ spectrum with a *high* resolution (FWHM=100 keV) is shown in Figure 2.3(a) for the MSOBEP interaction. The *low* resolution spectra for the MSOBEP (solid line) and MH (dashed line) interactions shown in Figure 2.3 (b) was obtained with FWHM=400 keV. One normalized factor is introduced in Figure 2.3 to make the areas proportional to the $B(\mathrm{GT}^-)$ strength. The $B(\mathrm{GT}^-)$ values extracted from the (p,n) data are compared with the theory in Table 2.1.

Table 2.1: Summary of the $B(\mathrm{GT}^-)$ and $B(\mathrm{GT}^+)$ values obtained from the experiments and compared to the theoretical calculations with the MSOBEP and the MH interactions.

| | $E_m$ (MeV) | Experiment[a)] | MSOBEP | MH |
|---|---|---|---|---|
| $\beta^-$ | 2.52–3.5 | 1.30 | 1.32 | 1.24 |
| | 3.5–14.5 | 8.61+2.86[b)] | 12.31 | 12.39 |
| | 16.8(T=4) | 0.45 | 0.42(0.62)[c] | 0.72(0.73)[c] |
| $\beta^+$ | 2.52 | 0.07 | 0.07 | 0.15 |
| | 3.0–6.0 | 0.49 | 0.50 | 0.51 |
| | > 6.0 | ? | 0.03 | 0.10 |

[a)] The experimental $B(\mathrm{GT}^-)$ and $B(\mathrm{GT}^+)$ strengths from [And 85] and [Alf 91].

[b)] The $B(\mathrm{GT})$ in the experimental background in the region of $4.5 \le E_m \le 14.5$MeV [And 85].

[c)] The first number is the strength in the single strongest T=4 state whereas the number in the bracket includes the additional strength from small states ±500 keV on either side of the strongest state.

For the broad peak between 4.5 ~ 14.5 MeV, the minimum experimental value of 8.61 corresponds to the spectrum in Figure 2.3(c). An additional amount of 2.86 was estimated to be in the background not shown in Figure 2.3(c) [And 85].

The theoretical and experimental shapes are qualitatively the same as well as the $B(\mathrm{GT}^-)$ strength values themselves (see Table 2.1). But quantitatively there are some interesting differences which indicate a preference for the MSOBEP over the MH interaction. In the pure j-j coupling model, the first $1^+$ excited state in $^{48}$Sc can be understood as a $(\pi f_{7/2} \nu f_{7/2}{}^{-1})$ particle-hole configuration. The theoretical calculation based on the MSOBEP interaction and the experimental data are both in good agreement with this simple picture. But for the MH interaction, this particle-hole state is the second $1^+$ excited state located at 3.13 MeV. The first $1^+$ of $^{48}$Sc in the MH calculation has a negligibly small $B(\mathrm{GT}^-)$ value. This state, however,

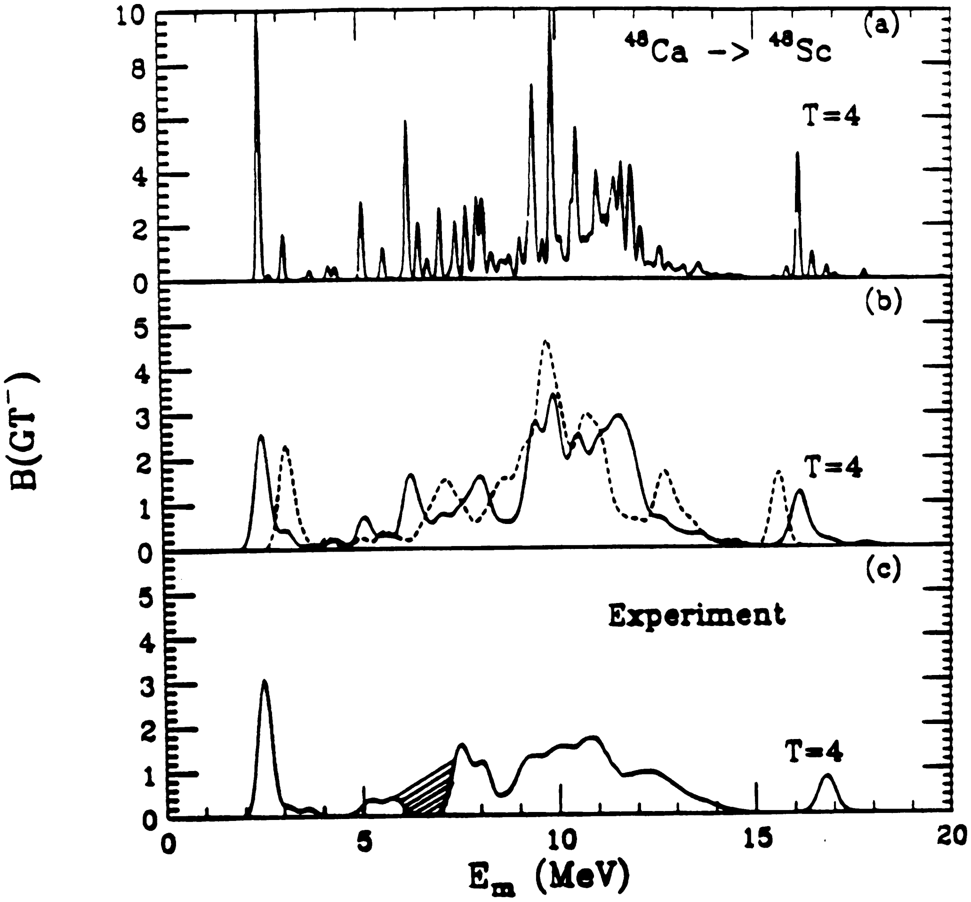

Figure 2.3: The $B(\mathrm{GT}^-)$ spectra for ${}^{48}\mathrm{Ca}\rightarrow{}^{48}\mathrm{Sc}$. The spectrum with FWHM = 100 keV obtained with the MSOBEP interaction is shown in (a). The spectra with FWHM = 400 keV obtained with the MSOBEP (solid line) and MH interaction (dashed line ) are shown in (b). The effective operator defined in Eq.(2.1) is employed in our calculations. The experimental $B(\mathrm{GT}^-)$ from [And 85] and B.D. Anderson (private communication) is presented in (c). The hatched area indicates the uncertainty resulting from subtracting the Fermi strength in the $0^+$(T=4) state at 6.8 MeV.

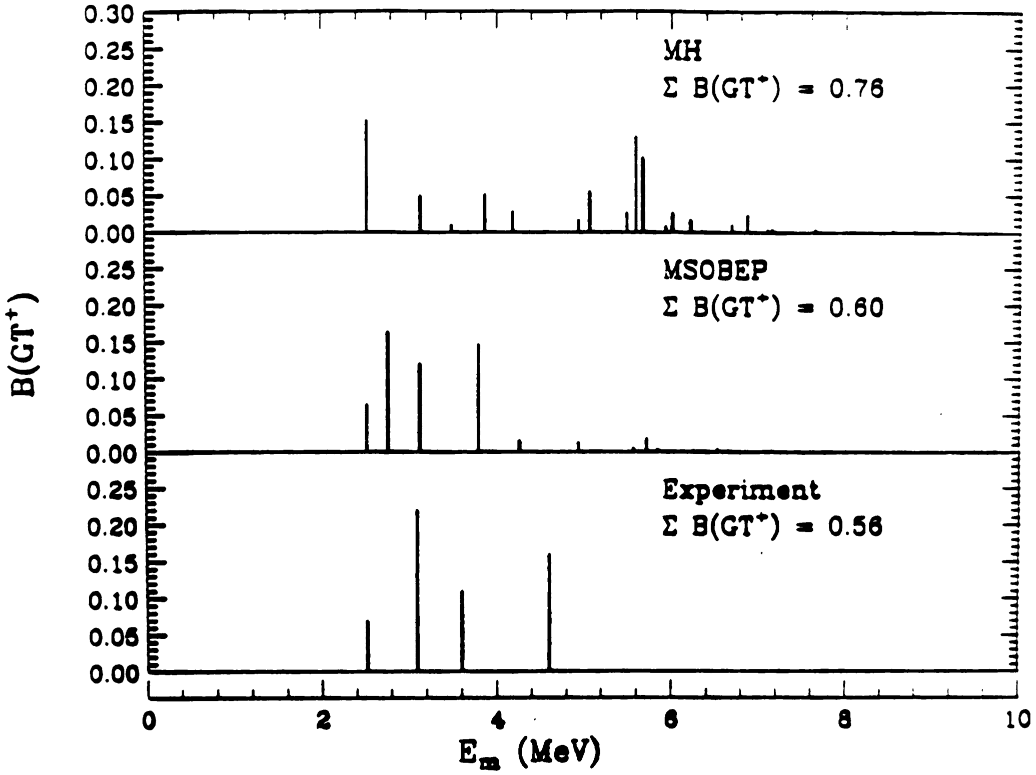

Figure 2.4: The $B(\mathrm{GT}^+)$ values for $^{48}$Ti →$^{48}$Sc. The experimental values from [Alf 91] are compared to the results obtained with the MSOBEP and MH interactions. The effective operator defined in Eq. (2.1) is employed in our calculations.

has a relatively large overlap with $^{46}$Ca plus a deuteron-cluster configuration, which explains why the state comes low in energy.

The total $B(\mathrm{GT}^-)$ strengths in T=4 states are 0.78 and 0.77 for the MSOBEP and MH interactions, respectively. For the MSOBEP interaction, only $B(\mathrm{GT}^-)$=0.42 contributes to the single state at 16.1 MeV, the rest is spread between 15 $\sim$ 20 MeV. ( see Figure 2a ). But for the MH interaction, most of the $B(\mathrm{GT}^-)$ strength (0.72) is in a single state at 15.4 MeV. Thus comparison with experiment again favors the MSOBEP interaction ( see Table 2.1 ).

The $\beta^+$ strength distribution and total strengths for theory and experiment [Alf 91] are compared in Figure 2.4 and in Table 2.1. There is the possibility for $B(\mathrm{GT}^+)$ strength above 6 MeV in the data [Alf 91] not shown in Figure 2.4. We see that the $\beta^+$ spectrum and $\sum B(\mathrm{GT}^+)$ are strongly dependent on the effective interactions. The spectrum for the MSOBEP interaction is in best agreement with the experiment, especially for the first state (see Table 2.1).

The calculated $M_{\mathrm{GT}}^{2\nu}$ values are presented in Table 2.2, and compared with previous calculations. We have modified the results from previous calculation to take into account the effective operator of Eq. (2.2). We note that the value of $< E_m >$=5.86 MeV assumed by Haxton is too large in agreement with the conclusion of [Tsu 84]. We also note the excellent agreement between our result with the MH interaction and the result obtained with the new method of Ogawa and Horie [Oga 89] who also used the MH interaction. This new method implicitly takes into account the spectrum of intermediate states exactly in the full basis. But it does not produce the explicit intermediate state spectrum which was important for the $\beta^-$ and $\beta^+$ comparisons made above. Also we note that the results obtained with the MSOBEP and MH interactions are not very different, indicating the relative stability of the calculation

Table 2.2: Comparison of the nuclear matrix elements $B(cls)$ and $M^{2\nu}_{\mathrm{GT}}$, the average excited energy $< E_m >$ and half life $T_{1/2}$. The shell-model space configurations are described by $f^{8-n}_{7/2}(p_{3/2}f_{5/2}p_{1/2})^n$ with n=0 to $\mathrm{n}_{max}$ for the fp shell referring to the initial(i), intermediate(m) and final(f) states.

| Reference | Interaction | | $\mathrm{n}_{max}$ | | $B(cls)$ | $M^{2\nu}_{\mathrm{GT}}$ | $< E_m >$ | $T_{1/2}$ |
|---|---|---|---|---|---|---|---|---|
| | | i | m | f | | $(\mathrm{MeV})^{-1}$ | (MeV) | $(10^{19}\mathrm{yr})$ |
| Experiment | | | | | | | | $> 3.6$ |
| present | MSOBEP | 4 | 5 | 4 | 0.204 | 0.070 | 1.06 | 1.9 |
| present | MH | 4 | 5 | 4 | 0.213 | 0.055 | 2.01 | 3.0 |
| Oga89 [a] | MH | 8 | 8 | 8 | | 0.053 | | 3.3 |
| Hax84 [a] | KB | 8 | | 4 | 0.266 | | | 7.2[b](1.1[c]) |
| Tsu84 [a] | MH | 2 | 2 | 2 | 0.278 | 0.073 | 1.94 | 1.7 |
| Zam82 [a] | MBZ | 0 | | 0 | 0.216 | | | |
| Sko83 [a] | KB | 0 | | 0 | 0.150 | | | |

[a] Modified by taking into account the effective operator in Eq.(2).

[b] Based on an assumed $< E_m >= 5.86$ MeV.

[c] Based on the exact $< E_m >= 1.06$ MeV.

with respect to reasonable variations in the interaction.

There are several reasons why $M^{2\nu}_{\mathrm{GT}}$ in the $2\nu\beta\beta$ decay of $^{48}$Ca is relatively small. The energy region of the strongest $B(\mathrm{GT}^-)$ strength (6∼10 MeV) is mismatched from the region of strongest $B(\mathrm{GT}^+)$ strength (2.52∼6 MeV ). Also there is a systematic cancellation between the $M^m_{\mathrm{GT}}$ in the low and the high energy part (see Figure 2.2). The qualitative reason for this behaviour can be understood as follows. In the simple j-j coupling model where the initial and final states are pure $f_{7/2}$ configurations, the only partitions for the intermediate $1^+$ states which can be reached by $\beta^-$ and $\beta^+$ transition are A($\pi f_{7/2}\nu f^{-1}_{7/2}$), B($\pi f_{5/2}\nu f^{-1}_{7/2}$) and C($\pi f_{7/2}\nu f_{5/2}\nu f^{-2}_{7/2}$). $\beta^-$ transitions can go to A or B and $\beta^+$ transitions can go to A or C. Thus the $\beta\beta$ transition can only go through A. These partitions will be mixed in the physical system, and in particular

Table 2.3: The first ten $B(\mathrm{GT}^-)$, $B(\mathrm{GT}^+)$ and $\mathrm{M}_{GT}^m$ values obtained with the MSOBEP interaction

| $E_m$ | $(< 1_m^+ \|\| \tilde{\sigma} t^- \|\| 0_i^+ >)^2$ | $(< 1_m^+ \|\| \tilde{\sigma} t^+ \|\| 0_f^+ >)^2$ | $\frac{<0_f^+ \|\| \tilde{\sigma} t^- \|\| 1_m^+><1_m^+ \|\| \tilde{\sigma} t^- \|\| 0_i^+>}{E_m+E_0}$ |
|---|---|---|---|
| 2.520 | 1.102 | 0.065 | 0.061 |
| 2.759 | 0.022 | 0.163 | -0.013 |
| 3.122 | 0.180 | 0.120 | 0.030 |
| 3.620 | 0.010 | 0.000 | 0.000 |
| 3.789 | 0.037 | 0.146 | 0.013 |
| 4.257 | 0.053 | 0.015 | 0.005 |
| 4.425 | 0.048 | 0.000 | 0.000 |
| 4.934 | 0.002 | 0.014 | -0.001 |
| 5.104 | 0.305 | 0.001 | -0.002 |
| 5.568 | 0.006 | 0.006 | 0.001 |

mixing of B and C will lead to two states $|1_1^+ >= \alpha|B> + \beta|C>$ and $|1_2^+ >= \beta|B> - \alpha|C>$, which can both be reached by $\beta^-$ and $\beta^+$ transitions. The numerator of the $\beta\beta$ matrix element will then have the form $< 0_f^+||\sigma t^-||1_1^+ >< 1_1^+||\sigma t^-||0_i^+ > + < 0_f^+||\sigma t^-||1_2^+ >< |1_2^+||\sigma t^-||0_i^+ >= \alpha\beta < 0_f^+||\sigma t^-||C >< B||\sigma t^-||0_i^+ > -\alpha\beta < 0_f^+||\sigma t^-||C >< B||\sigma t^-||0_i^+ >$. Thus we find two $\beta\beta$ routes each of which is nonzero but differing in sign so that they cancel. Mixing of B and C into A is important in modifying the $\beta\beta$ strength through the lowest $1^+$ state relative to pure j-j coupling. This aspect of the $\beta\beta$ strength function shows up qualitatively in all of our calculations (see Figure 2.2). And it is remarkable in our most complete calculations with the MSOBEP interaction that the total $M_{\mathrm{GT}}^{2\nu}$ matrix element(0.070) is nearly exactly equal to the contribution from the first state alone(0.061).

We give the $B(\mathrm{GT}^-)$, $B(\mathrm{GT}^+)$ and $M_{\mathrm{GT}}(E_m)$ values for the first ten eigenstates in Table 2.3 obtained with the MSOBEP interaction. They are the main positive contributions to $M_{\mathrm{GT}}^{2\nu}$. The states with small $B(\mathrm{GT}^-)$ and $B(\mathrm{GT}^+)$ strengths will be missed in the experiment because of the finite resolution. Consequently some states will be seen in (p,n) and not (n,p) and visa versa. Nevertheless, the results given in Table 2.3 are in excellent agreement with the analysis of [Alf 91] based entirely on experimental data.

To study the effects of truncation, now we discuss the several cases of interest shown in Table 2.4. The $M^{2\nu}_{\mathrm{GT}}$ for $^{48}$Ca in more highly truncated fp-shell spaces are presented, where only the MSOBEP interaction is used. One of them is obtained from the truncation ($n_{max}$ =2) for $^{48}$Ca, $^{48}$Sc and $^{48}$Ti used by Tsuboi et al with the MH interaction. (We note that at this level of truncation the MH interaction gives the lowest $1^+$ state with a structure as expected in the simple picture discussed above.) The $B(\mathrm{GT})$ strengths from this space will not give the sum rule (Eq. (2.1)) because the intermediate state is incomplete. However, The $M^{2\nu}_{\mathrm{GT}}$ is changed very little when $n_{max}$ =3 is allowed for $^{48}$Sc. This indicates that the sum rule violation is not so important for $M^{2\nu}_{\mathrm{GT}}$. From the Table 2.4, we find that the $M^{2\nu}_{\mathrm{GT}}$ in the highly truncated spaces differ significantly from the one in our expanded basis. The $M_{\mathrm{GT}}(E_m)$ spectra in Figure 2.2(b) show these differences in detail.

To test the accuracy of our truncation, we compare the calculations for $M^{2\nu}_{\mathrm{GT}}$ values in the space we used and in the full-basis for $^{22}$O in the sd shell and $^{46}$Ca in the fp shell. These comparisons indicate that the truncation we used is a good approximation to the full space results. We may expect that the present $M^{2\nu}_{\mathrm{GT}}$ value of $^{48}$Ca will be reduced a further 5$\sim$10% if the full-basis in the fp shell is employed. (Compared with these more complete calculations, a previous estimate [BAB 85] of the extrapolation from the $n_{max}$ =2 space to the full-space value for $M^{2\nu}_{\mathrm{GT}}$ is found to be in error by about a factor of two.)

Beyond the fp shell model space there are several processes which we should consider. The role of $\Delta$-isobar admixtures have been investigated in previous work

Table 2.4: Comparison of $M^{2\nu}_{\rm GT}$ in different truncations. The shell-model space configurations are described by $f^{8-n}_{7/2}(p_{3/2}f_{5/2}p_{1/2})^n$ for the fp shell and $d^{6-n}_{5/2}(s_{1/2}d_{3/2})^n$ for the sd shell referring to the initial(i), intermediate(m) and final(f) states with n=0 to $n_{max}$. The full-basis means $n_{max}$=8 in the fp shell or $n_{max}$=6 in the sd shell. The MSOBEP interaction was used for $^{48}$Ca and $^{46}$Ca and the interaction [Wil 84] was used for $^{22}$O.

| | $n_{max}$ | | | $M^{2\nu}_{\rm GT}$ |
|---|---|---|---|---|
| | i | m | f | |
| $^{48}\mathrm{Ca} \rightarrow {}^{48}\mathrm{Ti}$ | 0 | 0 | 0 | 0.124 |
| | 0 | 1 | 0 | 0.143 |
| | 1 | 2 | 1 | 0.049 |
| | 2 | 2 | 2 | 0.086 |
| | 2 | 3 | 2 | 0.088 |
| | 4 | 5 | 4 | 0.070 |
| $^{46}\mathrm{Ca} \rightarrow {}^{46}\mathrm{Ti}$ | 4 | 5 | 4 | 0.134 |
| | Full | Full | Full | 0.127 |
| $^{22}\mathrm{O} \rightarrow {}^{22}\mathrm{Ne}$ | 2 | 2 | 2 | 0.077 |
| | 4 | 5 | 4 | 0.041 |
| | Full | Full | Full | 0.039 |

[Goo 81, Boh 81, Ari 87, Tow 87], The contribution from the direct excitation of the $\Delta$-isobar nucleon-hole configuration, for which the excitation energy is about 300 MeV, is negligible [Zam 82, Gro 86] because of the cancellation between $\beta^+$ and $\beta^-$ and because of the large energy denominator in Eq. (2.3). The $\Delta$-isobar admixtures in the low-lying states are already approximately taken into account in our calculation in the effective operator $\tilde{\sigma} t$ of Eq. (2.2) as well as in the effective interaction. In addition, 2p2h admixtures beyond the fp shell can lead to $B(\mathrm{GT})$ strength at higher excitation [Ber 82]. The possible strength seen experimentally in the background above 6 MeV in $\beta^+$ and 15 MeV in $\beta^-$ may be due to these 2p2h admixtures. The effect of these 2p2h admixtures in the low-lying states are also approximately taken account in the effective operator and effective interaction. The contribution from the direct excitation of the 2p2h configurations may again be small because of cancellation and large energy denominator but should be investigated further.

## 2.4 Summary

In summary, we have studied the $2\nu\beta\beta$ decay of $^{48}$Ca in a large basis shell-model space. An effective Gamow-Teller operator $\tilde{\sigma}t$ is employed, which well describes $B(\mathrm{GT}^-)$ and $B(\mathrm{GT}^+)$ behaviour in the energy region (2.5∼15.0 MeV). Of two effective interactions we have employed, new MSOBEP interaction seems to be a better interaction for the $\beta^-$ and $\beta^+$ spectra. With this interaction we predict the $2\nu\beta\beta$ decay matrix element of $^{48}$Ca is $M^{2\nu}_{\mathrm{GT}}$=0.070 giving a half life $T_{1/2}$= $1.9\times10^{19}$yr, which differs by nearly a factor of two from the experimental limit [Bar 70] of $T_{1/2} > 3.6\times10^{19}$ yr. We believe that the most important aspect of these calculations which cannot be directly tested by the (p,n) and (n,p) experiments is the amount of strength in the (n,p) $\beta^+$ spectrum above 5 MeV in excitation. This is because there is a large uncertainty in the amount of Gamow-Teller strength in the background above this energy. The Gamow-Teller strength in this region may be sensitive to further refinements in the effective interaction as well as to direct excitation of 2p2h states, and should be studied further. In addition, we believe that it is important to confirm and improve upon the present experimental limit.

# Chapter 3

# Comparison between pnQRPA and Shell Model I: $\beta^+$ Decay

## 3.1 Introduction

The Gamow-Teller transitions are of interest in their own right in addition to their role as virtual transitions in $\beta\beta$ decay. The transition strengths of $\beta^+$ decay in heavy nuclei are understood poorly [Wap 71, Kle 85].

In recent years, the pnQRPA theory has been employed to calculate the $\beta$ Gamow-Teller transitions in heavy nuclei [Cha 83, Sub 88]. In the pnQRPA, the proton-neutron correlation plays an important role. This equation contains two types of interactions, particle-particle and particle-hole, but the former was neglected in early calculations [Hal 67]. Recently several authors have investigated the particle-particle interaction term which was reintroduced by Cha [Cha 83], and found that the $\beta^+$ transition matrix elements are sensitive to this term [Cha 83, Sub 88].

As mentioned in Chapter 1, the pnQRPA is an approximation model, so there may be some correlations that could be important in $\beta^+$ decay which are not included in the pnQRPA. Therefore it is very important to examine the validity and accuracy of the pnQRPA approach. These tests can be achieved by making a comparison of the pnQRPA and full-basis shell-model calculations in the nuclear mass regions where the full-basis shell-model calculations are possible. The full-basis shell-model calculations include all types of the correlations within a major shell. We believe that such a comparison is meaningful if and only if the pnQRPA and shell-model calculations are performed in the same model space and use the same effective interaction.

This kind of comparison has been made by Lauritzen [Lau 88] for several sd shell nuclei, Brown and Zhao [Brz 89] for $^{28}$Mg and Civitarese, et.al. [Civ 91] for $^{26}$Mg. Lauritzen and Brown and Zhao have concluded that the pnQRPA does not include some important correlations in $\beta^+$ decay and fails to reproduce the shell-model results. Civitarese contradicts this conclusion. However, their comparisons only concentrate on total $B(\mathrm{GT}^+)$ and strength distributions, and relative contributions of the various single-particle state in Gamow-Teller transitions are not considered.

In this Chapter, a self-consistent BCS-pnQRPA is developed in sections 3.2.1 and 3.2.2. In section 3.2.4, we introduce the coherent one-body transition density (COBTD) and coherent transition matrix element (CTME), which can describe the single-particle state effects in one-body transitions. Our comparison between the pnQRPA and shell model is presented in section 3.3, where we investigate total $B(\mathrm{GT}^+)$ strengths, strength distributions and COBTD and CTME. In our study, $^{46}$Ti $\beta^+$ decay is the example. The model space is the full fp shell and the effective interaction used is MSOBEP [Ric 91] (see Chapter 2). We give the summary and conclusions in section 3.4.

## 3.2 Formalism

### 3.2.1 pnQRPA equations

We start with the equation of motion [Row 70, Rin 80], where the excited eigenstates $|\nu>$ are constructed from the phonon creation operator $Q_\nu^\dagger$ which is defined by

$$|\nu>= Q_\nu^\dagger|0>, \quad \text{and } Q_\nu|0>= 0, \quad \text{for all } \nu \tag{3.1}$$

where $|\nu>$ and $|0>$ are the excited eigenstates and the physical ground state. They satisfy the Schrödinger equation,

$$H|\nu>= E_\nu|\nu> \text{ and } H|0>= E_0|0>. \tag{3.2}$$

Then one obtains the following equation of motion from the above relations;

$$[H, Q_\nu^\dagger]|0>= (E_\nu - E_0)Q_\nu^\dagger|0>. \tag{3.3}$$

Multiplying from the left with an arbitrary state of the form $<0|\delta Q_\nu$, we get

$$<0|[\delta Q_\nu, [H, Q_\nu^\dagger]]|0>= \hbar\omega <0|[\delta Q_\nu, Q_\nu^\dagger]|0>, \tag{3.4}$$

where $\hbar\omega = E_\nu - E_0$.

In order to obtain the pnQRPA equation, the phonon creation operators in the angular momentum coupled representation are written as [Hal 67, Cha 83, Lau 88],

$$\begin{aligned}
Q_\nu^\dagger(J, M) &= \sum_{p,n}(X_\nu^{pn}\mathcal{A}_{\rm pn}^\dagger(pn, JM) - Y_\nu^{pn}\tilde{\mathcal{A}}_{\rm pn}(pn, JM)), && (3.5)\\
\mathcal{A}_{\rm pn}^\dagger(pn, JM) &= \sum_{m_p,m_n} <j_pm_pj_nm_n|JM> c_{j_pm_p}^\dagger c_{j_nm_n}^\dagger, && (3.6)\\
\tilde{\mathcal{A}}_{\rm pn}(pn, JM) &= (-1)^{J+M}\mathcal{A}_{\rm pn}(pn, J-M), && (3.7)
\end{aligned}$$

where $c^{\dagger}_{j_{p(n)}}$ is the quasiproton (quasineutron) creation operator. In terms of the spherical shell-model states, the particle and quasiparticle creation and annihilation operators are related by the Bogoliubov transformation, e.g. for proton

$$c^{+}_{j_p m_p} = u_p a^{+}_{j_p m_p} + (-)^{j_p + m_p} v_p a_{j_p - m_p}, \tag{3.8}$$

where $u_p^2 + v_p^2 = 1$, and $a^{\dagger}_{j_p}(a_{j_p})$ is the proton creation (destruction) operator for the single-particle state. $v_p^2$ turns out to be the occupation probability. The eigenvalue $\hbar\omega$ and the forward- and backward- going amplitudes $X$ and $Y$ are obtained by solving the pnQRPA equation

$$\begin{pmatrix} A & B \\ -B^* & -A^* \end{pmatrix} \begin{pmatrix} X \\ Y \end{pmatrix} = \hbar\omega \begin{pmatrix} X \\ Y \end{pmatrix}, \tag{3.9}$$

with the orthogonality and normalization relation

$$\sum_{pn} [X^{pn}_{\nu} X^{pn}_{\nu'} - Y^{pn}_{\nu} Y^{pn}_{\nu'}] = \delta_{\nu\nu'}. \tag{3.10}$$

The matrix elements A and B are explicitly given by [Hal 67, Cha 83, Lau 88, Sub 88]

$$\begin{aligned} A^J_{pnp'n'} &= \, < \mathrm{QRPA}|[\mathcal{A}_{\mathrm{pn}}(pn, JM), [H, \mathcal{A}^{\dagger}_{\mathrm{pn}}(p'n', JM)]]|\mathrm{QRPA} > \\ &\simeq \, < \mathrm{BCS}|[\mathcal{A}_{\mathrm{pn}}(pn, JM), [H, \mathcal{A}^{\dagger}_{\mathrm{pn}}(p'n', JM)]]|\mathrm{BCS} > \\ &= (E_p + E_n)\delta_{pp'}\delta_{nn'} + (H^{\mathrm{pn}}_{22})^J_{pnp'n'}, \end{aligned} \tag{3.11}$$

$$\begin{aligned} B^J_{pnp'n'} &= \, < \mathrm{QRPA}|[\mathcal{A}_{\mathrm{pn}}(pn, JM), [H, \tilde{\mathcal{A}}_{\mathrm{pn}}(p'n', JM)]]|\mathrm{QRPA} > \\ &\simeq \, < \mathrm{BCS}|[\mathcal{A}_{\mathrm{pn}}(pn, JM), [H, \tilde{\mathcal{A}}_{\mathrm{pn}}(p'n', JM)]]|\mathrm{BCS} > \\ &= -(G^{\mathrm{pn}})^J_{pnp'n'}, \end{aligned} \tag{3.12}$$

with

$$\begin{aligned} (H^{\mathrm{pn}}_{22})^J_{pnp'n'} &= g_{pp} V^J_{pnp'n'}(u_p u_n u_{p'} u_{n'} + v_p v_n v_{p'} v_{n'}) \\ &\quad + g_{ph} W^J_{pnp'n'}(u_p v_n u_{p'} v_{n'} + v_p u_n v_{p'} u_{n'}), \end{aligned} \tag{3.13}$$

$$\begin{aligned}(G^{\mathrm{pn}})^J_{pnp'n'} &= g_{pp}V^J_{pnp'n'}(u_pu_nv_{p'}v_{n'}+v_pv_nu_{p'}u_{n'}) \\ &\quad -g_{ph}W^J_{pnp'n'}(v_pu_nu_{p'}v_{n'}+u_pv_nv_{p'}u_{n'}).\end{aligned} \tag{3.14}$$

where $|\mathrm{QRPA}>$ is the QRPA ground state defined in Appendix A. The relation between the QRPA and pnQRPA is discussed in Appendix B. The quasiproton and quasineutron energies $E_p$ and $E_n$ and occupation factors $u, v$ are obtained by solving the BCS equation in section 3.2.2 or Chapter 5. The matrix elements of the particle-particle (V) and particle-hole (W) interaction are related by Pandya transformation,

$$W^J_{pn,p'n'} = -(-1)^{j_p+j_n+j_{p'}+j_{n'}}\sum_{J'}(2J'+1)\left\{\begin{array}{ccc} j_p & j_n & J \\ j'_p & j'_n & J'\end{array}\right\}V^{J'}_{pn',p'n}. \tag{3.15}$$

In order to discuss the results as a function of the strength associated with each part of the interaction, the multiplicative factors $g_{ph}$ and $g_{pp}$ are conventionally introduced for the particle-particle and particle-hole, respectively. They are both equal to one in the standard pnQRPA theory.

The charge-exchange transition matrix elements of the Gamow-Teller operator between the ground state $|0^+_i>$ and the excited state $|1^+_\nu>$ are given by

$$B(\mathrm{GT}) = \frac{1}{2J_i+1}(<1^+_\nu||\sigma t||0^+_i>)^2, \tag{3.16}$$

where $J_i = 0$. We denote

$$M_\nu(\mathrm{GT}) =< 1^+_\nu||\sigma t||0^+_i> , \tag{3.17}$$

where $\sigma$ is the Pauli spin operator. The isospin operator $t$ can be the raising or lowering operator, $t^+$ or $t^-$, which are corresponding to $\beta^+$ and $\beta^-$ Gamow-Teller transitions. In the pnQRPA, we can obtain

$$\begin{aligned} M_\nu(\mathrm{GT}^-) &= \sum_{pn} <p||\sigma||n>(X^{pn}_\nu u_pv_n + Y^{pn}_\nu v_pu_n), & (3.18)\\ M_\nu(\mathrm{GT}^+) &= -\sum_{pn} <p||\sigma||n>(X^{pn}_\nu v_pu_n + Y^{pn}_\nu u_pv_n). & (3.19)\end{aligned}$$

The above equations for $M_\nu(\mathrm{GT})$ in the pnQRPA can be rewritten as,

$$M_\nu(\mathrm{GT}) = \sum_{pn} < p||\sigma||n > \mathrm{OBTD}(p,n,\nu)_{\mathrm{QRPA}}, \tag{3.20}$$

where the $\mathrm{OBTD}(p,n,\nu)_{\mathrm{QRPA}}$ is a one-body transition density of the pnQRPA given by the Eq. (3.18) or Eq. (3.19) explicitly.

### 3.2.2 BCS equations

The BCS theory will be reviewed and extended in Chapter 5. Here we just present the standard BCS formalism for the proton-neutron system. In the BCS, the quasiproton energies $E_p$, occupation probabilities $v_p^2$ and pairing gaps $\Delta_p$ are given by

$$E_p = \sqrt{(\varepsilon_p - \lambda_\pi)^2 + \Delta_p^2}, \tag{3.21}$$

$$v_p^2 = \frac{1}{2}(1 - \frac{\varepsilon_p - \lambda_\pi}{\sqrt{(\varepsilon_p - \lambda_\pi)^2 + \Delta_p^2}}), \tag{3.22}$$

$$\Delta_p = -\sum_{p'} \sqrt{\frac{2j'_p + 1}{2j_p + 1}} u_{p'} v_{p'} V^{J=0}_{pp,p'p'}, \tag{3.23}$$

where $\lambda_\pi$ is the proton Fermi energy, $\varepsilon_p$ and $V_{pp,p'p'}$ are the single proton energy and proton two-body interaction, respectively. The above equations can be solved using the constraint for the total proton number

$$N_\pi = \sum_p (2j_p + 1) v_p^2, \tag{3.24}$$

to determine the constant $\lambda_\pi$. A similar set of the equations can be solved for neutrons. The single proton energies $\varepsilon_p$ are related to the bare single-particle proton energies $\varepsilon_p^0$ at the closed shell by addition of the rearrangement terms $\Gamma_p$

$$\varepsilon_p = \varepsilon_p^0 + \Gamma_p, \tag{3.25}$$

where

$$\Gamma_p = \frac{1}{2j_p+1}\sum_{p'}(1+\delta_{pp'})v_{p'}^2\sum_J(2J+1)V^J_{pp',pp'}$$

$$+\frac{1}{(2j_p+1)}\sum_{n'}v_{n'}^2\sum_J(2J+1)V^J_{pn',pn'}. \tag{3.26}$$

The first term refers to like particle correction and the second term to unlike particle correction. The rearrangement term for $\varepsilon_n$ has the same form but with the p/n indices interchange. Eq. (3.26) can be verified by simple shell-model calculations. The BCS equations (3.21-3.24) plus the rearrangement terms can be solved iteratively.

The Eqs. (3.9 − 3.14,3.21 − 3.26) are called the self-consistent BCS-pnQRPA equations. The *self-consistent* means that the input ingredients in the BCS-pnQRPA are consistent with those in the shell model, namely, the bare single particle energies $\varepsilon_j^0$ at the closed shell and two-body interaction matrix elements $V^J_{ijkl}$.

### 3.2.3 $B$(GT) in shell-model calculations

In the shell-model calculation, the Gamow-Teller strength is equal to the product of one-body transition density and single particle matrix element [Bru 77], and the matrix element $M_\nu$ in Eq. (3.17) is expressed by

$$M_\nu(\mathrm{GT}) = \sum_{pn} < p||\sigma||n > \mathrm{OBTD}(p,n,\nu)_{\mathrm{SM}}, \tag{3.27}$$

where

$$\mathrm{OBTD}(p,n,\nu)_{\mathrm{SM}} =< 1^+_\nu||\frac{[a^+_p\otimes\tilde{a}_n]^{\Delta J}}{\sqrt{2\Delta J+1}}||0^+_i > , \tag{3.28}$$

where $\Delta J$ = 1. The one-body transition density describes the shell configuration effects when a proton in $j_p$ orbit transfers to a neutron in $j_n$ orbit. In this work,

$\mathrm{OBTD}(p,n,\nu)_{\mathrm{SM}}$ is calculated from the OXBASH shell-model code [Etc 85]. The proton (neutron) occupation probabilities in the shell model are given by

$$v^2_{p(n)}(\mathrm{SM}) = \frac{<\mathrm{SM}|a^+_{p(n)}a_{p(n)}|\mathrm{SM}>}{2j_{p(n)}+1}, \tag{3.29}$$

where $|\mathrm{SM}>$ denotes the shell-model wave function.

### 3.2.4 The coherent one-body transition density

The $B(\mathrm{GT})$ spectrum itself lacks information about the single-particle state contributions in the charge-exchange process, because we sum over all single-particle state components $p, n$ in Eqs.(3.18–3.20) for the pnQRPA and Eq.(3.27) for the shell model. Therefore, we introduce two quantities which can describe such single-particle state effects in the Gamow-Teller transition. We define the *coherent one-body transition density* (COBTD) as

$$\mathrm{COBTD}(p,n) = \frac{1}{\sqrt{\sum_\nu B(\mathrm{GT})}}\sum_\nu M_\nu(\mathrm{GT})\mathrm{OBTD}(p,n,\nu), \tag{3.30}$$

where $M_\nu(\mathrm{GT})$ is given by Eq. (3.17). The OBTD is given by Eq. (3.28) and (3.20) for the shell model and the pnQRPA, respectively. Also the *coherent transition matrix element* (CTME) is defined by

$$\mathrm{CTME}(p,n) =< p||\sigma||n > \mathrm{COBTD}(p,n). \tag{3.31}$$

The COBTD and CTME are a function of the single-particle state components. All final states($\nu$) are summed up in Eq. (3.30). The relation between the $B(\mathrm{GT})$ and CTME is given by

$$\{\sum_{p,n}\mathrm{CTME}(p,n)\}^2 = \sum_\nu B(\mathrm{GT}). \tag{3.32}$$

In Appendix D, we will discuss the COBTD in detail.

Table 3.1: $^{46}$Ti: Proton and neutron: single particle energies $\varepsilon_i$ (MeV), gap parameters $\Delta_i$ (MeV) and occupation probabilities $v_i^2$ from BCS and the shell-model $E_i$(SM) and $v_i^2$(SM) . The Fermi energies obtained from the BCS calculation are −12.968 MeV and −10.868 MeV for proton and neutron, respectively.

| level | $\varepsilon_i$ | $\Delta_i$ | $v_i^2$ | $E_i$(BCS) | $E_i$(SM) | $v_i^2$(SM) |
|---|---|---|---|---|---|---|
| $\pi f_{7/2}$ | −12.234 | 1.206 | 0.239 | 1.412 | 1.412 | 0.187 |
| $\pi p_{3/2}$ | −8.194 | 0.911 | 0.009 | 4.861 | 4.305 | 0.078 |
| $\pi f_{5/2}$ | −5.739 | 1.314 | 0.008 | 7.347 | 6.845 | 0.022 |
| $\pi p_{1/2}$ | −5.994 | 0.874 | 0.004 | 7.028 | 6.431 | 0.031 |
| | | | | | | |
| $\nu f_{7/2}$ | − 10.809 | 1.447 | 0.480 | 1.448 | 1.414 | 0.404 |
| $\nu p_{3/2}$ | −6.852 | 1.104 | 0.018 | 4.164 | 3.336 | 0.092 |
| $\nu f_{5/2}$ | −4.044 | 1.574 | 0.013 | 7.003 | 6.099 | 0.054 |
| $\nu p_{1/2}$ | −4.553 | 1.069 | 0.007 | 6.405 | 5.564 | 0.040 |

## 3.3 Calculations and Discussions

### 3.3.1 Comparison of pnQRPA and shell model

We have presented the self-consistent BCS-pnQRPA equations in section 3.2.1 and 3.2.2. In the BCS equation, the pairing gaps are state dependent and are self-consistently calculated. But in practice, when the pnQRPA equation is used in heavier nuclei or in the simple BCS calculations, the quasiparticle energies and occupation probabilities are not obtained in this way, but rather based on some empirical value for the pairing gap $\Delta$ ( often one which is independent of single-particle state ) and on some interpolated values for the effective single-particle energies.

The single-particle energies with addition of rearrangement terms, quasiparticle energies, pairing gaps and occupation probabilities of $^{46}$Ti are given in Table 3.1. The proton pairing gaps are almost 40 % less than those obtained from the empirical formula $\Delta_p = 12A^{-1/2}$, where $A$ is total nucleon number in the nucleus [Rin 80].

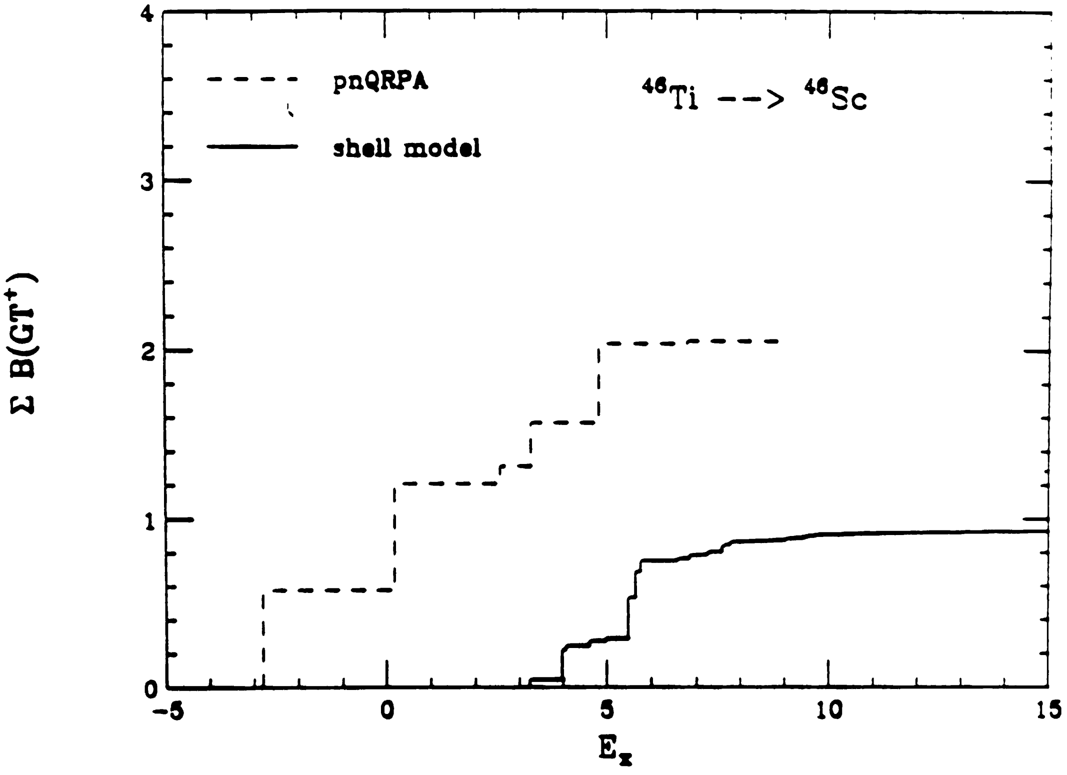

Figure 3.1: Summed Gamow-Teller strength for $^{46}$Ti →$^{46}$Sc. The solid line is the shell-model result while the dashed line is the pnQRPA result.

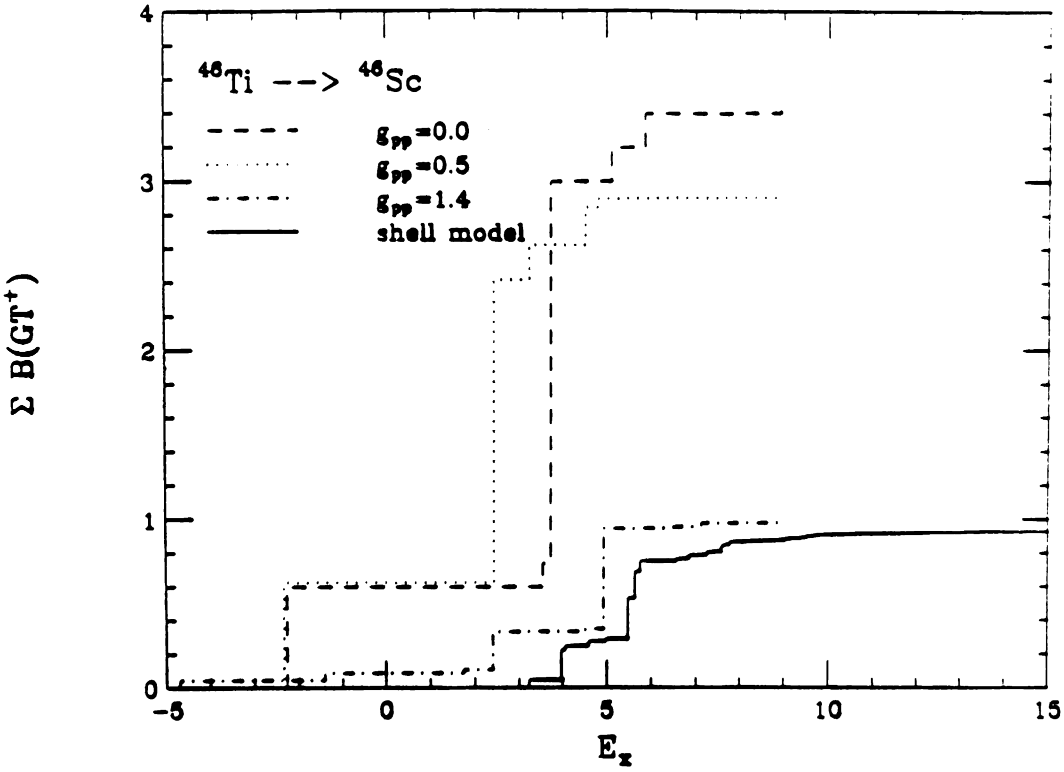

Figure 3.2: Summed Gamow-Teller strength for $^{46}$Ti $\rightarrow ^{46}$Sc with various particle-particle strength $g_{pp}$ where $g_{ph} = 1$.

We put these BCS parameters into the pnQRPA equation and obtain the pnQRPA $\beta^+$-decay spectrum. The full-basis shell-model calculation is carried out with the OXBASH code. The J-dimensions are 1514 and 2042 for the $^{46}$Ti ground state and the $^{46}$Sc $1^+$ excitations, respectively. Figure 3.1 presents the running sum $\sum B(\mathrm{GT}^+)$ as a function of the $^{46}$Sc $1^+$ excitation energy $\mathrm{E}_x$ corresponding to the $^{46}$Ti ground state. The running sum $\sum B(\mathrm{GT}^+)$ is defined by

$$\sum B(\mathrm{GT}^+) = \sum_{\nu=1}^{E_x} (< 1_\nu^+ || \sigma t^+ || 0_i^+ >)^2. \tag{3.33}$$

The pnQRPA and shell-model results are shown by dashed and solid lines, respectively. The Coulomb shift 7.586 MeV is taken into account [Bro 79].

We find that the pnQRPA calculation does not give sufficient suppression for the total $B(\mathrm{GT}^+)$. It overshoots by about 50 % compared to the shell-model result. The shapes of the two models are also different. The energies of the first excited state in the two models differs by about 6 MeV.

The coherent one-body transition densities and the coherent transition matrix elements defined by section 3.2.4 are given in Table 3.2 and Table 3.3 for the pnQRPA and shell model, (see columns (A) and (E)). There are significant difference between the two models. For example, the COBTD and CTME values in the pnQRPA and shell model have the opposite sign for the $f_{7/2} \rightarrow f_{7/2}$ and the $f_{5/2} \rightarrow f_{5/2}$.

Since the $B(\mathrm{GT}^+)$ strength are more sensitive to $g_{pp}$ than $g_{ph}$, we will set $g_{ph} = 1$ and discuss the dependence on $g_{pp}$. In Figure 3.2, the $B(\mathrm{GT}^+)$ spectra with various $g_{pp}$ values are presented. One can find the pnQRPA results are very sensitive to $g_{pp}$ values, which is in the agreement with the previous conclusions [Cha 83, Lau 88, Sub 88]. Especially, the strengths in the low-lying states decrease rapidly around the value $g_{pp} = 1$. The total shell-model $B(\mathrm{GT}^+)$ is reproduced by the pnQRPA with $g_{pp} = 1.4$,

Table 3.2: Comparison of the coherent one-body transition density (COBTD) obtained in the pnQRPA, modified pnQRPA and shell-model calculations of $^{46}$Ti.

(A): COBTD in the pnQRPA with BCS occupation and quasiparticle energies;
(B): COBTD in the pnQRPA with BCS occupation and SM quasiparticle energies;
(C): COBTD in the pnQRPA with SM occupation and BCS quasiparticle energies;
(D): COBTD in the pnQRPA with SM occupation and quasiparticle energies;
(E): COBTD in SM (shell-model).

| $j_p \to j_n$ | A | B | C | D | E |
|---|---|---|---|---|---|
| $f_{7/2} \to f_{7/2}$ | 0.034 | 0.019 | -0.005 | -0.031 | -0.096 |
| $f_{7/2} \to f_{5/2}$ | 0.443 | 0.448 | 0.310 | 0.315 | 0.386 |
| $p_{3/2} \to p_{3/2}$ | 0.002 | -0.001 | 0.075 | 0.072 | 0.006 |
| $p_{3/2} \to f_{5/2}$ | -0.001 | -0.001 | -0.006 | -0.010 | 0.017 |
| $p_{3/2} \to p_{1/2}$ | 0.005 | 0.003 | 0.087 | 0.088 | 0.060 |
| $f_{5/2} \to f_{7/2}$ | 0.088 | 0.099 | 0.091 | 0.109 | 0.086 |
| $f_{5/2} \to p_{3/2}$ | 0.001 | 0.002 | 0.006 | 0.009 | 0.010 |
| $f_{5/2} \to f_{5/2}$ | 0.001 | 0.003 | -0.007 | -0.005 | -0.011 |
| $p_{1/2} \to p_{3/2}$ | 0.003 | 0.005 | -0.012 | -0.006 | 0.009 |
| $p_{1/2} \to p_{1/2}$ | -0.001 | 0.000 | -0.012 | -0.013 | -0.003 |

Table 3.3: Comparison of the coherent transition matrix elements (CTME) obtained in the pnQRPA, modified pnQRPA and shell-model calculations of $^{46}$Ti. Labels (A), (B), (C), (D) and (E) are given by Table 3.2

| $j_p \rightarrow j_n$ | A | B | C | D | E |
|---|---|---|---|---|---|
| $f_{7/2} \rightarrow f_{7/2}$ | 0.108 | 0.062 | -0.017 | -0.099 | -0.308 |
| $f_{7/2} \rightarrow f_{5/2}$ | 1.641 | 1.661 | 1.149 | 1.167 | 1.431 |
| $p_{3/2} \rightarrow p_{3/2}$ | 0.005 | -0.002 | 0.195 | 0.186 | 0.014 |
| $p_{3/2} \rightarrow f_{5/2}$ | 0.000 | 0.000 | 0.000 | 0.000 | 0.000 |
| $p_{3/2} \rightarrow p_{1/2}$ | 0.011 | 0.006 | 0.200 | 0.202 | 0.139 |
| $f_{5/2} \rightarrow f_{7/2}$ | -0.325 | -0.366 | -0.338 | -0.403 | -0.319 |
| $f_{5/2} \rightarrow p_{3/2}$ | 0.000 | 0.000 | 0.000 | 0.000 | 0.000 |
| $f_{5/2} \rightarrow f_{5/2}$ | -0.002 | -0.005 | 0.014 | 0.010 | 0.024 |
| $p_{1/2} \rightarrow p_{3/2}$ | -0.006 | -0.011 | 0.027 | 0.013 | -0.020 |
| $p_{1/2} \rightarrow p_{1/2}$ | 0.000 | 0.000 | 0.010 | 0.011 | 0.002 |

but the shape of the strength distributions of two models are totally different.

When $g_{pp}$ increases up to a certain value, the lowest eigenvalue becomes the imaginary and the pnQRPA equation collapses. It means that the pnQRPA theory is no longer a valid model. Around this $g_{pp}$, the equation gives unrealistic large amplitudes $X$ and $Y$, and consequently presents an unphysical $B(\mathrm{GT}^+)$ strength.

### 3.3.2 Phenomenological improvements of pnQRPA

We now investigate various ways to understand and then improve the agreement between the pnQRPA and the full-basis shell model. First, we introduce shell-model quasiparticle energies. Since the BCS quasiparticle energies can be understood as the lowest excited energies of the odd nucleus [Row 70, Law 80], one may appropriately analyse the odd nucleus energy spectra in the shell-model calculations, and find those excited states which are qualitatively equivalent to the single quasiparticle $E_j$ excitations. The overlap method is employed to find these states [Etc 85]. For example, the shell-model quasineutron energies of $^{46}$Ti can be obtained as follows: the one-particle transfer amplitudes are calculated between the $^{46}$Ti ground state and the $^{47}$Ti excited states $J = 7/2^-$ (or $3/2^-$, $5/2^-$ and $1/2^-$). The eigenvalue of the state which has the largest overlap in one-particle transfer is considered as the shell-model quasineutron energy $E_{f7/2}$ (or $E_{p3/2}$, $E_{f5/2}$ and $E_{p1/2}$).

Possible improvements of the pnQRPA may be obtained by replacing the quasiparticle energies and occupation probabilities of the shell model to those of the BCS in the pnQRPA. The shell-model occupations of $^{46}$Ti ground state are evaluated with Eq. (3.29), where $|\mathrm{SM}>$ is the ground state wave function. The shell-model quasiproton and quasineutron energies are obtained by analysis of $^{46}$Ti isotopes and isotone in the shell-model calculations. These parameters are given in the Table 3.1. The modified models are called " hybrid " pnQRPA.

The calculations for three types of " hybrid " pnQRPA are shown in Figure 3.3. The dashed line is the pnQRPA with BCS occupations and shell-model quasiparticle energies. The dotted line is the pnQRPA with shell-model occupations and BCS quasiparticle energies. The dot-dashed line is the pnQRPA with shell-model occupations and quasiparticle energies. One finds that the total $B(\mathrm{GT}^+)$ strength is suppressed in the " hybrid " pnQRPA. That is 2.053 in the pnQRPA, 1.811 in the " hybrid " pnQRPA with the shell-model quasiparticle energies and the BCS occupation probabilities, 1.536 in the " hybrid " pnQRPA with the BCS quasiparticle energies and the shell-model occupation probabilities, and 1.181 in the " hybrid " pnQRPA with the shell-model quasiparticle energies and the occupation probabilities. It is close to 0.928, the total $B(\mathrm{GT}^+)$ in the full-basis shell model.

The " hybrid " models have not improved the strength distribution. But comparing to the shape of the spectrum of the pnQRPA with $g_{pp} = 1.4$ in Figure 3.2, the " hybrid " pnQRPA with the shell-model parameters (the dot-dashed line in Figure 3.3) still keeps a reasonable shape. We know both of them almost reproduce the shell-model total $B(\mathrm{GT}^+)$ value. In the " hybrid" pnQRPA, the position of the $1^+$ state almost remains the same, i.e., still differs by 6 MeV to the energy from the shell-model calculation.

The COBTD and CTME values of the " hybrid " pnQRPA are presented in the columns (B), (C)and (D) of Table 3.2 and Table 3.3. The COBTD and CTME in the column (B) are obtained by using the shell-model quasiparticle energies and the BCS occupation probabilities in the pnQRPA. We find that the difference between the columns (B) and (E) is decreased only for the transitions $f_{7/2} \rightarrow f_{7/2}$, but the COBTD and CTME in other transitions become worse or remain the same.

The COBTD and CTME values in the column (C), using the BCS quasiparticle energies and the shell-model occupation probabilities, and the column (D), using the shell-model quasiparticle energies and the occupation probabilities, present similar behaviour. The COBTD and CTME in the transition $f_{7/2} \rightarrow f_{7/2}$ now have the same sign as those in column (E). The COBTD and CTME for the transition $p_{3/2} \rightarrow p_{1/2}$ are and $f_{5/2} \rightarrow f_{5/2}$ have been improved over those in the pnQRPA. But other COBTD and CTME values become worse compared to those in the pnQRPA.

We compare the occupation factors between the BCS and shell-model in Table 3.1 and find in order to reproduce shell-model occupation factors, the pairing gap in the BCS equation should be unrealistically increased to around 4 Mev [Lau 88]. It requires a very strong and unrealistical effective interaction. The present BCS gaps are around 1 MeV.

We have made several similar comparisons for some nuclei in sd shell and $^{48}$Ti in fp shell. Similar conclusions are obtained. The detailed calculations for $^{48}$Ti have been shown in ref. [Brz 90].

## 3.4 Summary and Conclusions

We have investigated the pnQRPA as a model to study $\beta^+$ decay. The Gamow-Teller transition strength $B(\mathrm{GT}^+)$ for $^{46}\mathrm{Ti} \rightarrow ^{46}\mathrm{Sc}$, as an example, is calculated by the pnQRPA and full-basis shell model. The formulation of the self-consistent BCS-pnQRPA is given in the section 3.2. The coherent one-body transition densities (COBTD) and coherent transition matrix elements (CTME) are introduced and applied for analysis of the single-particle state contributions in $\beta^+$ decay. The comparison of the pnQRPA and shell model is made, including the total $B(\mathrm{GT}^+)$, shape of the strength distribution, COBTD and CTME values. Our comparison shows that the pnQRPA cannot reproduce the shell-model results. The large disagreements imply that there are some correlations which are important to $\beta^+$ decay but have not been taken into account in the BCS-pnQRPA equations. Our results agree with those of [Lau 88] and [Brz 89] who made similar comparisons for some sd shell nuclei.

We confirm that the particle-particle interactions in the pnQRPA provide the suppression mechanism in $\beta^+$ decay in agreement with previous studies. The total $B(\mathrm{GT}^+)$ is decreased when the parameter $g_{pp}$ is increased. But we note that the shape of the spectra is poor when $g_{pp}$ is increased beyond unity.

The shell-model quasiparticle energies and occupations are defined in section 3.3.2 and Eq. (3.29). Empirical improvements for the pnQRPA, namely, the " hybrid " pnQRPA, have been introduced by replacing the shell-model quasiparticle energies and/or occupation factors in the pnQRPA equation. Suppression of total $B(\mathrm{GT}^+)$ and some improvement in the COBTD and CTME are found in our study. The calculations show that the main suppression mechanism is from the shell-model occu-

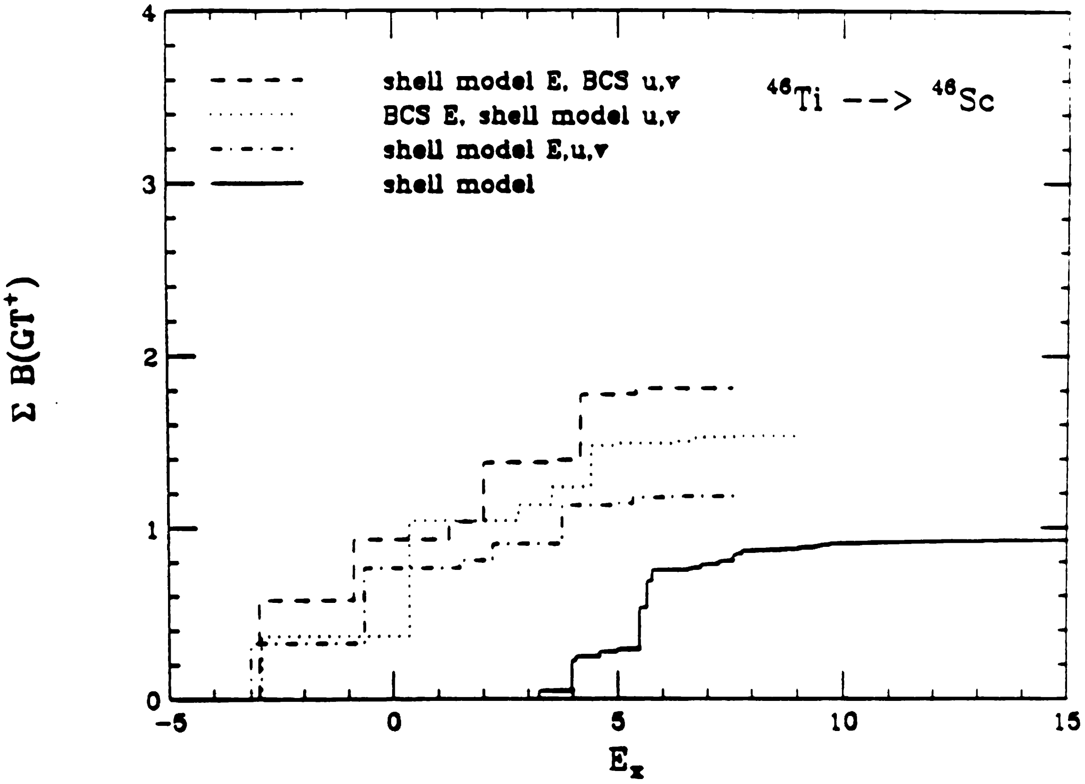

Figure 3.3: The pnQRPA result with the shell-model quasiparticle energies and/or occupation probabilities ( see Table 3.1 ).

pation factors. Thus we conclude it may be possible to put together "hybrid" models of this type that are more reliable than the conventional pnQRPA. Also we note that a solid theoretical study is necessary to generalize the pnQRPA model, and this will be discussed in Chapters 5 and 6.

# Chapter 4

# Comparison between pnQRPA and Shell Model II: $2\nu\beta\beta$ Decay

## 4.1 Introduction

Study of $2\nu\beta\beta$ decay is an important test of our understanding of nuclear structure properties since the decay process occurs within the standard weak interaction model. But until 1986, there have been large discrepancies between the experimental results and the simple shell model and/or other model's predictions. The theoretical half-lives of the double-beta decay nuclei are almost $5 \sim 100$ less than the experimental ones, i.e., the experimental $2\nu\beta\beta$ decay matrix elements are strongly suppressed (see Eq. (2.4)) [Hax 84, Doi 85].

In recent years, the pnQRPA has been applied to calculate $\beta\beta$ decay matrix elements [Vol 86, Civ 87, Eng 88, Mut 89]. Several calculations indicate that $2\nu\beta\beta$ decay matrix elements are suppressed if the particle-particle interaction term is included in the pnQRPA equation. They decrease rapidly when parameter $g_{pp}$ is increased ($g_{pp}$ is introduced as a multiplicative factor to the particle-particle interaction, see Eqs. (3.13,3.14)). Also previous studies have shown that the pnQRPA equation tends to be unstable and collapse when $g_{pp}$ is larger than unity [Vol 86, Civ 87, Eng 88,

Mut 89].

In Chapter 3, we concluded that the pnQRPA has not taken into account some correlations but which are important in $\beta^+$ decay. Therefore it is necessary to test the validity of the pnQRPA in $\beta\beta$ decay. In 1989, Brown and Zhao [Brz 89] made a comparison of the pnQRPA and full-basis shell-model calculations for hypothetical $\beta\beta$ decay of $^{28}$Mg in the sd shell. In their work, the BCS equation was solved by assuming a state-independent gap value which was obtained by analysing experimental data. Later Muto et. al. [Mut 91] presented a similar comparison for the $\beta\beta$ decay of $^{48}$Ca. But in their work, the model spaces of the pnQRPA and the shell model are not the same: the former is the (sd + fp + g) shells, where the g shell means $(1g_{9/2}, 1g_{7/2})$, and another is the fp shell only. Therefore the comparison may be meaningless because a meaningful comparison requires that the calculations of these models are performed in the same model space. On the other hand, the state-independent gap in the BCS was used in their work as well.

In this Chapter, the comparison of the pnQRPA and the full-basis shell-model calculations is made for $2\nu\beta\beta$decay of $^{46}$Ca. The model space and effective interaction are the fp shell and MSOBEP interaction, respectively. The self-consistent BCS-pnQRPA equations given in Chapter 3 are used. Two types of $2\nu\beta\beta$ decay matrix elements are discussed here, the energy dependent and the closure $\beta\beta$ decay matrix elements. The first gives the exact $2\nu\beta\beta$ decay matrix element, and the second relates an approximate method, namely, the closure approximation ( see Chapter 2 ).

The energy diagram for mass A=46 is presented in Figure 4.1. It is obvious that the $\beta\beta$ decay is the only decay mode for $^{46}$Ca ground state because all single $\beta$ decays are forbidden.

In section 4.2, the formulas for $2\nu\beta\beta$ decay matrix elements are presented. The

calculation results are given in section 4.3. The summary and conclusions are given in the final section.

## 4.2 Formalism of $2\nu\beta\beta$ Decay

In the shell-model calculations, the (intermediate state) energy dependent matrix element is defined by

$$M_{\mathrm{GT}}(E_m) = \sum_{m=1}^{E_m} \frac{< 0_f^+ || \sigma t^- || 1_m^+ >< 1_m^+ || \sigma t^- || 0_i^+ >}{E_m - E_i + T_0/2 + m_e c^2}, \tag{4.1}$$

where $E_m$ are the $1^+$ excitation energies of the intermediate states, $E_i$ is the intial state energy, $T_0/2$ is Q-value of $\beta\beta$ decay, for $^{46}$Ca, $T_0 = 0.986$ MeV. $m_e c^2$ is electron mass. The total matrix element for $2\nu\beta\beta$ is given by $M_{\mathrm{GT}} = M_{\mathrm{GT}}(E_m = \infty)$. The closure matrix element is defined by (see Chapter 2)

$$B_{\mathrm{CLS}}(E_m) = \sum_{m=1}^{E_m} < 0_f^+ || \sigma t^- || 1_m^+ >< 1_m^+ || \sigma t^- || 0_i^+ > . \tag{4.2}$$

The total matrix element is given by $B_{\mathrm{CLS}} = B_{\mathrm{CLS}}(E_m = \infty)$.

In the pnQRPA calculations, the $\beta\beta$ formulas become more complicated because the summation in Eqs. (4.1 – 4.2) involves the product of two transition matrix elements and each one contains the intermediate states of the intermediate nucleus. Of course, in the shell model, the intermediate states in the two transition matrix elements are the same. But in the pnQRPA, we recognize that the intermediate states in the two transition matrix elements are different. They depend on which parent nucleus is being considered. Thus a problem arises that the intermediate states resulting from the two different pnQRPA calculations are not orthogonal. Of course, they should be the same physically. In order to solve such a mismatch problem, we

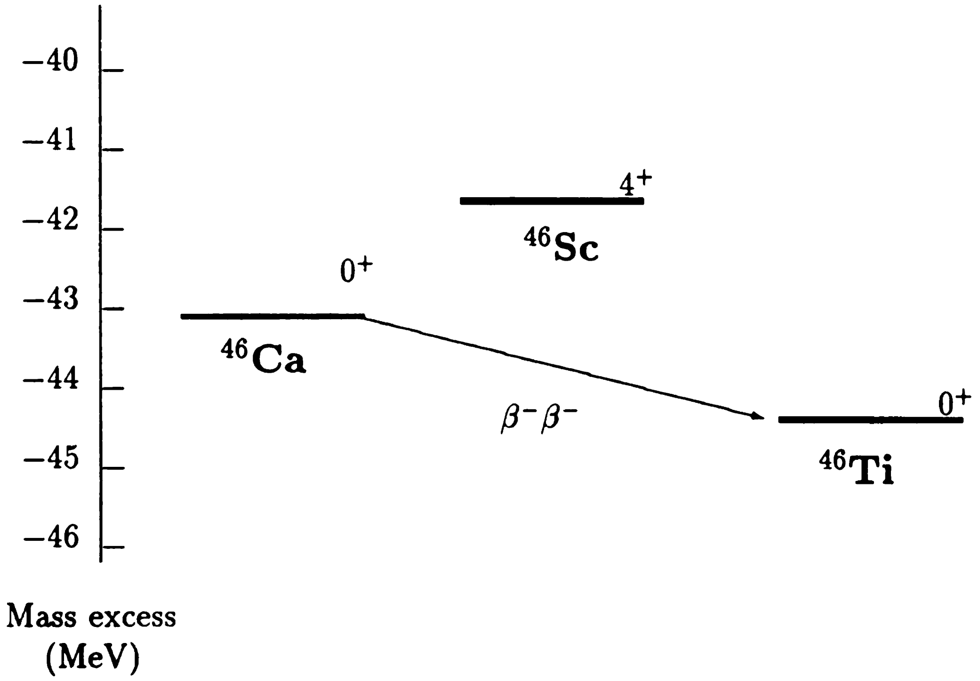
−40
−41
−42
−43
−44
−45
−46
Mass excess (MeV)
4+
$^{46}$Sc
0+
$^{46}$Ca
$\beta^-\beta^-$
0+
$^{46}$Ti

Figure 4.1: Mass spectrum for A=46 nuclei, where the double-beta decay is the only possible decay mode for the $^{46}$Ca. ground state

introduce an overlap matrix element between any two intermediate states $J^\pi_m$ and $J^\pi_{m'}$

$$< J^\pi_m | J^\pi_{m'} >= \sum_{pn} (\bar{X}^{pn,J^\pi}_{m'} X^{pn,J^\pi}_{m} - \bar{Y}^{pn,J^\pi}_{m'} Y^{pn,J^\pi}_{m}) \tag{4.3}$$

where $m$, $m'$ denote two states with eigenvectors $(X, Y)$ and $(\bar{X}, \bar{Y})$, which are constructed from intial and final states, respectively [Civ 87, Gro 86, Mut 89]. Obviously, if $(X, Y)$ and $(\bar{X}, \bar{Y})$ are identical, then we have $< J^\pi_m | J^\pi_{m'} >= \delta_{mm'}$ (see Eq. (3.10)). With the overlap matrix element, Eq. (4.1 - 4.3) can be rewritten by

$$M_{\mathrm{GT}}(E_m) = \sum_{m,m'} \frac{< 0^+_f || \sigma t^- || 1^+_m >< 1^+_m | 1^+_{m'} >< 1^+_{m'} || \sigma t^- || 0^+_i >}{E_m - E_i + T_0/2 + m_e c^2}, \tag{4.4}$$

$$B_{\mathrm{CLS}}(E_m) = \sum_{m,m'} < 0^+_f || \sigma t^- || 1^+_m >< 1^+_m | 1^+_{m'} >< 1^+_{m'} || \sigma t^- || 0^+_i > . \tag{4.5}$$

## 4.3 Results and Discussions

In this section, we compare the calculation results of the pnQRPA and full-basis shell model for the $2\nu\beta\beta$ of $^{46}$Ca. In this case, the initial (final) nucleus has 0 (2) protons and 6 (4) neutrons in the fp shell.

The double-beta decay matrix elements $M_{\mathrm{GT}}$ and/or $B_{\mathrm{CLS}}$ consist of the virtual decay routes, $\beta^-$ and $\beta^+$ decays. The $\beta^+$ Gamow-Teller transition strength in the pnQRPA was presented and discussed in Chapter 3. Here the running sums $\sum B(\mathrm{GT}^-)$ of the $\beta^-$ decay of $^{46}$Ca are shown in Figure 4.2. The dashed line is obtained from the BCS-pnQRPA and solid line from the full-basis shell model. The Coulomb shift 7.173 MeV is included in the calculations [Bro 79]. The matrix $B$ in the pnQRPA is zero because $v_p = 0$. Then the pnQRPA reduces to the pnQTDA. The amplitudes $Y$ are consequently equal to zero. The $\beta^+$ transition strength of $^{46}$Ca vanishes because there are no valence protons in the fp shell. So the total $B(\mathrm{GT}^-)$ strength is equal to 18 because of the sum rule Eq. (2.1). In Figure 4.2, the first $1^+$ eigenvalue of the pnQRPA differs by about 5 MeV to that of the shell model.

In Figure 4.3 and 4.4, we present the running sum of matrix element $M_{\rm GT}(E_m)$ and $B_{\rm CLS}(E_m)$ as a function of the $1^+$ excitation energies corresponding to the $^{46}$Ca ground state. The excitation energies are obtained by the pnQRPA calculation for $^{46}\mathrm{Ca} \rightarrow {}^{46}\mathrm{Sc}$, and are employed to evaluate the energy denominator in Eq. (4.4). Qualitatively the pnQRPA and shell-model show a similar behaviour. There is a cancellation between the matrix elements in the low- and high-lying states. The relative shapes qualitatively agree but quantitatively disagree with each other. We find the pnQRPA does not provide enough suppression for total $M_{\rm GT}$ and $B_{\rm CLS}$, which are about three times larger than those in the full-basis shell-model calculation. In detail, the matrix elements in the low-lying states are rather different between the two models, for example, the first $B_{\rm CLS}(E_1)$ is almost 8 times larger than the corresponding shell-model result. On the other hand, in the pnQRPA, the first $B(\mathrm{GT}^-)$ and $B(\mathrm{GT}^+)$ are dominated by the transition $f_{7/2} \rightarrow f_{7/2}$, but in the shell-model, this transition contributes only about 50 %.

We present the running sum of $B_{\rm CLS}(E_m)$ with respect to various $g_{pp}$ values in Figure 4.5 to 4.7, where we keep $g_{ph} = 1$. The particle-particle interaction suppresses the total matrix elements in agreement with previous studies [Vol 86, Civ 87, Eng 88, Mut 89]. If the particle-particle channel is shut off ($g_{pp} = 0$ ), the cancellation of $B_{\rm CLS}(E_m)$ between the low- and high-lying excitations disappears as shown in Figure 4.5. However, the cancellation emerges and becomes stronger and stronger as $g_{pp}$ is increased.

At $g_{pp} = 1.28$ (Figure 4.7), the pnQRPA agrees with the total shell-model $B_{\rm CLS}$ but fails to reproduces the relevant shape. At $g_{pp} = 1.20$ (Figure 4.8) the pnQRPA

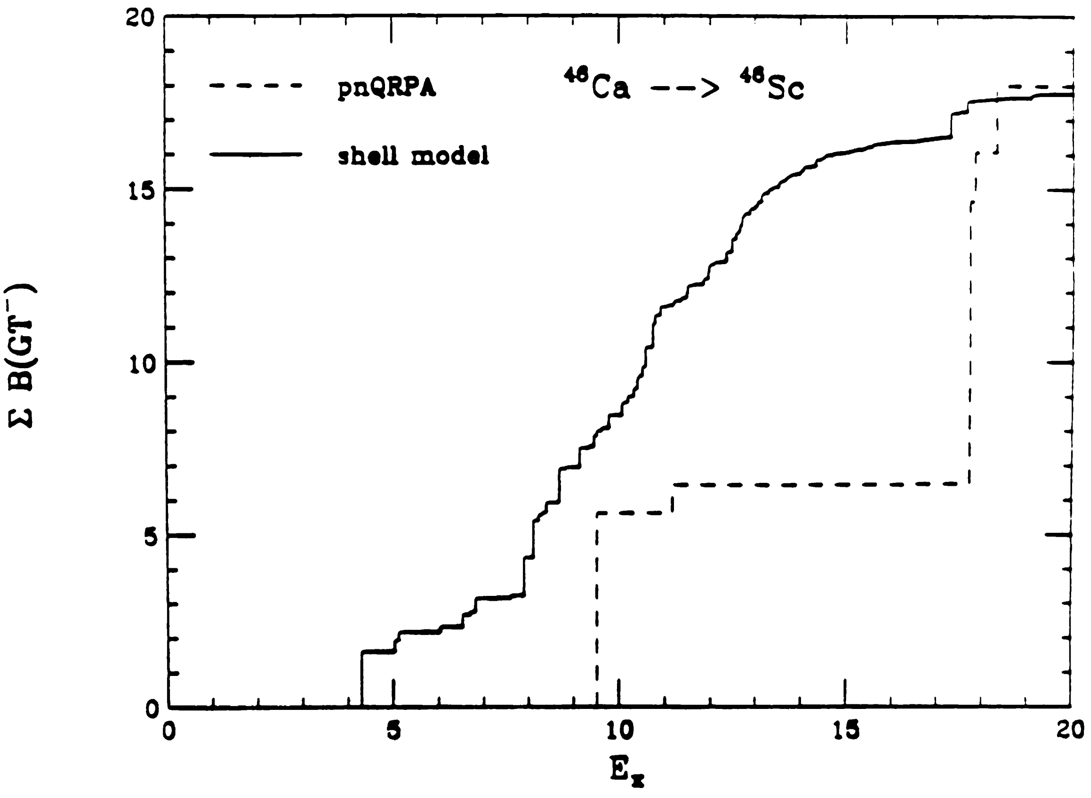

Figure 4.2: Summed Gamow-Teller strength $B(\mathrm{GT}^-)$ of $^{46}$Ca $\rightarrow^{46}$Sc. The dashed and solid lines are the pnQRPA and shell-model results, respectively

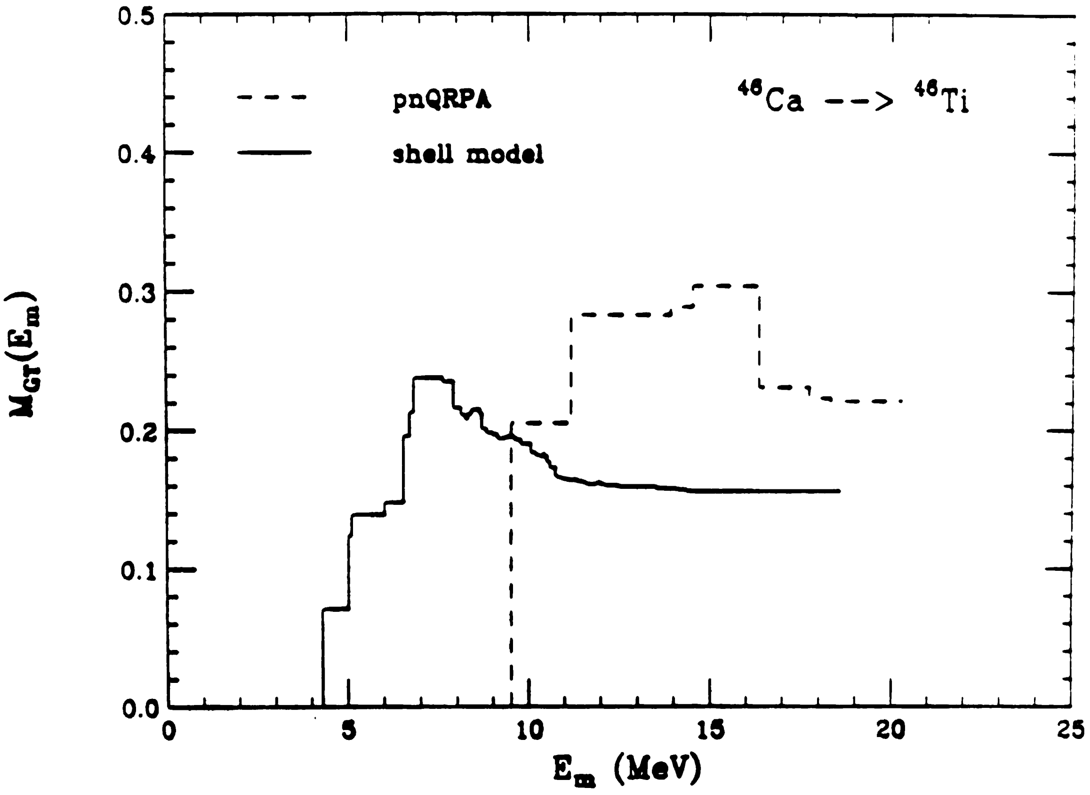

Figure 4.3: Summed energy dependent $2\nu\beta\beta$ decay matrix element $M_{\rm GT}(E_m)$ as the function of the excitation energies, the solid line and dashed line are the shell-model and pnQRPA results, respectively

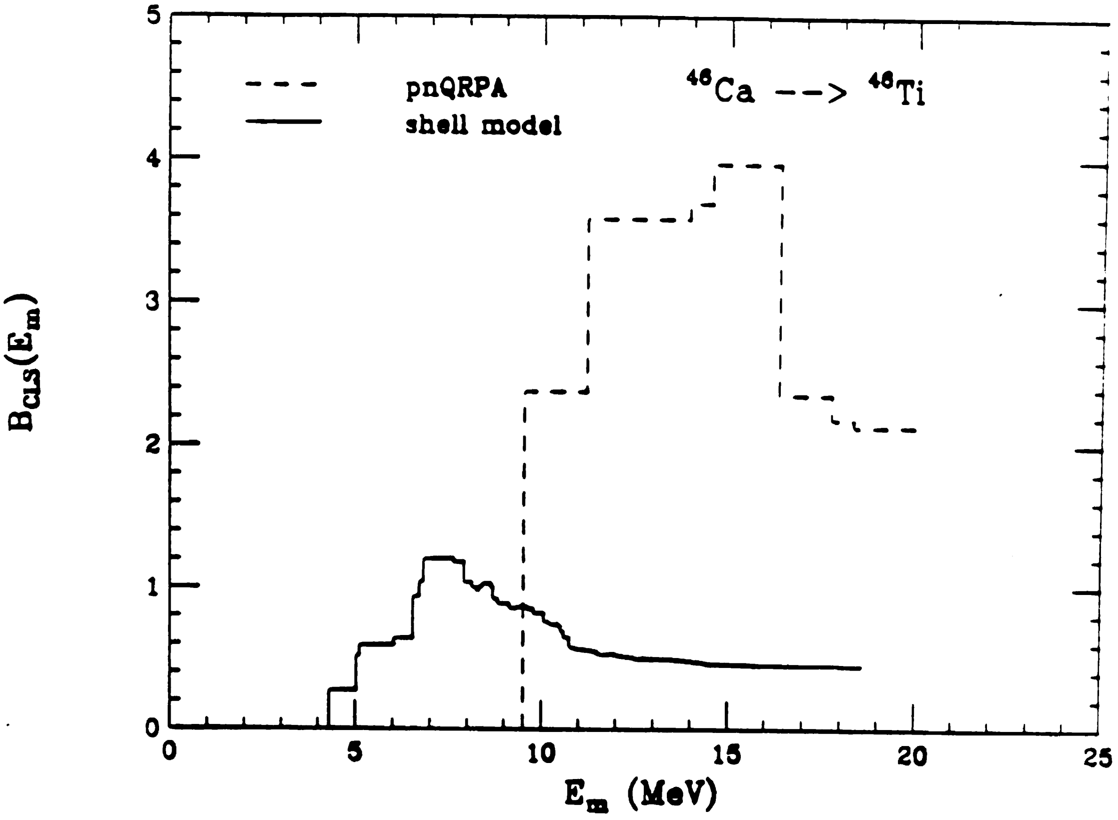

Figure 4.4: Summed closure $2\nu\beta\beta$ decay matrix element $B_{CLS}(E_m)$ as the function of the excitation energies, the solid line and dashed line are the shell-model and pnQRPA results, respectively

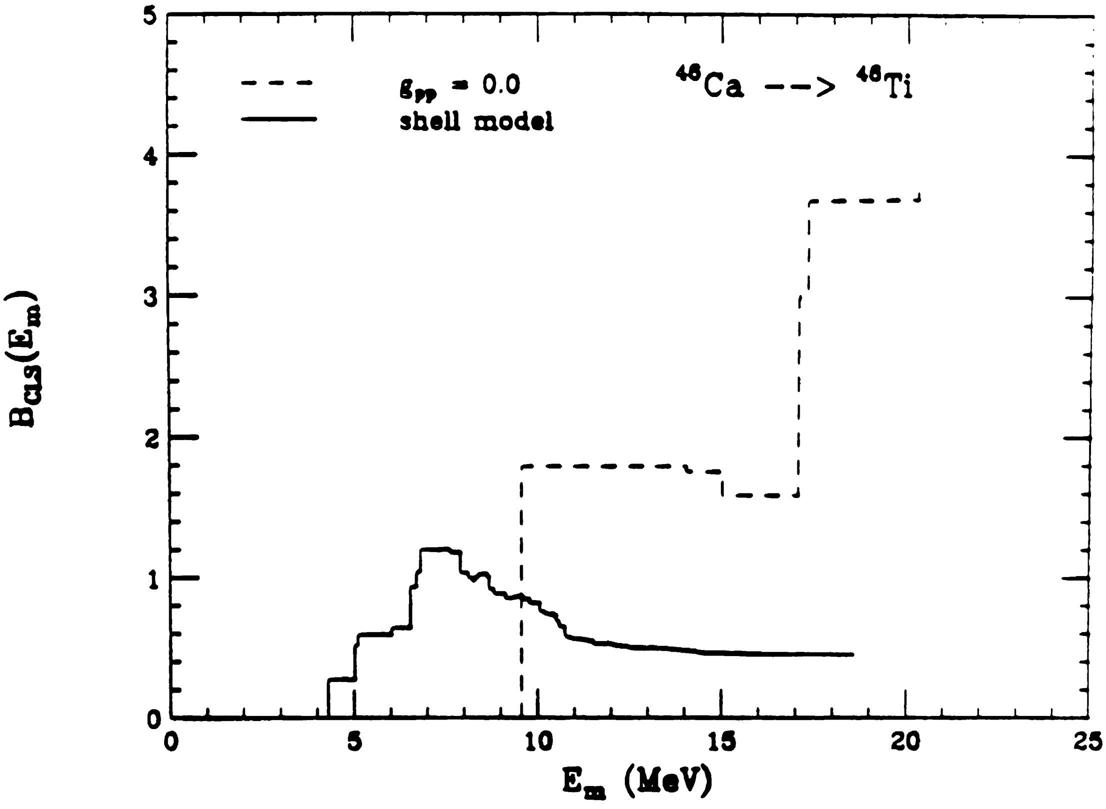

Figure 4.5: Summed closure matrix element $B_{\text{CLS}}(E_m)$, the solid line is from the shell-model calculation, the dashed line is pnQRPA result with $g_{pp} = 0.0$ and $g_{ph} = 1.0$

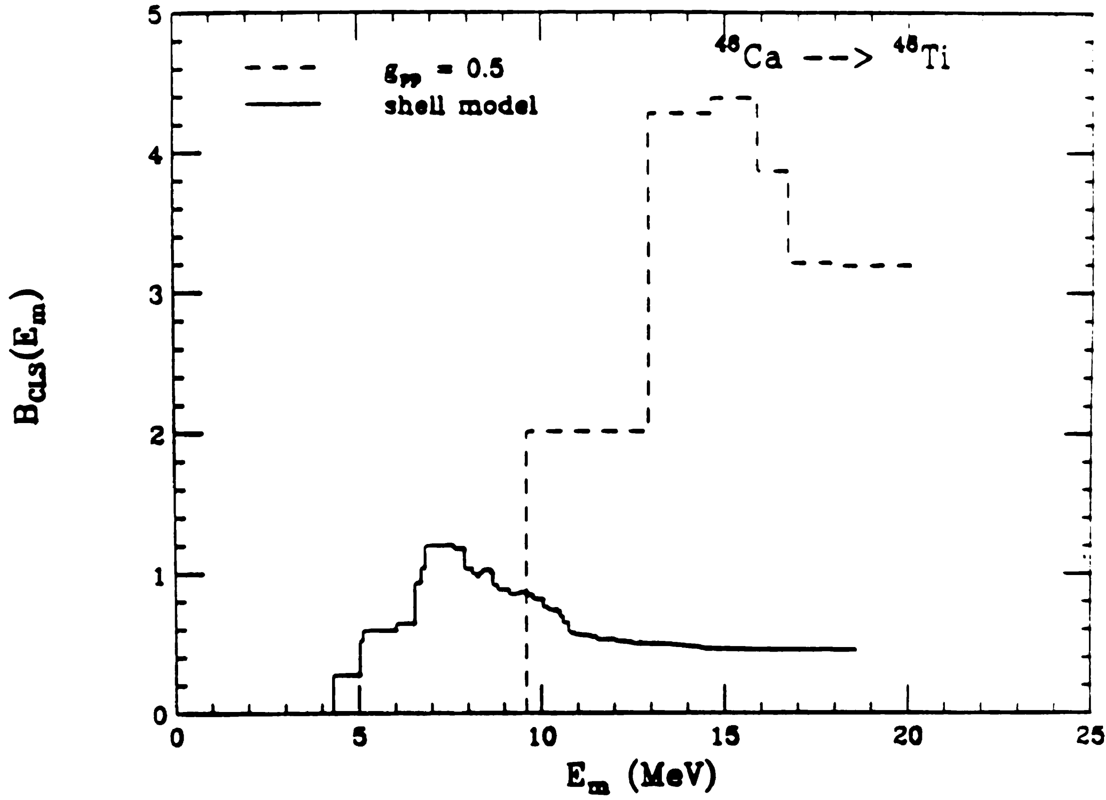

Figure 4.6: Summed closure matrix element $B_{\rm CLS}(E_m)$, the solid line is from the shell-model calculation, the dashed line is pnQRPA result with $g_{pp} = 0.5$ and $g_{ph} = 1.0$

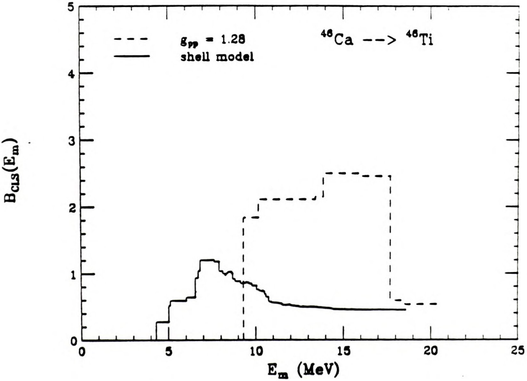

Figure 4.7: Summed closure matrix element $B_{\mathrm{CLS}}(E_m)$, the solid line is from the shell-model calculation, the dashed line is pnQRPA result with $g_{pp} = 1.28$ and $g_{ph} = 1.0$. The pnQRPA reproduces shell-model total $B_{\mathrm{CLS}}$ value.

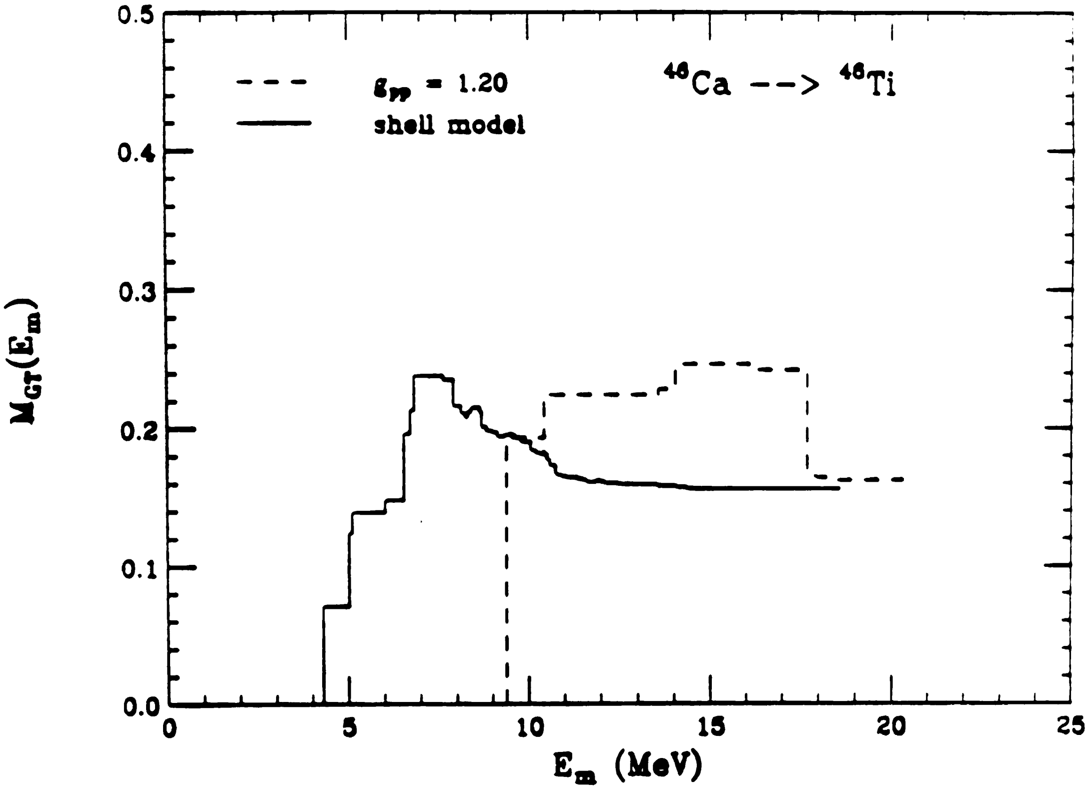

Figure 4.8: Summed energy dependent matrix element $M_{\mathrm{GT}}(E_m)$, the solid line is from the shell-model calculation, the dashed line is pnQRPA result with $g_{pp} = 1.2$ and $g_{ph} = 1.0$. The pnQRPA reproduces shell-model total $M_{\mathrm{GT}}$ value.

Table 4.1: $^{46}$Ca: Neutron single particle energies $\varepsilon_i$ (MeV), gap parameters $\Delta_i$ (MeV) and occupation probabilities $v_i^2$ and quasineutron energies $E_i$ (MeV) from BCS, the shell-model $E_i$(SM), $v_i^2$(SM) defined in Chapter 3. The neutron Fermi energy is −8.712 MeV.

| level | $\varepsilon_i$ | $\Delta_i$ | $v_i^2$ | $E_i$ | $E_i$(SM) | $v_i^2$(SM) |
|---|---|---|---|---|---|---|
| $\nu f_{7/2}$ | − 9.395 | 1.347 | 0.726 | 1.510 | 1.700 | 0.703 |
| $\nu p_{3/2}$ | − 5.507 | 1.042 | 0.025 | 3.370 | 3.343 | 0.049 |
| $\nu f_{5/2}$ | − 3.354 | 1.455 | 0.013 | 5.552 | 6.377 | 0.025 |
| $\nu p_{1/2}$ | − 3.107 | 1.026 | 0.008 | 5.698 | 5.830 | 0.016 |

agrees with the total shell-model $M_{\mathrm{GT}}$ but fails to reproduce the relevant shape as well.

Encouraged by the successes of the improvements of the pnQRPA in Chapter 3, we also consider the use of “ hybrid ” models for the $\beta\beta$ decay matrix elements. The shell-model quasiparticle energies and occupation probabilities for the initial and final nuclei are given in Table 3.1 and Table 4.1. In the following, we compare the following three curves, the dashed line is obtained by the pnQRPA, the dotted line by the “hybrid” model, and the solid line by the shell model. In Figure 4.9, one uses the shell-model quasiparticle energies and finds that $B_{\mathrm{CLS}}$ is suppressed. In Figure 4.10, one uses the shell-model occupation numbers and finds that $B_{\mathrm{CLS}}$ is unfortunately enhanced. In Figure 4.11, one uses all shell-model parameters and finds that $B_{\mathrm{CLS}}$ is suppressed. But suppressions in Figure 4.9 and 4.11 are not enough to reproduce the shell-model results. One may conclude the “ hybrid ” models do not work well for $2\nu\beta\beta$ decay.

Finally, we notice that there is a some arbitrariness to the choice of the energy denominator in Eq. (4.4) for calculating $M_{\mathrm{GT}}$ in the pnQRPA. This is because the intermediate states constructed from the initial and final states are mismatched. The

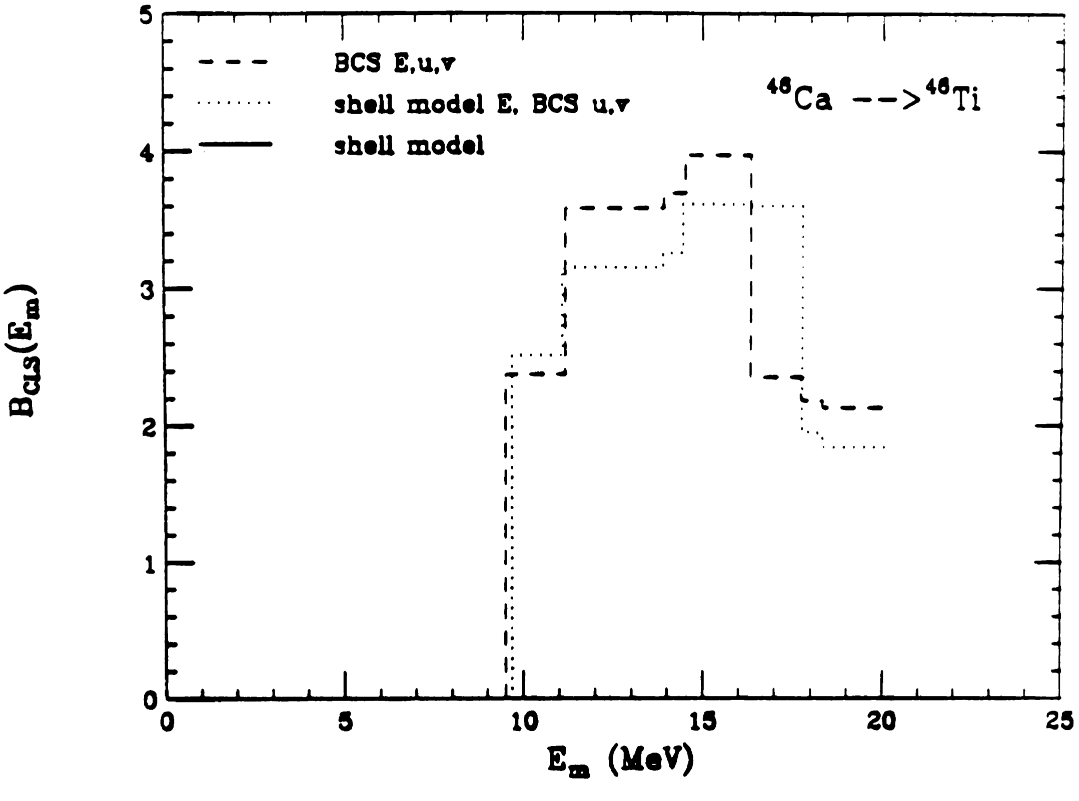

Figure 4.9: Summed closure matrix element $B_{\mathrm{CLS}}(E_m)$, the dashed line obtained by the pnQRPA with E, u,v from BCS and the dotted line with E from shell model and u,v from BCS, respectively.

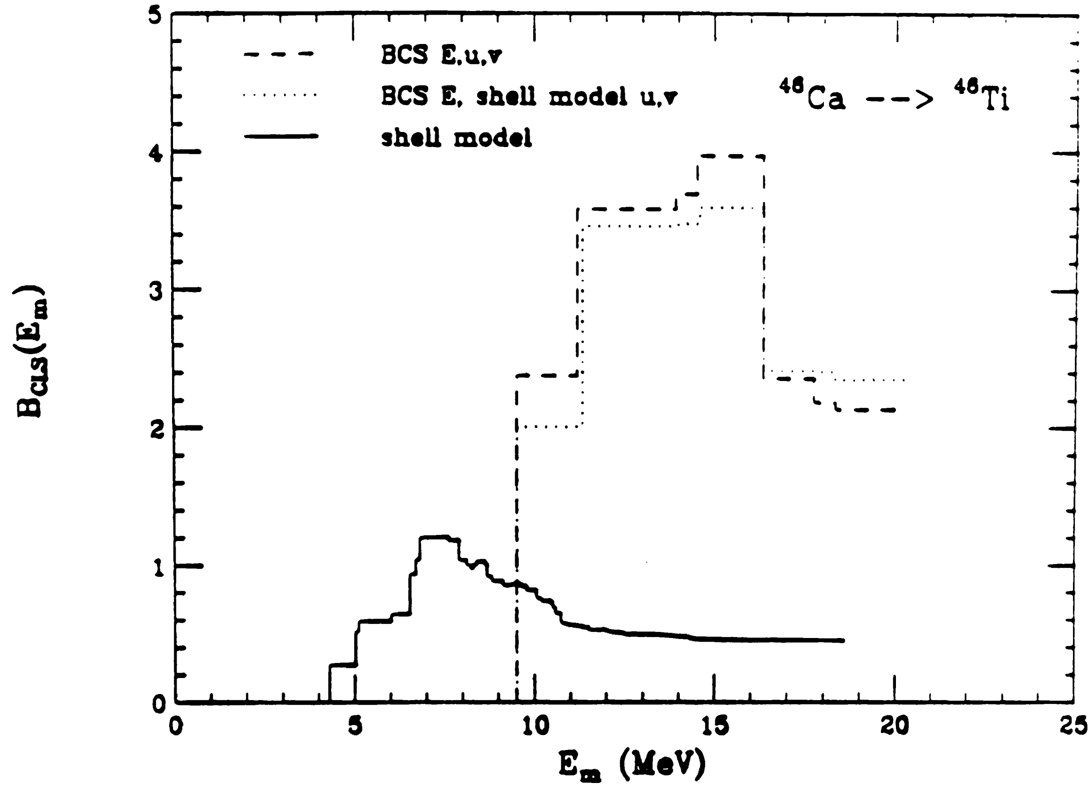

Figure 4.10: Summed closure matrix element $B_{\mathrm{CLS}}(E_m)$, the dashed line obtained by the pnQRPA with E, u,v from BCS and the dotted line with E from BCS and u,v from shell model, respectively.

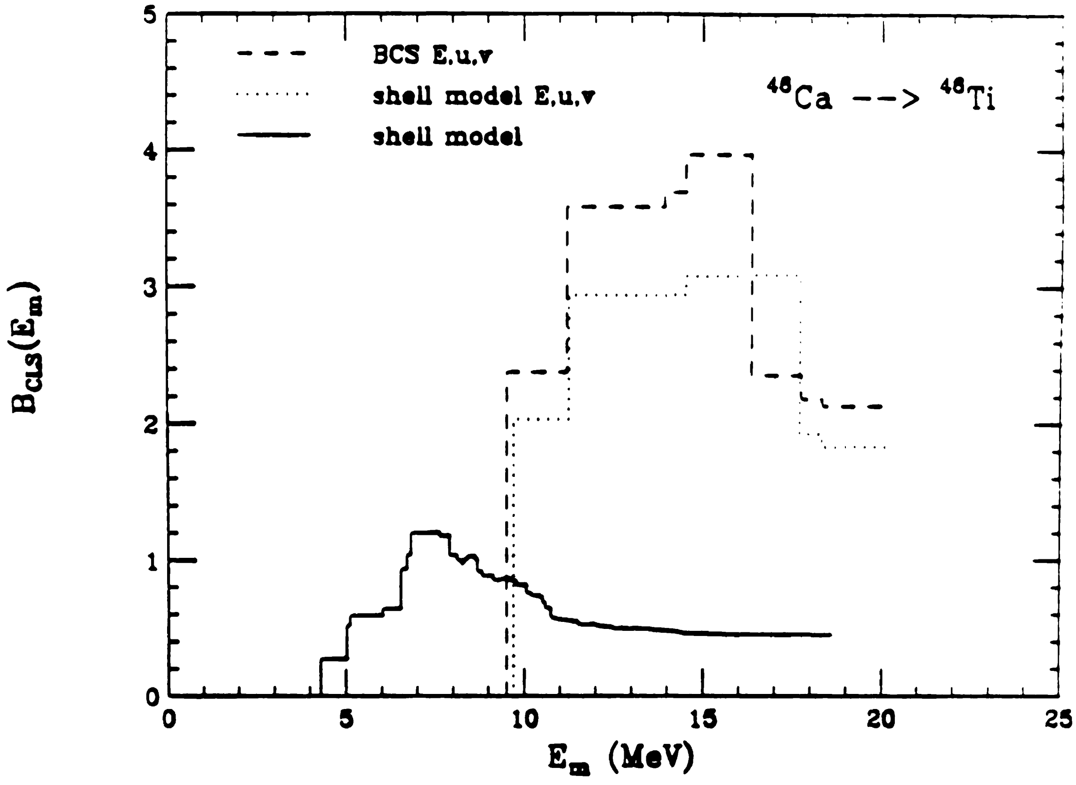

Figure 4.11: Summed closure matrix element $B_{\mathrm{CLS}}(E_m)$, the dashed line obtained by the pnQRPA with E, u,v from BCS and the dotted line with u,v and E from shell model, respectively.

simplest way is to let $E_m - E_i$ be the excitation energies from $^{46}$Ca $\rightarrow^{46}$Sc calculation as we used before. Another approach is using the relation $E_m - E_i = E_m - E_f + \Delta M$ and calculating $E_m - E_f$ from $^{46}$Ti $\rightarrow^{46}$Sc, where $\Delta M = -0.986$ MeV is mass difference between $^{46}$Ca and $^{46}$Ti. In fact, there is no big difference between the two methods in our calculations.

## 4.4 Summary and Conclusions

In this Chapter, we have made a comparison of the pnQRPA and shell-model calculations for the $2\nu\beta\beta$ decay matrix elements of $^{46}$Ca in the fp shell. The comparison not only gives insight into the total matrix elements as in previous studies, but also investigates the relevant matrix element distributions. The self-consistent BCS-pnQRPA equations given in Chapter 3 are used to calculate $\beta^-$ and $\beta^+$ Gamow-Teller components involved in the $2\nu\beta\beta$ decay formulas. Since the intermediate states constructed from the initial and final states are mismatched mathematically in the pnQRPA, the overlap matrix is introduced and used to match $\beta^-$ and $\beta^+$ virtual decay routes.

Two types of matrix element are investigated, the energy dependent $M_{\mathrm{GT}}(E_m)$ which is the exact $2\nu\beta\beta$ decay matrix element, and closure $B_{\mathrm{CLS}}(E_m)$ which is related to the closure approximation. In our work, we confirm that the suppression mechanism of the $2\nu\beta\beta$ matrix elements is due to the particle-particle interaction. $M_{\mathrm{GT}}$ and $B_{\mathrm{GT}}$ decrease when $g_{pp}$ value increases. Our calculations show the discrepancies between the pnQRPA and shell-model are not only in the total $M_{\mathrm{GT}}$ and $B_{\mathrm{CLS}}$ values but also in the shape of the matrix element distribution. The disagreements between the two models mainly come from the low-lying excitations, where the pnQRPA gives relatively large $\beta\beta$ matrix elements compared to the shell model.

The $2\nu\beta\beta$ decay matrix elements are also calculated by “ hybrid ” pnQRPA models, i.e., using the shell-model quasiparticle energies and/or occupations in the pn-QRPA. Suppressions in the “ hybrid ” are found, but are not enough to reproduce the shell-model calculations.

# Chapter 5

# BCS Theory and Extension

## 5.1 Introduction

The BCS theory developed by Bardeen, Cooper and Schrieffer [BCS 57] has successfully explained the superconductivity of the superconducting metals at very low temperature. The adoption of the BCS theory into nuclear physics followed the suggestions of Bohr, Mottelson and Pines and the exploratory work of Belyaev [BMP 58, Bel 59]. The first application is to even number semi-magic nuclei, where the ground states are considered to be constructed by pairing configurations. This model is a useful tool to explain a large variety of nuclear properties[Law 80, Rin 80]. The best known form of this theory is obtained by means of the Bogoliubov transformation and Ritz variational principle. The BCS is an independent quasiparticle theory and its ground state is the quasiparticle vacuum. The disadvantage of BCS is that particle number is not conserved.

The application of the BCS theory to a proton-neutron (*pn*) system, i.e., open proton and neutron shells, is complicated because we have two types of interacting particles. Of course, these particles can been rewritten as identical particles if another quantum number—isospin— is introduced. But we will not use isospin formalism here because the pnQRPA equation is more easily derived keeping protons and neutrons separate and it is usually applied in heavy nuclei with a large neutron excess where the *pn* formalism is more appropriate.

Several theories were suggested in order to describe *pn* system. The simplest method provides separate Bogoliubov transformations for protons and neutrons, respectively. Thus the quasiprotons and quasineutrons are well defined, and the ground state is the vacuum corresponding to both types of quasiparticles. In this formalism, the BCS equations for protons and neutrons retain the same form as those obtained from the semi-magic nuclei case, and they are just coupled through the mean field. In this model, only *pp*− and *nn*− pairing are taken into account. Another formulation that has been proposed by Lane [Lan 64] and considered by a number of authors[Row 70, Goo 70, Goo 79] is to give up the distinction between the protons and neutrons by using a generalized Bogoliubov transformation that mixes protons and neutrons to obtain two kinds of new mixed quasiparticles. BCS types of equations can be derived. They include all kinds of pairing, i.e. *pp*−, *nn*− and *pn*− pairing, where complex mean field and potentials are required [Goo 79].

In this Chapter, we concentrate on the first method because well defined quasiprotons and quasineutrons are necessary when one develops pnQRPA theory. In section 5.2, we re-derive the BCS equation in angular momentum coupling space for the proton-neutron system. Also a correlated BCS wave function is introduced through perturbation theory and the extended BCS equation are given in section 5.3. The spurious states are discussed as well in this section. The summary and conclusions are given in section 5.4.

## 5.2 BCS Theory for Proton-Neutron System

### 5.2.1 Nuclear Hamiltonian in quasiparticle space

In the shell-model basis, the nuclear Hamiltonian in the second quantization formalism can be written as

$$\begin{aligned} H &= T + V \\ &= \sum_{\alpha} \varepsilon^0_\alpha a^+_\alpha a_\alpha + \frac{1}{4} \sum_{\alpha\beta\gamma\delta} < \alpha\beta|V|\gamma\delta > a^+_\alpha a^+_\beta a_\delta a_\gamma, \qquad (5.1) \end{aligned}$$

where $\varepsilon^0_\alpha$ is the single-particle energy and $< \alpha\beta|V|\gamma\delta >$ is the antisymmetric two-body interaction matrix element. The labels $(\alpha\beta\gamma\delta)$ refer to the particular state $(n, l, j, m, t_z)$ in the shell-model basis, where $n$ is principle quantum number, $l$ is orbital momentum, $j$ and $m$ are angular momentum and its third component, and $t_z$ is isospin third component, where isospin $t = 1/2$ for proton and neutron. For simplicity, $(n, l, j, m, t_z)$ is denoted as $(jmt_z)$ and then the Hamiltonian can be rewritten as

$$\begin{aligned} H = & \sum_{jmt_z} \varepsilon^0_{jt_z} a^+_{jmt_z} a_{jmt_z} + \\ & \frac{1}{4} \sum_{\substack{j_a m_a, \cdots j_d m_d \\ t_{za}, \cdots t_{zd}}} < j_a m_a t_{za}, j_b m_b t_{zb} | V | j_c m_c t_{zc}, j_d m_d t_{zd} > \\ & a^+_{j_a m_a t_{za}} a^+_{j_b m_b t_{zb}} a_{j_d m_d t_{zd}} a_{j_c m_c t_{zc}}. \qquad (5.2) \end{aligned}$$

Eq. (5.2) is called the m-scheme formalism.

The above Hamiltonian can be expressed in proton-neutron formalism with the definition of isospin of proton $(t, t_z) = (1/2, -1/2)$ and neutron $(t, t_z) = (1/2, 1/2)$,

$$\begin{aligned} H = & \sum_{j_p m_p} \varepsilon^0_{j_p} a^+_{j_p m_p} a_{j_p m_p} + \sum_{j_n m_n} \varepsilon^0_{j_n} a^+_{j_n m_n} a_{j_n m_n} \\ & + \frac{1}{4} \sum_{\substack{j_{p_1}, \cdots j_{p_4} \\ m_{p_1} \cdots m_{p_4}}} < j_{p_1} m_{p_1} j_{p_2} m_{p_2} | V | j_{p_3} m_{p_3} j_{p_4} m_{p_4} > a^+_{j_{p_1} m_{p_1}} a^+_{j_{p_2} m_{p_2}} a_{j_{p_4} m_{p_4}} a_{j_{p_3} m_{p_3}} \end{aligned}$$

$$+\frac{1}{4}\sum_{\substack{j_{n_1},\cdots j_{n_4}\\ m_{n_1}\cdots m_{n_4}}} < j_{n_1}m_{n_1}j_{n_2}m_{n_2}|V|j_{n_3}m_{n_3}j_{n_4}m_{n_4} > a^{+}_{j_{n_1}m_{n_1}}a^{+}_{j_{n_2}m_{n_2}}a_{j_{n_4}m_{n_4}}a_{j_{n_3}m_{n_3}}$$

$$+\sum_{\substack{j_{p_1}\cdots j_{n_2}\\ m_{p_1}\cdots m_{n_2}}} < j_{p_1}m_{p_1}j_{n_1}m_{n_1}|V|j_{p_2}m_{p_2}j_{n_2}m_{n_2} > a^{+}_{j_{p_1}m_{p_1}}a^{+}_{j_{n_1}m_{n_1}}a_{j_{n_2}m_{n_2}}a_{j_{p_2}m_{p_2}} \tag{5.3}$$

where $p, n$ label proton and neutron. We are reminded that additional terms which contain matrix elements such as $< pp|V|pn >, < pn|V|nn >$ and $< pp|V|nn >$ are dropped since the nuclear interactions conserve charge numbers.

We introduce the two-proton, two-neutron and proton-neutron creation operators defined by

$$A^{\dagger}_{\mathrm{pp}}(p_1p_2, JM) = \sum_{m_{p_1}m_{p_2}} \frac{< j_{p_1}m_{p_1}j_{p_2}m_{p_2}|JM >}{\sqrt{1+\delta_{p_1p_2}}} a^{\dagger}_{j_{p_1}m_{p_1}}a_{j_{p_2}m_{p_2}} \tag{5.4}$$

$$A^{\dagger}_{\mathrm{nn}}(n_1n_2, JM) = \sum_{m_{n_1}m_{n_2}} \frac{< j_{n_1}m_{n_1}j_{n_2}m_{n_2}|JM >}{\sqrt{1+\delta_{n_1n_2}}} a^{\dagger}_{j_{n_1}m_{n_1}}a_{j_{n_2}m_{n_2}} \tag{5.5}$$

$$A^{\dagger}_{\mathrm{pn}}(p_1n_1, JM) = \sum_{m_{p_1}m_{n_1}} < j_{p_1}m_{p_1}j_{n_1}m_{n_1}|JM > a^{\dagger}_{j_{p_1}m_{p_1}}a_{j_{n_1}m_{n_1}}. \tag{5.6}$$

The Hermitian adjoint operators are defined by

$$A_{\mathrm{pp}} = (A^{\dagger}_{\mathrm{pp}})^{\dagger}, \tag{5.7}$$

$$A_{\mathrm{nn}} = (A^{\dagger}_{\mathrm{nn}})^{\dagger}, \tag{5.8}$$

$$A_{\mathrm{pn}} = (A^{\dagger}_{\mathrm{pn}})^{\dagger}. \tag{5.9}$$

Thus the Hamiltonian given by Eq. (5.3) can been written as

$$H = \sum_{p}\varepsilon^0_p\sqrt{2j_p+1}(a^{+}_{j_p}\otimes\tilde{a}_{j_p})^{J=0,M=0} + \sum_{n}\varepsilon^0_n\sqrt{2j_n+1}(a^{+}_{j_n}\otimes\tilde{a}_{j_n})^{J=0,M=0}$$

$$+\frac{1}{4}\sum_{\substack{p_1\cdots p_4\\ JM}}(1+\delta_{p_1p_2})(1+\delta_{p_3p_4})V^{J}_{p_1p_2p_3p_4}A^{\dagger}_{\mathrm{pp}}(p_1p_2, JM)A_{\mathrm{pp}}(p_3p_4, JM)$$

$$+\frac{1}{4}\sum_{\substack{n_1,\cdots n_4\\ JM}}(1+\delta_{n_1n_2})(1+\delta_{n_3n_4})V^J_{n_1n_2n_3n_4}A^\dagger_{\rm nn}(n_1n_2,JM)A_{\rm nn}(n_3n_4,JM)$$

$$+\sum_{\substack{p_1n_1p_2n_2\\ JM}}V^J_{p_1n_1p_2n_2}A^\dagger_{\rm pn}(p_1n_1,JM)A_{\rm pn}(p_2n_2,JM), \tag{5.10}$$

where $V^J_{ijkl} =< ij|V|kl >^J$ and the label $p$ and $n$ represent proton's and neutron's $(nlj)$. The Hamiltonian in Eq. (5.10) is called the J-scheme coupling in proton-neutron formalism.

The quasiprotons and quasineutrons are introduced by the Bogoliubov transformations, in the spherical shell-model basis,

$$c^+_{j_pm_p} = u_p a^+_{j_pm_p} + (-1)^{j_p+m_p} v_p a_{j_p-m_p}, \tag{5.11}$$

$$c^+_{j_nm_n} = u_n a^+_{j_nm_n} + (-1)^{j_n+m_n} v_n a_{j_n-m_n}, \tag{5.12}$$

with

$$u_p^2 + v_p^2 = u_n^2 + v_n^2 = 1. \tag{5.13}$$

Eq. (5.13) is required if the quasiparticles are assumed to be fermions[Row 70, Law 80, Rin 80].

In order to derive the BCS equation, we relax the fixed proton and neutron number restriction and introduce the extra terms to the Hamiltonian.

$$\tilde{H} = H - \lambda_\pi \hat{N}_\pi - \lambda_\nu \hat{N}_\nu, \tag{5.14}$$

where $\hat{N}_\pi$ and $\hat{N}_\nu$ are proton and neutron number operators. The Lagrange multipliers $\lambda_\pi$ and $\lambda_\nu$ turn out to have the physical interpretation of proton and neutron Fermi energies. They are chosen to ensure that mean proton and neutron numbers are correct.

After carrying out the Bogoliubov transformation, the Hamiltonian can be rewritten as

$$\tilde{H} = H_{\mathrm{BCS}} + H_{\mathrm{int}}, \tag{5.15}$$

where

$$\begin{aligned} H_{\mathrm{BCS}} &= H_0 + H_{11}^{\mathrm{pp}} + H_{11}^{\mathrm{nn}} + (H_{20}^{\mathrm{pp}} + h.c) + (H_{20}^{\mathrm{nn}} + h.c), & (5.16)\\ H_{\mathrm{int}} &= H_{\mathrm{int}}^{\mathrm{pp}} + H_{\mathrm{int}}^{\mathrm{nn}} + H_{\mathrm{int}}^{\mathrm{pn}}, & (5.17) \end{aligned}$$

where the numerical subscripts indicate the number of quasiparticle creation and annihilation operators in each piece of the Hamiltonian. We also require that the above equations should be *normal ordered*, that is, destruction operators $c$ stand to the right of creation operators $c^\dagger$. $H_{\mathrm{int}}$ will be discussed in section 5.3.1.

### 5.2.2 BCS equations ( independent quasiparticle )

The BCS equations only depend on $H_{\mathrm{BCS}}$ in Eq. (5.16). The terms in $H_{\mathrm{BCS}}$ are given by

$$\begin{aligned} H_0 &= \sum_p (2j_p+1)(\varepsilon_p - \lambda_\pi - \frac{1}{2}\Gamma_p)v_p^2 + \sum_n (2j_n+1)(\varepsilon_n - \lambda_\nu - \frac{1}{2}\Gamma_n)v_n^2 \\ &\quad -\frac{1}{2}\sum_p (2j_p+1)\Delta_p u_p v_p - \frac{1}{2}\sum_n (2j_n+1)\Delta_n u_n v_n, & (5.18)\\ H_{11}^{\mathrm{pp}} &= \sum_{p,m_p} \{(\varepsilon_p - \lambda_\pi)(u_p^2 - v_p^2) + 2u_p v_p \Delta_p\} c_{j_p m_p}^\dagger c_{j_p m_p}, & (5.19)\\ H_{11}^{\mathrm{nn}} &= \sum_{n,m_n} \{(\varepsilon_n - \lambda_\nu)(u_n^2 - v_n^2) + 2u_n v_n \Delta_n\} c_{j_n m_n}^\dagger c_{j_n m_n}, & (5.20)\\ H_{20}^{\mathrm{pp}} &= \sum_p (-1)^{j_p+m_p} \{(\varepsilon_p - \lambda_\pi)u_p v_p - \frac{1}{2}(u_p^2 - v_p^2)\Delta_p\} c_{j_p m_p}^\dagger c_{j_p -m_p}^\dagger, & (5.21)\\ H_{20}^{\mathrm{nn}} &= \sum_n (-1)^{j_n+m_n} \{(\varepsilon_n - \lambda_\nu)u_n v_n - \frac{1}{2}(u_n^2 - v_n^2)\Delta_n\} c_{j_n m_n}^\dagger c_{j_n -m_n}^\dagger, & (5.22) \end{aligned}$$

with

$$\varepsilon_p = \varepsilon_p^0 + \Gamma_p, \tag{5.23}$$

$$\varepsilon_n = \varepsilon_n^0 + \Gamma_n, \tag{5.24}$$

$$\Gamma_p = \frac{1}{2j_p+1}[\sum_{p',J}(1+\delta_{pp'})(2J+1)v_{p'}^2 V_{pp'pp'}^J + \sum_{n',J}(2J+1)v_{n'}^2 V_{pn'pn'}^J], \tag{5.25}$$

$$\Gamma_n = \frac{1}{2j_n+1}[\sum_{n',J}(1+\delta_{nn'})(2J+1)v_{n'}^2 V_{nn'nn'}^J + \sum_{p',J}(2J+1)v_{p'}^2 V_{p'np'n}^J], \tag{5.26}$$

$$\Delta_p = -\sum_{p'}\sqrt{\frac{2j_p'+1}{2j_p+1}}u_{p'}v_{p'}V_{ppp'p'}^{J=0}, \tag{5.27}$$

$$\Delta_n = -\sum_{n'}\sqrt{\frac{2j_n'+1}{2j_n+1}}u_{n'}v_{n'}V_{nnn'n'}^{J=0}, \tag{5.28}$$

$\Gamma_p$ and $\Gamma_n$ the are proton and neutron single-particle energy rearrangements. $\Delta_p$ and $\Delta_n$ are proton and neutron gaps. The r.h.s. of the gap equations ( Eq. (5.27,5.28)) only depend on J=0 interaction matrix elements. The $J \neq 0$ terms are automatically equal to zero due to Clebsch-Gordan coefficient coupling. So the BCS is an S-pair theory. Also one finds only *pp*− or *nn*− paring is involved in the proton or neutron gap equation.

In order to derive the BCS equations, we will drop quasiparticle interaction terms $H_{\text{int}}$, and let the BCS ground state be the vacuum corresponding to quasiprotons and quasineutrons introduced in Eqs. (5.11,5.12), i.e.,

$$c_{j_p m_p}|\text{BCS}> = 0, \tag{5.29}$$

$$c_{j_n m_n}|\text{BCS}> = 0, \tag{5.30}$$

where $|\text{BCS}>$ is the BCS ground state.

The BCS equations can be obtained from the Ritz variation principle, in which the expectation value of $\tilde{H}$ is minimized [Row 70, Rin 80, Zha 92]. It requires the coefficients of $H_{20}^{\mathrm{pp}}$ and $H_{20}^{\mathrm{nn}}$ in Eqs. (5.21,5.22) to be equal to zero, i.e.,

$$(\varepsilon_p - \lambda_\pi)u_p v_p - \frac{1}{2}(u_p^2 - v_p^2)\Delta_p = 0, \tag{5.31}$$

$$(\varepsilon_n - \lambda_\nu)u_n v_n - \frac{1}{2}(u_n^2 - v_n^2)\Delta_n = 0. \tag{5.32}$$

We introduce the quasiproton and quasineutron energies defined by

$$E_p = \sqrt{(\varepsilon_p - \lambda_\pi)^2 + \Delta_p^2}, \tag{5.33}$$

$$E_n = \sqrt{(\varepsilon_n - \lambda_\nu)^2 + \Delta_n^2}. \tag{5.34}$$

Then one solves Eqs. (5.31,5.32,5.13) and obtains

$$v_p^2 = \frac{1}{2}(1 - \frac{\varepsilon_p - \lambda_\pi}{E_p}), \tag{5.35}$$

$$v_n^2 = \frac{1}{2}(1 - \frac{\varepsilon_n - \lambda_\nu}{E_n}). \tag{5.36}$$

The BCS wave function has a trial form in the particle basis [Law 80],

$$\begin{aligned} |\mathrm{BCS}> &= \prod_{\substack{j_p m_p>0 \\ j_n m_n>0}} (u_p + v_p a^\dagger_{j_p m_p}\tilde{a}^\dagger_{j_p m_p})(u_n + v_n a^\dagger_{j_n m_n}\tilde{a}^\dagger_{j_n m_n})|> \\ &= \prod_{j_p j_n}\{u_p^{\Omega_p}\exp[-\frac{v_p}{u_p}S_+(j_p)]u_n^{\Omega_n}\exp[-\frac{v_n}{u_n}S_+(j_n)]\}|> , \end{aligned} \tag{5.37}$$

where

$$\tilde{a}^\dagger_{jm} = (-1)^{j+m}a^\dagger_{j-m}, \tag{5.38}$$

$$\Omega = \frac{2j+1}{2} \tag{5.39}$$

$$\begin{aligned} S_+(j) &= \sum_{jm>0}(-1)^{j-m}a^\dagger_{jm}a^\dagger_{j-m} \\ &= \sum_{jm>0}\sqrt{2j+1} < jmj-m|00 > a^\dagger_{jm}a^\dagger_{j-m}, \end{aligned} \tag{5.40}$$

where $|>$ is the particle vacuum, i.e., $a_{jm}|>= 0$. Eqs. (5.37,5.40) imply that the BCS wave function has seniority-zero and consequently represent a $0^+$ state in an even-even nucleus. Since the BCS equation is obtained by dropping quasiparticle interaction $H_{\text{int}}$ terms, the BCS is an independent quasiparticle theory.

The BCS wave function is required to have correct mean particle numbers. Thus the proton and neutron Fermi energies $\lambda_\pi$ and $\lambda_\nu$ are chosen so that the mean proton and neutron numbers in BCS satisfy

$$< \text{BCS}|\hat{N}_\pi|\text{BCS} > \;=\; \sum_p (2j_p+1)v_p^2 = N_\pi, \tag{5.41}$$

$$< \text{BCS}|\hat{N}_\nu|\text{BCS} > \;=\; \sum_n (2j_n+1)v_n^2 = N_\nu, \tag{5.42}$$

where $N_\pi$ and $N_\nu$ are the proton and neutron numbers in the nuclear system. At this stage, parameters $v_p^2$ and $v_n^2$ introduced in Bogoliubov transformations turn out to have the physical meaning of proton and neutron occupation probabilities.

Eqs. (5.23-5.28,5.33-5.36,5.41,5.42) are called the BCS equation. They can be solved iteratively. In the BCS equations, we can find that the equations for protons and neutrons are coupled only through the proton-neutron interaction terms in the rearrangement $\Gamma_p$ and $\Gamma_n$.

We reiterate that the BCS theory ceases to conserve particle numbers. The particle-number uncertainty can be calculated as

$$(\Delta N)^2 =< \text{BCS}|\hat{N}^2|\text{BCS} > -N^2 = \sum_j (2j+1)u_j^2 v_j^2. \tag{5.43}$$

The fractional uncertainty in particle number is defined by

$$\frac{(\Delta N)}{N}. \tag{5.44}$$

When $v_p^2$ and $v_n^2$ satisfy Eqs. (5.35,5.36), the BCS Hamiltonian in Eq. (5.16) becomes

$$H_{\text{BCS}} = H_0 + \sum_{p,m_p} E_p c^\dagger_{j_p m_p} c_{j_p m_p} + \sum_{n,m_n} E_n c^\dagger_{j_n m_n} c_{j_n m_n}. \tag{5.45}$$

and the Hamiltonian in Eq. (5.15)

$$\tilde{H} = H_0 + \sum_{p,m_p} E_p c^{\dagger}_{j_p m_p} c_{j_p m_p} + \sum_{n,m_n} E_n c^{\dagger}_{j_n m_n} c_{j_n m_n} + H_{\text{int}}, \tag{5.46}$$

Then Hamiltonian given by Eq. (5.1) is expressed by

$$H = H_{\text{BCS}} + H_{\text{int}} + \lambda_\pi \hat{N}_\pi + \lambda_\nu \hat{N}_\nu. \tag{5.47}$$

### 5.2.3 BCS energy spectrum

The BCS ground state energy is given by

$$\begin{aligned} E_{\text{BCS}} &= < \text{BCS}|H_{\text{BCS}} + \lambda_\pi \hat{N}_\pi + \lambda_\nu \hat{N}_\nu|\text{BCS} > \\ &= H_0 + \lambda_\pi N_\pi + \lambda_\nu N_\nu \\ &= \sum_p (2j_p + 1)(\varepsilon_p - \frac{1}{2}\Gamma_p) v_p^2 + \sum_n (2j_n + 1)(\varepsilon_n - \frac{1}{2}\Gamma_n) v_n^2 \\ &\quad -\frac{1}{2}\sum_p (2j_p + 1)\Delta_p u_p v_p - \frac{1}{2}\sum_n (2j_n + 1)\Delta_n u_n v_n. \end{aligned} \tag{5.48}$$

The BCS excitations, sometimes called unperturbed states ( which refers to dropping the $H_{\text{int}}$,) are defined as

$$|h_{\text{qp}} l_{\text{qn}} >= \prod_{i=1}^{h} \prod_{j=1}^{l} c^{\dagger}_{j_{p_i} m_{p_i}} c^{\dagger}_{j_{n_j} m_{n_j}} |\text{BCS} > . \tag{5.49}$$

The excitation energy is

$$E_{h_{\text{qp}} l_{\text{qn}}} = E_{\text{BCS}} + \sum_{i=1}^{h} E_{p_i} + \sum_{j=1}^{l} E_{n_j}. \tag{5.50}$$

The configuration corresponding to this excitation is obtained by creating $h$ quasiprotons and $l$ quasineutrons with respect to the ground state $|\text{BCS}>$.

## 5.3 Extended BCS Theory

### 5.3.1 Interactions between quasiparticles

As we mentioned before, the $H_{\text{int}}$ terms describe the interactions between the quasiparticles, consisting of like particle interaction $H_{\text{int}}^{\text{pp}}$ and $H_{\text{int}}^{\text{nn}}$ and unlike particle interaction $H_{\text{int}}^{\text{pn}}$. Since $H_{\text{int}}^{\text{nn}}$ is identical with $H_{\text{int}}^{\text{pp}}$ if p/n labels are interchanged, we will give $H_{\text{int}}^{\text{pp}}$ here. Now the expressions of each term in $H_{\text{int}}$ are given by

$$\begin{aligned} H_{\text{int}}^{\text{pp}} &= H_{22}^{\text{pp}} + (H_{31}^{\text{pp}} + h.c) + (H_{40}^{\text{pp}} + h.c) && (5.51) \\ H_{\text{int}}^{\text{pn}} &= H_{22}^{\text{pn}} + (H_{40}^{\text{pn}} + h.c) + (P_{31}^{\text{pn}} + h.c) \\ &\quad + (N_{31}^{\text{pn}} + h.c) + P_{22}^{\text{pn}} + N_{22}^{\text{pn}}, && (5.52) \end{aligned}$$

where the numerical subscripts again indicate the number of quasiparticle creation and annihilation operators in each piece of $H_{\text{int}}$.

$$\begin{aligned} H_{40}^{\text{pp}} &= -\frac{1}{4} \sum_{\substack{p_1 \cdots p_4, \\ JM}} (1+\delta_{p_1p_2})(1+\delta_{p_3p_4}) u_{p_1} u_{p_2} v_{p_3} v_{p_4} V^J_{p_1p_2p_3p_4} \\ &\quad \mathcal{A}^\dagger_{\text{pp}}(p_1p_2, JM) \tilde{\mathcal{A}}^\dagger_{\text{pp}}(p_3p_4, JM), && (5.53) \\ H_{31}^{\text{pp}} &= -\frac{1}{2} \sum_{\substack{p_1 \cdots p_4, \\ JM}} (1+\delta_{p_1p_2})(1+\delta_{p_3p_4}) V^J_{p_1p_2p_3p_4} \\ &\quad (u_{p_1} u_{p_2} u_{p_3} v_{p_4} - v_{p_1} v_{p_2} v_{p_3} u_{p_4}) \mathcal{A}^\dagger_{\text{pp}}(p_1p_2, JM) \tilde{\mathcal{D}}^\dagger_{\text{pp}}(p_3p_4, JM), && (5.54) \\ H_{22}^{\text{pp}} &= \frac{1}{4} \sum_{\substack{p_1 \cdots p_4, \\ JM}} \{(1+\delta_{p_1p_2})(1+\delta_{p_3p_4})(u_{p_1} u_{p_2} u_{p_3} u_{p_4} + v_{p_1} v_{p_2} v_{p_3} v_{p_4}) V^J_{p_1p_2p_3p_4} \\ &\quad + 4 u_{p_1} v_{p_2} u_{p_3} v_{p_4} W^J_{p_1p_2p_3p_4} \sqrt{(1+\delta_{p_1p_2})(1+\delta_{p_3p_4})(1+\delta_{p_1p_3})(1+\delta_{p_2p_4})}\} \\ &\quad \mathcal{A}^\dagger_{\text{pp}}(p_1p_2, JM) \mathcal{A}^\dagger_{\text{pp}}(p_3p_4, JM), && (5.55) \\ H_{40}^{\text{pn}} &= -\sum_{\substack{p_1 n_1 p_2 n_2, \\ JM}} V^J_{p_1n_1p_2n_2} u_{p_1} u_{n_1} v_{p_2} v_{n_2} \mathcal{A}^\dagger_{\text{pn}}(p_1n_1, JM) \tilde{\mathcal{A}}^\dagger_{\text{pn}}(p_2n_2, JM), && (5.56) \\ P_{31}^{\text{pn}} &= -\sum_{\substack{p_1 n_1 p_2 n_2, \\ JM}} V^J_{p_1n_1p_2n_2} \{u_{p_1} u_{n_1} v_{p_2} u_{n_2} \mathcal{A}^\dagger_{\text{pn}}(p_1n_1, JM) \mathcal{P}^\dagger_{\text{pn}}(p_2n_2, JM) \end{aligned}$$

$$
\begin{aligned}
& +v_{p_1}v_{n_1}u_{p_2}v_{n_2}\tilde{\mathcal{A}}^{\dagger}_{\rm pn}(p_1n_1,JM)\tilde{\mathcal{P}}^{\dagger}_{\rm pn}(p_2n_2,JM)\}, && (5.57)\\
N^{\rm pn}_{31} &= -\sum_{\substack{p_1n_1p_2n_2,\\ JM}} V^{J}_{p_1n_1p_2n_2}\{u_{p_1}u_{n_1}u_{p_2}v_{n_2}\mathcal{A}^{\dagger}_{\rm pn}(p_1n_1,JM)\mathcal{N}^{\dagger}_{\rm pn}(p_2n_2,JM) \\
& +v_{p_1}v_{n_1}u_{p_2}u_{n_2}\tilde{\mathcal{A}}^{\dagger}_{\rm pn}(p_1n_1,JM)\tilde{\mathcal{N}}^{\dagger}_{\rm pn}(p_2n_2,JM)\}, && (5.58)\\
H^{\rm pn}_{22} &= \sum_{\substack{p_1n_1p_2n_2,\\ JM}} \{(u_{p_1}u_{n_1}u_{p_2}u_{n_2}+v_{p_1}v_{n_1}v_{p_2}v_{n_2})V^{J}_{p_1n_1p_2n_2} \\
& +(u_{p_1}v_{n_1}u_{p_2}v_{n_2}+v_{p_1}u_{n_1}v_{p_2}u_{n_2})W^{J}_{p_1n_1p_2n_2}\} \\
& \mathcal{A}^{\dagger}_{\rm pn}(p_1n_1,JM)\mathcal{A}_{\rm pn}(p_2n_2,JM), && (5.59)\\
P^{\rm pn}_{22} &= -\sum_{\substack{p_1n_1p_2n_2,\\ JM}} V^{J}_{p_1n_1p_2n_2}u_{p_1}v_{n_1}v_{p_2}u_{n_2}\tilde{\mathcal{P}}^{\dagger}_{\rm pn}(p_1n_1,JM)\mathcal{P}^{\dagger}_{\rm pn}(p_2n_2,JM), && (5.60)\\
N^{\rm pn}_{22} &= -\sum_{\substack{p_1n_1p_2n_2,\\ JM}} V^{J}_{p_1n_1p_2n_2}v_{p_1}u_{n_1}u_{p_2}v_{n_2}\tilde{\mathcal{N}}^{\dagger}_{\rm pn}(p_1n_1,JM)\mathcal{N}^{\dagger}_{\rm pn}(p_2n_2,JM). && (5.61)
\end{aligned}
$$

The notations used in the above equations are defined by

$$
\begin{aligned}
\mathcal{A}^{\dagger}{}_{\rm pp}(p_1p_2,JM) &= \sum_{m_{p_1}m_{p_2}} \frac{<j_{p_1}m_{p_1}j_{p_2}m_{p_2}|JM>}{\sqrt{1+\delta_{p_1p_2}}}c^{\dagger}_{j_{p_1}m_{p_1}}c^{\dagger}_{j_{p_2}m_{p_2}}, && (5.62)\\
\mathcal{D}_{\rm pp}(p_1p_2,JM) &= \sum_{m_{p_1}m_{p_2}} <j_{p_1}m_{p_1}j_{p_2}m_{p_2}|JM>c^{\dagger}_{j_{p_1}m_{p_1}}\tilde{c}_{j_{p_2}m_{p_2}}, && (5.63)\\
\mathcal{A}^{\dagger}_{\rm pn}(p_1n_1,JM) &= \sum_{m_{p_1}m_{n_1}} <j_{p_1}m_{p_1}j_{n_1}m_{n_1}|JM>c^{\dagger}_{j_{p_1}m_{p_1}}c^{\dagger}_{j_{n_1}m_{n_1}}, && (5.64)\\
\mathcal{P}_{\rm pn}(p_1n_1,JM) &= \sum_{m_{p_1}m_{n_1}} <j_{p_1}m_{p_1}j_{n_1}m_{n_1}|JM>\tilde{c}^{\dagger}_{j_{p_1}m_{p_1}}c_{j_{n_1}m_{n_1}}, && (5.65)\\
\mathcal{N}_{\rm pn}(p_1n_1,JM) &= \sum_{m_{p_1}m_{n_1}} <j_{p_1}m_{p_1}j_{n_1}m_{n_1}|JM>\tilde{c}^{\dagger}_{j_{n_1}m_{n_1}}c_{j_{p_1}m_{p_1}}, && (5.66)
\end{aligned}
$$

with

$$
\begin{aligned}
\mathcal{A}(j_1j_2,JM) &= (\mathcal{A}^{\dagger}(j_1j_2,JM))^{\dagger}, && (5.67)\\
\tilde{\mathcal{A}}(j_1j_2,JM) &= (-1)^{J+M}\mathcal{A}(j_1j_2,J-M), && (5.68)\\
\tilde{c}_{jm} &= (-1)^{j+m}c_{j-m}. && (5.69)
\end{aligned}
$$

$W^J$ is particle-hole interaction defined by the Pandy transformation given in Eq. (3.15).

### 5.3.2 Correlated BCS wave function

Since the quasiparticle interaction term $H_{\text{int}}$ is dropped in the BCS, we can incorporate its effects approximately by using it to improve our lowest-order results with the Rayleigh-Schrödinger perturbation theory. The first-order correction terms are rather easily evaluated if we are only interested in the BCS ground state. $H_{31}$ and $H_{22}$ both contain an annihilation operator $c$ as the rightmost operator and hence give zero when operating on the BCS ground state (quasiparticle vacuum). This means that, in this order, the corrections mix the unperturbed four quasiparticle excitations with the quasiparticle vacuum via $H_{40}$. The unperturbed four quasiparticle excitations are given by section 5.2.3.

Since $H_{40}$ consists of three terms $H_{40}^{\text{pp}}$, $H_{40}^{\text{nn}}$ and $H_{40}^{\text{pn}}$, the unperturbed quasiparticle excitations connected to the ground state corrections contains three kinds of configuration, four-quasiproton, four-quasineutron and two-quasiproton two-quasineutron excitations. They are denoted as $|4\text{qp}>$, $|4\text{qn}>$ and $|2\text{qpn}>$, and corresponding to $(h = 4, l = 0)$, $(h = 0, l = 4)$ and $(h = 2, l = 2)$ in Eq. (5.49), respectively. Therefore excitation energies are given by Eq. (5.50). The *correlated* BCS ground state wave function can be represented as

$$
\begin{aligned}
|\text{CBCS}> &= \mathcal{N}(|\text{BCS}> + \sum_k \frac{<k|H_{\text{int}}|\text{BCS}>}{E_{\text{BCS}} - E_k}|k>) \\
&= \mathcal{N}(|\text{BCS}> + \sum_{4\text{qp}} \frac{<4\text{qp}|H_{40}^{\text{pp}}|\text{BCS}>}{E_{\text{BCS}} - E_{4\text{qp}}}|4\text{qp}> \\
&\quad + \sum_{4\text{qn}} \frac{<4\text{qn}|H_{40}^{\text{nn}}|\text{BCS}>}{E_{\text{BCS}} - E_{4\text{qn}}}|4\text{qn}>
\end{aligned}
$$

$$+\sum_{2\mathrm{qpn}} \frac{<2\mathrm{qpn}|H_{40}^{\mathrm{pn}}|\mathrm{BCS}>}{E_{\mathrm{BCS}}-E_{2\mathrm{qpn}}}|2\mathrm{qpn}>), \tag{5.70}$$

where $\mathcal{N}$ is the normalization factor, and $|k>$ denotes any unperturbed excitations. However, this correction is expected to be small so that the gap properties of the pairing solution are not destroyed.

In order to simplify our calculation, the interactions between like particle are assumed to be relatively small and dropped. Thus Eq. (5.70) becomes

$$|\mathrm{CBCS}>\approx \mathcal{N}(|\mathrm{BCS}>+\sum_{2\mathrm{qpn}} \frac{<2\mathrm{qpn}|H_{40}^{\mathrm{pn}}|\mathrm{BCS}>}{E_{\mathrm{BCS}}-E_{2\mathrm{qpn}}}|2\mathrm{qpn}>). \tag{5.71}$$

The word *correlated* implies including the quasiparticle correlation terms in Eqs.(5.70,5.71).

### 5.3.3 Construction of two-quasiproton two-quasineutron excitations in the J-scheme

The two-proton and two-neutron doublet excitations $|2\mathrm{qpn}>$ are simply obtained by choosing $h = l = 2$ in Eq. (5.49) in the m-scheme, where one normalized factor may be introduced. But if we are only interested in some special J values, the J-scheme representation is useful because of rather smaller dimensions involved. For example, only J=1 excitations are needed in Gamow-Teller transitions. Thus we define a two-quasiproton two-quasineutron doublet creation operator in the J-scheme,

$$\begin{aligned} B^{\dagger}_{J'J''}(p_1n_1p_2n_2,JM) &= N_B(\mathcal{A}^{\dagger}(p_1n_1,J'M')\otimes\mathcal{A}^{\dagger}(p_2n_2,J''M''))^{JM} \\ &= N_B\sum_{M'M''} <J'M'J''M''|JM> \\ &\quad \times\mathcal{A}^{\dagger}(p_1n_1,J'M')\mathcal{A}^{\dagger}(p_2n_2,J''M''), \end{aligned} \tag{5.72}$$

where $N_B$ is the normalization factor of $B^+$. The two-quasiproton two-quasineutron excitations are given by

$$|2\mathrm{qpn}>=B^{\dagger}_{J'J''}(p_1n_1p_2n_2,JM)|\mathrm{BCS}>. \tag{5.73}$$

However, when one constructs the $|2\text{qpn}>$ excitations, identical states must be excluded in order to avoid double counting.

The normalization factor $N_B$ is determined by

$$\begin{aligned} <2\text{qpn}|2\text{qpn}> &= <\text{BCS}|B_{J'J''}(p_1n_1p_2n_2, JM)B^{\dagger}_{J'J''}(p_1n_1p_2n_2, JM)|\text{BCS}> \\ &= 1. \end{aligned} \tag{5.74}$$

Then we obtain,

$$\begin{aligned} N_B^{-2} &= 1 + (-1)^{j_{n_1}+j_{n_2}+J}(2J+1)(2J'+1)(2J''+1)\delta_{p_1p_2}\begin{Bmatrix} j_{p_1} & j_{n_1} & J' \\ j_{n_2} & j_{p_2} & J'' \\ J'' & J' & J \end{Bmatrix} \\ &\quad +(-1)^{j_{p_1}+j_{p_2}+J}(2J+1)(2J'+1)(2J''+1)\delta_{n_1n_2}\begin{Bmatrix} j_{n_1} & j_{p_1} & J' \\ j_{p_2} & j_{n_2} & J'' \\ J'' & J' & J \end{Bmatrix}. \\ &\quad +\delta_{J'J''}\delta_{p_1p_2}\delta_{n_1n_2}. \end{aligned} \tag{5.75}$$

Since the BCS ground state has spin $J = 0$ (see Eq. (5.37)), only $J = 0$ two-quasiproton two-quasineutron excitations in Eq. (5.73) contribute to the ground state correction. Therefore we have $J' = J''$ and $M' = -M''$. Then two-quasiproton two-quasineutron excitations used in the correlated BCS wave function are restricted to

$$\begin{aligned} |2\text{qpn}> &= N_B B^{\dagger}_{J'J'}(p_1n_1p_2n_2, 00)|\text{BCS}> \\ &= |(p_1n_1)^{J'}(p_2n_2)^{J'}> . \end{aligned} \tag{5.76}$$

The last notation will be frequently used in later discussions.

According to perturbation theory, all unperburbed states involved in Eq. (5.71) must form an orthogonal basis. But the excitations created by Eq. (5.73) or (5.76) are not orthogonal each other. Let's consider any two states,

$$|k> \;=\; |2\text{qpn}>= N_B B^{\dagger}_{JJ}(p_1 n_1 p_2 n_2, 00)|\text{BCS}> , \tag{5.77}$$

$$|k'> \;=\; |2\text{qpn}'>= N_{B'} B^{\dagger}_{J'J'}(p'_1 n'_1 p'_2 n'_2, 00)|\text{BCS}> . \tag{5.78}$$

The orthogonal condition requires $< k|k' >= \delta_{kk'}$. But the overlap between them is

$$\begin{aligned}
\chi_{kk'} &= < \text{BCS}|B_{JJ}(p_1 n_1 p_2 n_2, 00) B^{\dagger}_{J'J'}(p'_1 n'_1 p'_2 n'_2, 00)|\text{BCS}> \\
&= N_B N_{B'}\{\delta_{p_1 p'_1}\delta_{n_1 n'_1}\delta_{p_2 p'_2}\delta_{n_2 n'_2}\delta_{JJ'} \\
&\quad +(-1)^{j_{n_1}+j_{n_2}+J+J'}(2J+1)(2J'+1)\left\{\begin{array}{ccc} j_{p_1} & j_{n_1} & J \\ j_{n_2} & j_{p_2} & J \\ J' & J' & 0 \end{array}\right\}\delta_{p_1 p'_2}\delta_{n_1 n'_1}\delta_{p_2 p'_1}\delta_{n_2 n'_2} \\
&\quad +(-1)^{j_{p_1}+j_{p_2}+J+J'}(2J+1)(2J'+1)\left\{\begin{array}{ccc} j_{n_1} & j_{p_1} & J \\ j_{p_2} & j_{n_2} & J \\ J' & J' & 0 \end{array}\right\}\delta_{p_1 p'_1}\delta_{n_1 n'_2}\delta_{p_2 p'_2}\delta_{n_2 n'_1} \\
&\quad +\delta_{p_1 p'_2}\delta_{n_1 n'_2}\delta_{p_2 p'_1}\delta_{n_2 n'_1}\delta_{JJ'}\},
\end{aligned} \tag{5.79}$$

where $N_B$ and $N_{B'}$ are the normalization factors for states $|2\text{qpn} >$ and $|2\text{qpn}' >$.

The $\chi_{kk'}$ is nonzero only for the following cases,

(A) $p_1 = p'_1 \; n_1 = n'_1 \; p_2 = p'_2 \; n_2 = n'_2 \; J = J'$

(B) $p_1 = p'_2 \; n_1 = n'_2 \; p_2 = p'_1 \; n_2 = n'_1 \; J = J'$

(C) $p_1 = p'_2 \; n_1 = n'_1 \; p_2 = p'_1 \; n_2 = n'_2 \; J, \; J'$

(D) $p_1 = p'_2 \; n_1 = n'_2 \; p_2 = p'_2 \; n_2 = n'_2 \; J, \; J'$.

For case (A) or (B), it is easy to obtain $\chi = 1$. It indicates that states $|2\text{qpn} >$ and $|2\text{qpn}' >$ are identical. On the other hand, we can exclude all double counted $|2\text{qpn} >$ states through this overlap procedure. For cases (C) and (D), $0 < \chi < 1$ implies that two states are not orthogonal.

We have to use the Gram-Schmidt orthogonalization procedure to obtain normalized orthogonal states from the normalized nonorthogonal states |2qpn > ( in fact, they are not linearly independent ). Finally, we obtain

$$|p_1n_1p_2n_2,k>=\sum_i \alpha_{ik}|(p_1n_1)^{J_i}(p_2n_2)^{J_i}> . \tag{5.80}$$

The coefficients $\alpha$ are obtained from orthogonalization which relate to $\chi$. For the new state $|p_1n_1p_2n_2,k>$, we have

$$<p_1n_1p_2n_2,k|p_1n_1p_2n_2,k'>=\delta_{kk'}. \tag{5.81}$$

These states will be employed to calculate the first-order perturbation.

The excitation energy for state $|p_1n_1p_2n_2,k>$ is given by

$$E_k=(E_{\text{BCS}}+E_{p_1}+E_{p_2}+E_{n_1}+E_{n_2}). \tag{5.82}$$

So the energy denominator in Eq. (5.71) is

$$E_{\text{BCS}}-E_k=-(E_{p_1}+E_{p_2}+E_{n_1}+E_{n_2}). \tag{5.83}$$

### 5.3.4 Formalism of extended BCS theory

Based on the discussions in the last subsection, we can start to work on the formalism of the extended BCS theory. In this subsection, we will derive the correlated BCS wave function expression, occupation probability and energy shift, and so on. One inserts $|p_1n_1p_2n_2,k>$ into Eq. (5.71) instead of |2qpn >, the correction terms become

$$\sum_{\text{2qpn}}\frac{<\text{2qpn}|H_{40}^{\text{pn}}|\text{BCS}>}{E_{\text{BCS}}-E_{\text{2qpn}}}|\text{2qpn}>$$

$$=-\sum_{\substack{p_1n_1p_2n_2\\k}}\frac{<p_1n_1p_2n_2,k|H_{40}^{\text{pn}}|\text{BCS}>}{E_{p_1}+E_{n_1}+E_{p_2}+E_{n_2}}|p_1n_1p_2n_2,k>$$

$$= - \sum_{\substack{p_1 n_1 p_2 n_2 \\ k}} \frac{\sum_i \alpha_{ki} < \mathrm{BCS}|B_{J_iJ_i}(p_1n_1p_2n_2,00)H_{40}^{\mathrm{pn}}|\mathrm{BCS} >}{E_{p_1} + E_{n_1} + E_{p_2} + E_{n_2}}$$

$$\times \sum_j \alpha_{kj} B^{\dagger}_{J_jJ_j}(p_1n_1p_2n_2,00)|\mathrm{BCS}>$$

$$= - \sum_{\substack{p_1 n_1 p_2 n_2 \\ j}} \frac{\sum_k \sum_i \alpha_{ki}\alpha_{kj} < \mathrm{BCS}|B_{J_iJ_i}(p_1n_1p_2n_2,00)H_{40}^{\mathrm{pn}}|\mathrm{BCS} >}{E_{p_1} + E_{n_1} + E_{p_2} + E_{n_2}}$$

$$\times B^{\dagger}_{J_jJ_j}(p_1n_1p_2n_2,00)|\mathrm{BCS}> , \tag{5.84}$$

where the matrix element in above equation is

$$< \mathrm{BCS}|B_{J_iJ_i}(p_1n_1p_2n_2,00)H_{40}^{\mathrm{pn}}|\mathrm{BCS} >= -N_{Bi}\sqrt{2J_i+1}G^{J_i}_{p_1n_1p_2n_2}, \tag{5.85}$$

with

$$\begin{aligned} G^{J_i}_{p_1n_1p_2n_2} &= V^{J_i}_{p_1n_1p_2n_2}(u_{p_1}u_{n_1}v_{p_2}v_{n_2} + v_{p_1}v_{n_1}u_{p_2}u_{n_2}) \\ &\quad -W^{J_i}_{p_1n_1p_2n_2}(v_{p_1}u_{n_1}u_{p_2}v_{n_2} + u_{p_1}v_{n_1}v_{p_2}u_{n_2}). \end{aligned} \tag{5.86}$$

Therefore the correlated BCS wave function in Eq. (5.71) is given by

$$|\mathrm{CBCS} >= \mathcal{N}\{1 + \sum_{\substack{p_1 n_1 p_2 n_2 \\ j}} \frac{F_{p_1n_1p_2n_2}}{E_{p_1} + E_{n_1} + E_{p_2} + E_{n_2}} B^{\dagger}_{J_jJ_j}(p_1n_1p_2n_2,00)\}|\mathrm{BCS}> , \tag{5.87}$$

where

$$F_{p_1n_1p_2n_2} = \sum_k \sum_i N_{Bi}\alpha_{ki}\alpha_{kj}\sqrt{2J_i+1}G^{J_i}_{p_1n_1p_2n_2}. \tag{5.88}$$

One finds $F$ is a function of $j$ where $k$ and $i$ are already summed over. The normalization factors in Eq. (5.87) can be calculated from,

$$< \mathrm{CBCS}|\mathrm{CBCS} >= 1. \tag{5.89}$$

Then we obtain

$$\mathcal{N}^{-2} = 1 + \sum_{\substack{p_1 n_1 p_2 n_2 \\ p_1' n_1' p_2' n_2'}} \frac{F_{p_1 n_1 p_2 n_2} F_{p_1' n_1' p_2' n_2'} \chi_{p_1 n_1 p_2 n_2, p_1' n_1' p_2' n_2'}}{(E_{p_1} + E_{n_1} + E_{p_2} + E_{n_2})(E_{p_1'} + E_{n_1'} + E_{p_2'} + E_{n_2'})}, \tag{5.90}$$

where $\chi$ is the overlap between states $|(p_1 n_1)^{J_i}(p_2 n_2)^{J_i} >$ and $|(p_1' n_1')^{J_i'}(p_2' n_2')^{J_i'} >$, which is presented in Eq. (5.79).

The correlated BCS wave function is required to have correct mean proton and neutron numbers, and we have

$$< \mathrm{CBCS}|\hat{N}_\pi|\mathrm{CBCS} > \; = \; N_\pi \tag{5.91}$$

$$< \mathrm{CBCS}|\hat{N}_\nu|\mathrm{CBCS} > \; = \; N_\nu \tag{5.92}$$

where $\hat{N}_\pi(\hat{N}_\nu)$ is the proton ( neutron ) number operator. We evaluate the left side of these equations and obtain,

$$N_\pi \; = \; \sum_p (2j_p + 1)v_p^2 + \mathcal{N}^2 \sum_{p_1 n_1 p n_2} \left(\frac{F_{p_1 n_1 p n_2}}{E_{p_1} + E_{n_1} + E_p + E_{n_2}}\right)^2, \tag{5.93}$$

$$N_\nu \; = \; \sum_n (2j_n + 1)v_n^2 + \mathcal{N}^2 \sum_{p_1 p_2 n_1 n} \left(\frac{F_{p_1 n_1 p_2 n}}{E_{p_1} + E_{n_1} + E_{p_2} + E_n}\right)^2. \tag{5.94}$$

Eqs. (5.23-5.28,5.33-5.36,5.93,5.94 ) are called the extended BCS equations. They can be solved iteratively as well. We point out that parameters $v_p^2$ and $v_n^2$ have lost the physical interpretations of occupation probabilities, because of the existing additional terms in Eq. (5.93,5.94).

The correlated BCS ground state energy $E_{\mathrm{corr}}$ is obtained by second-order perturbation theory,

$$E_{\mathrm{corr}} = E_{\mathrm{BCS}} + E^{(1)} + E^{(2)}. \tag{5.95}$$

where

$$
\begin{aligned}
E^{(1)} &= 0, && (5.96)\\
E^{(2)} &= \sum_{\substack{p_1 n_1 p_2 n_2\\ k}} \frac{|<k|H_{40}^{\mathrm{pn}}|\mathrm{BCS}>|^2}{E_{\mathrm{BCS}}-E_k} \\
&= -\sum_{\substack{p_1 n_1 p_2 n_2\\ k}} \frac{(\sum_i \alpha_{ki} N_{Bi}\sqrt{2J_i+1}\,G^{J_i}_{p_1 n_1 p_2 n_2})^2}{E_{p_1}+E_{n_1}+E_{p_2}+E_{n_2}}. && (5.97)
\end{aligned}
$$

$E_{\mathrm{BCS}}$ is given by Eq. (5.48).

## 5.4 Application

We have applied the extended BCS theory to study the ground state properties of $^{46}$Ti. The occupation probabilities and the quasiparticle energies are calculated from the extended BCS equation Eqs. (5.23-5.28,5.33-5.36,5.93,5.94). They are solved iteratively with constrained proton and neutron numbers to be 2 and 4, respectively. In our calculation, the spurious states discussed in Appendix F are not projected out yet.

The occupation probabilities obtained from the extended BCS $<\mathrm{CBCS}|a_j^\dagger a_j|\mathrm{CBCS}>/(2j+1)$ are given in Table 5.1 and compared to the BCS and the full-basis shell-model calculations. We find the extended BCS calculation improves upon the BCS occupation numbers, bring them more in line with the full-basis shell-model result.

The extended BCS parameters are presented in Table 5.2. We find that $v^2$ are not equal to the relevant occupation probabilities given in Table 5.1. In the extended BCS, the Fermi level of proton and neutron are −13.216 MeV and −10.942 MeV. In the BCS, they are −12.968 MeV and −10.868 MeV, respectively.

Table 5.1: $^{46}$Ti: The occupation probabilities $< |a^{\dagger}_{jm} a_{jm}| > /(2j+1)$ for protons and neutrons obtained from the BCS, extended BCS (EBCS) and shell-model calculations, respectively.

| level | BCS | EBCS | Shell model |
|---|---|---|---|
| $\pi f_{7/2}$ | 0.239 | 0.222 | 0.187 |
| $\pi p_{3/2}$ | 0.009 | 0.022 | 0.078 |
| $\pi f_{5/2}$ | 0.008 | 0.020 | 0.022 |
| $\pi p_{1/2}$ | 0.004 | 0.008 | 0.031 |
| | | | |
| $\nu f_{7/2}$ | 0.480 | 0.459 | 0.404 |
| $\nu p_{3/2}$ | 0.018 | 0.036 | 0.092 |
| $\nu f_{5/2}$ | 0.013 | 0.027 | 0.054 |
| $\nu p_{1/2}$ | 0.007 | 0.011 | 0.040 |

Table 5.2: The extended BCS parameters, $u_i^2$, $v_i^2$, gap parameters $\Delta_i$ (MeV) and quasiparticle energies $E_i$ (MeV) for $^{46}$Ti

| level | $u_i^2$ | $v_i^2$ | $\Delta_i$ | $E_i$ |
|---|---|---|---|---|
| $\pi f_{7/2}$ | 0.817 | 0.183 | 1.203 | 1.556 |
| $\pi p_{3/2}$ | 0.992 | 0.008 | 0.911 | 5.105 |
| $\pi f_{5/2}$ | 0.993 | 0.007 | 1.314 | 7.592 |
| $\pi p_{1/2}$ | 0.996 | 0.004 | 0.874 | 7.275 |
| | | | | |
| $\nu f_{7/2}$ | 0.546 | 0.454 | 1.447 | 1.453 |
| $\nu p_{3/2}$ | 0.983 | 0.017 | 1.104 | 4.236 |
| $\nu f_{5/2}$ | 0.987 | 0.013 | 1.574 | 7.076 |
| $\nu p_{1/2}$ | 0.993 | 0.007 | 1.069 | 6.478 |

## 5.5 Summary

In this Chapter, we re-derived the BCS equations for proton-neutron systems in an angular momentum coupling space. The correlated BCS wave function is introduced through first-order perturbation theory, where the quasiparticle interactions $H_{\text{int}}$ dropped in BCS theory are incorporated approximately. In order to simplify our calculations, we only consider the proton-neutron interaction term in $H_{\text{int}}$ which is believed to be more important than the like particle interactions. The two-quasiproton two-quasineutron doublet excitations in the correlated BCS ground state are introduced and discussed in the J-scheme. Since the excitations may be not orthogonal to each other, the Gram-Schmidt orthogonalization method is employed to obtain a new orthogonal basis.

We also present the extended BCS equations based on the correlated BCS wave function. We applied the extended BCS equation to the study of the ground state properties of $^{46}$Ti and found that the the occupation probabilities have been improved compared to the standard BCS. The correlated BCS wave function will be employed to develop the extended pnQRPA equation in the next Chapter.

The extended BCS equations in angular momentum coupled space is given in Appendix E. The spurious states due to the violation of particle-number conservation will be discussed in Appendix F.

# Chapter 6

# Extended pnQRPA Theory and Applications

## 6.1 Introduction

In Chapter 3 and Chapter 4, we tested the validity and accuracy of the pnQRPA as a model to study $\beta^+$ and $\beta\beta$ decays. The tests were carried out by making the comparisons of the pnQRPA and the full-basis shell-model calculations. The comparison consisted of (1) for $\beta^+$ decay: the total $B(\mathrm{GT}^+)$ value, strength distributions, COBTD and CTME, (2) for $2\nu\beta\beta$ decay: the energy-dependent and the closure double-beta decay matrix elements ($M_{\mathrm{GT}}$ and $B_{\mathrm{CLS}}$), and their distributions with respect to the excitations. We found that the pnQRPA does not give a sufficient suppression for transition strength and presents a large discrepancy between the pnQRPA and shell model in the shape of the strength distributions. We concluded that maybe some correlations which are important to $\beta^+$ and $\beta\beta$ decay have not been included in the pnQRPA. The " hybrid " models, where the shell-model parameters are used in the pnQRPA, improve the calculations in $\beta^+$ decay but fail in $2\nu\beta\beta$ decay. On the other hand, the " hybrid " models are purely empirical improvements, which lack any solid theoretical background. Thus it is important and may be possible to develop a new kind of equation, in which more correlations are taken into account from the theory of many-body problem.

In Chapter 5, the correlated BCS wave function was introduced and the relevant extended BCS equation was derived as well. In this Chapter, we will derive an extended pnQRPA equation based on using the correlated BCS wave function to calculate the matrix elements in the equation. In section 6.2 and 6.3, the derivations and applications of the extended pnQRPA are presented. $\beta^+$ decay of $^{46}$Ti and $\beta\beta$ decay of $^{46}$Ca are employed again as examples. In section 6.4, we give a summary and conclusion.

## 6.2 Extended pnQRPA Equations

We start with the equation of motion which we discussed in Chapter 3,

$$<\mathrm{QRPA}|[\delta Q_\nu,[H,Q_\nu^\dagger]]|\mathrm{QRPA}>=\hbar\omega<\mathrm{QRPA}|[\delta Q_\nu,Q_\nu^\dagger]|\mathrm{QRPA}> \tag{6.1}$$

where $\hbar\omega = E_\nu - E_0$ and $Q_\nu^\dagger$ is phonon creation operator,

$$Q_\nu^\dagger(J,M)=\sum_{p,n}(X_\nu^{pn}\mathcal{A}_{\mathrm{pn}}^\dagger(pn,JM)-Y_\nu^{pn}\tilde{\mathcal{A}}_{\mathrm{pn}}(pn,JM)). \tag{6.2}$$

The excitations are given by

$$|\nu>=Q^\dagger|\mathrm{QRPA}>. \tag{6.3}$$

The operators $\mathcal{A}_{\mathrm{pn}}^\dagger(pn,JM)$ are two quasiparticle creation and destruction operators defined by Eq. (3.5) and $\tilde{\mathcal{A}}_{\mathrm{pn}}(pn,JM)$ is defined by Eq. (3.7). The Hamiltonian is given by Eq. (5.45). $|\mathrm{QRPA}>$ is the QRPA ground state defined in Appendix A.

By choosing variational operators $\delta Q_\nu$ as $\mathcal{A}_{\rm pn}(pn, JM)$ and $\tilde{\mathcal{A}}^\dagger_{\rm pn}(pn, JM)$, we obtain

$$\begin{pmatrix} A & B \\ -B^* & -A^* \end{pmatrix} \begin{pmatrix} X \\ Y \end{pmatrix} = \hbar\omega \begin{pmatrix} X \\ Y \end{pmatrix} . \tag{6.4}$$

It appears the same as the pnQRPA form (Eq. (3.9)). But the matrix elements $A$ and $B$ derived by using the |CBCS > rather than the |BCS > as follows are given by

$$\begin{aligned} A^J_{pnp'n'} &= <\mathrm{QRPA}|[\mathcal{A}_{\rm pn}(pn, JM), [H, \mathcal{A}^\dagger_{\rm pn}(p'n', JM)]]|\mathrm{QRPA}> \\ &\simeq <\mathrm{CBCS}|[\mathcal{A}_{\rm pn}(pn, JM), [H, \mathcal{A}^\dagger_{\rm pn}(p'n', JM)]]|\mathrm{CBCS}> \\ &\simeq (E_p + E_n)\delta_{pp'}\delta_{nn'} + (H^{\rm pn}_{22})^J_{pnp'n'} + (\Delta A)^J_{pnp'n'} \qquad (6.5) \\ B^J_{pnp'n'} &= <\mathrm{QRPA}|[\mathcal{A}_{\rm pn}(pn, JM), [H, \tilde{\mathcal{A}}_{\rm pn}(p'n', JM)]]|\mathrm{QRPA}> \\ &\simeq <\mathrm{CBCS}|[\mathcal{A}_{\rm pn}(pn, JM), [H, \tilde{\mathcal{A}}_{\rm pn}(p'n', JM)]]|\mathrm{CBCS}> \\ &\simeq -(G^{\rm pn})^J_{pnp'n'} + (\Delta B)^J_{pnp'n'} \qquad (6.6) \end{aligned}$$

where

$$\begin{aligned} (H^{\rm pn}_{22})^J_{pnp'n'} &= g_{pp} V^J_{pnp'n'}(u_p u_n u_{p'} u_{n'} + v_p v_n v_{p'} v_{n'}) \\ &\quad + g_{ph} W^J_{pnp'n'}(u_p v_n u_{p'} v_{n'} + v_p u_n v_{p'} u_{n'}) \qquad (6.7) \\ (G^{\rm pn})^J_{pnp'n'} &= g_{pp} V^J_{pnp'n'}(u_p u_n v_{p'} v_{n'} + v_p v_n u_{p'} u_{n'}) \\ &\quad - g_{ph} W^J_{pnp'n'}(v_p u_n u_{p'} v_{n'} + u_p v_n v_{p'} u_{n'}) \qquad (6.8) \end{aligned}$$

In Eqs. (6.5,6.6), we approximate |QRPA > by |CBCS >. ( In the pnQRPA, we approximate |QRPA > to |BCS >, see Eqs. (3.11,3.12)). |CBCS > is the correlated BCS wave function introduced in Chapter 5. The corrections are expressed by

$$\begin{aligned} (\Delta A)^J_{pnp'n'} &= 2\delta_{pp'}\delta_{nn'}\{ \sum_{\substack{p_1 p_2 n_2 \\ J'}} \frac{G^{J'}_{p_1 n p_2 n_2} F_{p_1 n p_2 n_2}}{E_{p_1} + E_n + E_{p_2} + E_{n_2}} (\frac{\sqrt{2J'+1}}{2j_n + 1}) \\ &\quad + \sum_{\substack{p_2 n_1 n_2 \\ J'}} \frac{G^{J'}_{p n_1 p_2 n_2} F_{p n_1 p_2 n_2}}{E_p + E_{n_1} + E_{p_2} + E_{n_2}} (\frac{\sqrt{2J'+1}}{2j_p + 1}) \} \qquad (6.9) \end{aligned}$$

$$
\begin{aligned}
(\Delta B)^{J}_{pnp'n'} &= 4\sum_{\substack{p_1 n_1 \\ J'}} \sqrt{2J'+1} \left\{ \begin{array}{ccc} j_p & j_n & J \\ j_{p'} & j_{n'} & J' \end{array} \right\} \{ \frac{(H^{pn}_{22})^{J'}_{pn'p_1n_1} F_{p_1n_1p'n}}{E_{p_1}+E_{n_1}+E_{p'}+E_n} \\
&\quad + \frac{(H^{pn}_{22})^{J'}_{p'np_1n_1} F_{p_1n_1pn'}}{E_{p_1}+E_{n_1}+E_{p}+E_{n'}} \} \qquad (6.10)
\end{aligned}
$$

The quasiparticle energies $E$ and parameters $u, v$ are obtained by solving the extended BCS equation in subsection 5.3.4. The quantities $F_{p_1n_1p_2n_2}$ are given by Eq. (5.88). And (V) and (W) are the particle-particle and particle-hole interaction matrix elements, respectively. In $\Delta A$, all off-diagonal matrix elements are equal to zero because of Clebsch-Gordan coefficient coupling. However, they are not zeros in m-scheme or uncoupled space. Eqs. (6.4—6.10) are called the extended pnQRPA equations.

Now we calculate the transition matrix elements between excited states and ground state for a one-body operator $\hat{O}$,

$$
\begin{aligned}
< \nu|\hat{O}|\mathrm{QRPA} > &= < \mathrm{QRPA}|[Q_\nu, \hat{O}]|\mathrm{QRPA} > \\
&\simeq < \mathrm{CBCS}|[Q_\nu, \hat{O}]|\mathrm{CBCS} > \\
&= \mathcal{N}^2 \{ < \mathrm{BCS}|[Q_\nu, \hat{O}]|\mathrm{BCS} > \\
&\quad + \sum_{\substack{2\mathrm{qpn} \\ 2\mathrm{qpn}'}} \frac{< 2\mathrm{qpn}|H^{\mathrm{pn}}_{40}|\mathrm{BCS} >< 2\mathrm{qpn}'|H^{\mathrm{pn}}_{40}|\mathrm{BCS} >}{(E_{\mathrm{BCS}} - E_{2\mathrm{qpn}})(E_{\mathrm{BCS}} - E_{2\mathrm{qpn}'})} \\
&\quad \times < 2\mathrm{qpn}'|[Q_\nu, \hat{O}]|2\mathrm{qpn} > \qquad (6.11) \\
&\simeq < \mathrm{BCS}|[Q_\nu, \hat{O}]|\mathrm{BCS} > . \qquad (6.12)
\end{aligned}
$$

In Eq. (6.12), we keep the zero-order term and drop the second-order terms. The first-order term is zero. Therefore for Gamow-Teller operator, the transition matrix elements are given by

$$
\begin{aligned}
B(\mathrm{GT}^-) &= \{M_\nu(\mathrm{GT}^-)\}^2 \simeq \{\sum_{pn} < p||\sigma||n > (X^{pn}_\nu u_p v_n + Y^{pn}_\nu v_p u_n)\}^2 \qquad (6.13) \\
B(\mathrm{GT}^+) &= \{M_\nu(\mathrm{GT}^+)\}^2 \simeq \{-\sum_{pn} < p||\sigma||n > (X^{pn}_\nu v_p u_n + Y^{pn}_\nu u_p v_n)\}^2 \qquad (6.14)
\end{aligned}
$$

where $\sigma$ is the Pauli spin operator. Although above equations have the same expression as Eqs.(3.18,3.19) in Chapter 3, the amplitudes $X$ and $Y$ are obtained by the extended pnQRPA rather than the pnQRPA, and $u, v$ factors are obtained by the extended BCS in Chapter 5 rather than the standard BCS.

## 6.3 Application and Discussions

We apply the extended pnQRPA equation to study the $\beta^+$ Gamow-Teller transition of $^{46}\mathrm{Ti} \rightarrow ^{46}\mathrm{Sc}$. The running sum $B(\mathrm{GT}^+)$ in the extended pnQRPA is presented in Figure 6.1 as a function of the excitation energy and compared with those in the pnQRPA and shell model. We find that total $B(\mathrm{GT}^+)$ is suppressed. It goes about half way between the pnQRPA and shell-model results. Actually, there is a competition between a suppression and an enhancement mechanism in our case. The suppression mechanisms are mainly from the off-diagonal terms in $\Delta B$ and the new $u, v$ parameters. The enhancement mechanisms are due to the positive $\Delta A$ values in the extended pnQRPA. In our calculation, almost all strengths are suppressed except the first one. The relatively strong enhancement in the $B(\mathrm{GT}^+)$ at the first excited state arises in the $\Delta A$ term from the $(\pi f_{7/2} \nu f_{7/2}, \pi f_{7/2} \nu f_{7/2})$ four quasiparticle configuration, which corresponds to the smallest energy denominator in Eq. (6.9). We know the first $B(\mathrm{GT}^+)$ is dominated by this configuration. Our calculation shows the enhanced strength is almost equal to the suppressed strength so that the first $B(\mathrm{GT}^+)$ is unchanged. The energy of the lowest state is shifted up about 0.1 MeV. The calculation has shown that the $B(\mathrm{GT}^+)$ strength in the second state has the largest suppression, which decreases 30 %.

The COBTD and CTME values are given in Table 6.1 and 6.2. Comparing to the pnQRPA and shell-model calculations, the COBTD and the CTME for $f_{7/2} \rightarrow f_{5/2}$

Table 6.1: Comparison of the coherent one-body transition density (COBTD) obtained for the pnQRPA, extended pnQRPA and shell model calculations of $^{46}$Ti. The labels represent (A): COBTD in the pnQRPA ; (B): COBTD in the extended pnQRPA ; (C): COBTD in the shell model.

| $j_p \rightarrow j_n$ | A | B | C |
|---|---|---|---|
| $f_{7/2} \rightarrow f_{7/2}$ | 0.034 | 0.048 | -0.096 |
| $f_{7/2} \rightarrow f_{5/2}$ | 0.443 | 0.375 | 0.386 |
| $p_{3/2} \rightarrow p_{3/2}$ | 0.002 | 0.001 | 0.006 |
| $p_{3/2} \rightarrow f_{5/2}$ | -0.001 | -0.001 | 0.017 |
| $p_{3/2} \rightarrow p_{1/2}$ | 0.005 | 0.005 | 0.060 |
| $f_{5/2} \rightarrow f_{7/2}$ | 0.088 | 0.081 | 0.086 |
| $f_{5/2} \rightarrow p_{3/2}$ | 0.001 | 0.001 | 0.010 |
| $f_{5/2} \rightarrow f_{5/2}$ | 0.001 | -0.002 | -0.011 |
| $p_{1/2} \rightarrow p_{3/2}$ | 0.003 | 0.003 | 0.009 |
| $p_{1/2} \rightarrow p_{1/2}$ | -0.001 | 0.000 | -0.003 |

is improved but the $f_{7/2} \rightarrow f_{7/2}$ and $f_{5/2} \rightarrow f_{7/2}$ terms become worse, and the $p \rightarrow p$ terms are almost the same as those in the pnQRPA.

We note the sum rule in Eq. (2.1) is violated in our calculations. This is because we have dropped the second-order terms in Eqs. (6.13, 6.14). (There are about twenty terms in the second-order corrections.) The violation is around 10 % in our example.

We now apply the extended pnQRPA to calculate the double-beta decay matrix elements of $^{46}$Ca. Figure 6.2 and 6.3 show the running sum of the closure matrix element $B_{\mathrm{CLS}}$ and energy dependent matrix element $M_{\mathrm{GT}}$ as the function of the excitation energy. Suppression of the transition is found but not enough to reproduce the shell-model result. For $^{46}$Ca, since the proton occupations are zero, we have $v_p = 0$ and $G^{J'}_{p_1 n_1 p_2 n_2} = 0$, so consequently all the corrections are zero, the extended pnQRPA reduces to the pnQRPA. Thus the excitation energies in the extended pnQRPA shown in Figure 6.2 are identical to those of the pnQRPA.

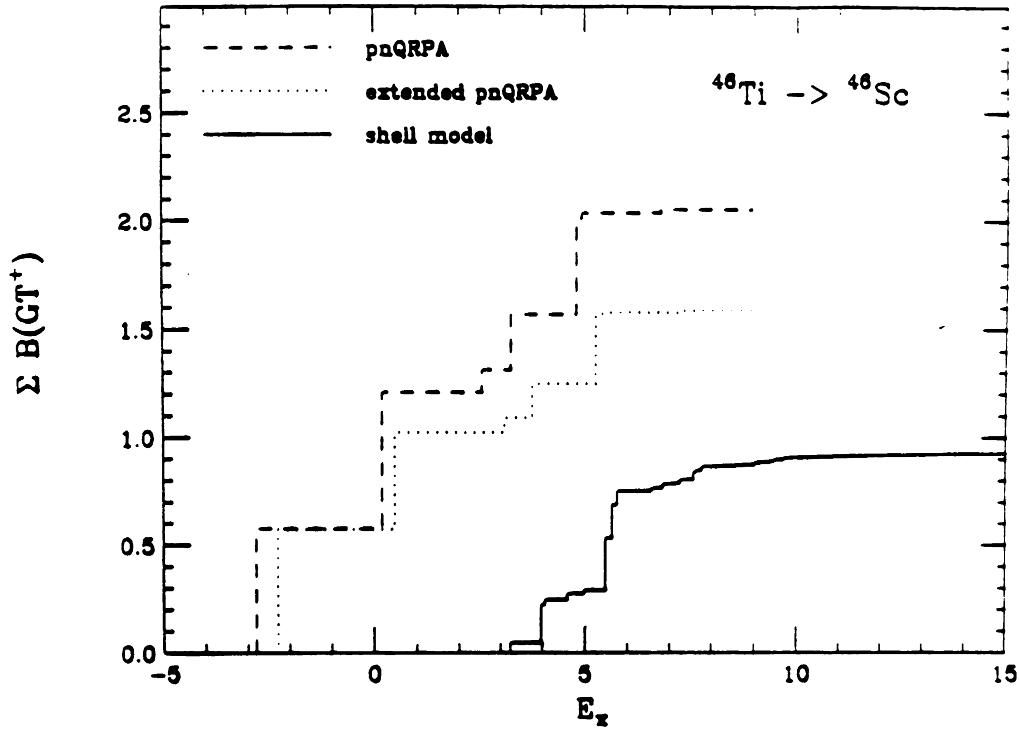

Figure 6.1: Summed Gamow-Teller strength for $^{46}$Ti $\rightarrow$$^{46}$Sc. The solid line, the dashed line and the dotted line are obtained by the shell model, pnQRPA and extended pnQRPA, respectively.

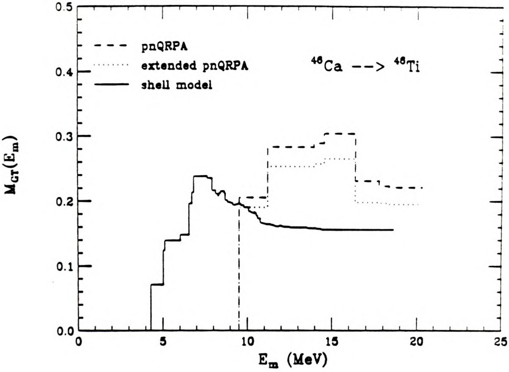

Figure 6.2: Summed energy dependent $2\nu\beta\beta$ decay matrix element $M_{\rm GT}(E_m)$ as the function of the excitation energies, the solid line, the dashed line and the dotted line are obtained by the shell model, pnQRPA and extended pnQRPA, respectively

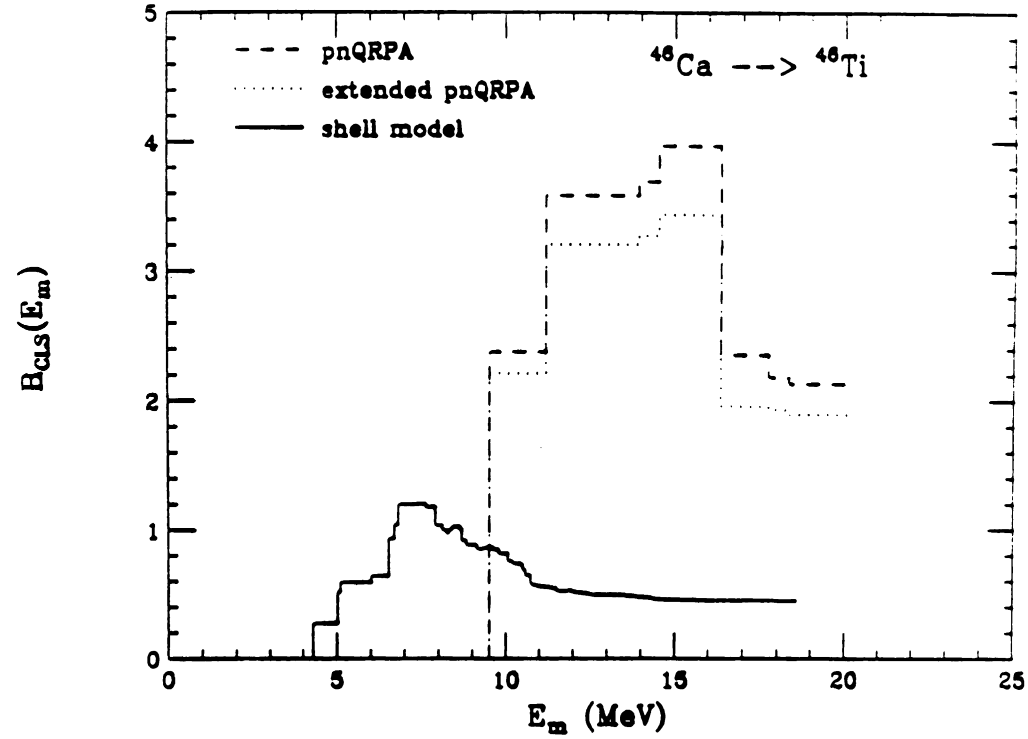

Figure 6.3: Summed closure $2\nu\beta\beta$ decay matrix element $B_{\mathrm{CLS}}(E_m)$ as the function of the excitation energies, the solid line, the dashed line and the dotted line are obtained by the shell model, pnQRPA and extended pnQRPA, respectively

Table 6.2: Comparison of the coherent transition matrix elements (CTME) obtained in the pnQRPA, extended pnQRPA and shell model calculations of $^{46}$Ti. Labels (A), (B) and (C) are given by Table 6.1

| $j_p \rightarrow j_n$ | A | B | C |
|---|---|---|---|
| $f_{7/2} \rightarrow f_{7/2}$ | 0.108 | 0.155 | -0.308 |
| $f_{7/2} \rightarrow f_{5/2}$ | 1.641 | 1.387 | 1.431 |
| $p_{3/2} \rightarrow p_{3/2}$ | 0.005 | 0.003 | 0.014 |
| $p_{3/2} \rightarrow f_{5/2}$ | 0.000 | 0.000 | 0.000 |
| $p_{3/2} \rightarrow p_{1/2}$ | 0.011 | 0.011 | 0.139 |
| $f_{5/2} \rightarrow f_{7/2}$ | -0.325 | -0.299 | -0.319 |
| $f_{5/2} \rightarrow p_{3/2}$ | 0.000 | 0.000 | 0.000 |
| $f_{5/2} \rightarrow f_{5/2}$ | -0.002 | 0.003 | 0.024 |
| $p_{1/2} \rightarrow p_{3/2}$ | -0.006 | -0.006 | -0.020 |
| $p_{1/2} \rightarrow p_{1/2}$ | 0.000 | 0.000 | 0.002 |

## 6.4 Summary and Conclusions

We have derived an extended pnQRPA equation, in which the correlated BCS ground state is used to calculate the extended pnQRPA matrix elements. The equation has the pnQRPA form but the matrix elements include additional first-order correction terms which are due to the correlated BCS ground state. The equation is applied to study the $\beta^+$ decay of $^{46}$Ti. Around 40 % suppression of total $B(\mathrm{GT}^+)$ has been found. But the $B(\mathrm{GT}^+)$ strength distribution in the extended pnQRPA still differs with the shell-model results. We also discuss the suppression and enhancement mechanisms in the $^{46}\mathrm{Ti} \rightarrow ^{46}\mathrm{Sc}$ transition. We find the sum rule is violated around 10 %. This is because the second-order terms are dropped in the transition matrix element formula.

The extended pnQRPA has also been applied to calculate $\beta\beta$ decay of $^{46}$Ca. The suppression of the total double-beta decay matrix elements is found but not enough to reproduce the shell-model results. Like the application of the extended pnQRPA in $\beta^+$ decay, the $\beta\beta$ matrix element distribution with respect to the excitations is not yet improved.

# Chapter 7

# Further Improvements and Considerations

## 7.1 Introduction

In Chapter 6, we derived the extended pnQRPA equation in which the correlated BCS ground state is used. Our calculation showed that the total $B(\mathrm{GT}^+)$ and $2\nu\beta\beta$ decay matrix elements are suppressed but not enough to reproduce the shell-model results. Also the shapes of the strength distributions are still in poor agreement with those obtained in shell-model calculations.

In this Chapter, we explore another possible technique in theory of many-body problem to improve the pnQRPA, namely, the second pnQRPA theory. In this model, we concentrate on the extensions of the phonon creation operator, which will be expanded up to four quasiparticle creation and destruction operators. But the BCS ground state is still used to calculate the matrix elements in the equation.

Also we can combine the extended and second pnQRPA, i.e., the phonon operators include two and four quasiparticle creation and destruction operators and the correlated BCS ground state is used to calculate the relevant matrix elements. This extension is called the extended second pnQRPA equation.

We will derive the second pnQRPA equation in section 7.2 and the extended second pnQRPA in section 7.3. The derivations are both obtained in angular momentum uncoupled space where a REDUCE [Hea 88] algebra code is used to calculate the expression of the operator in the second quantization scheme. The summary is given in section 7.3.

## 7.2 Second pnQRPA Equations

In order to include higher-order correlation terms in charge-exchange mode, we extend the phonon creation operator $Q^\dagger_\nu$ to four quasiparticle creation and destruction operators which can contribute to charge exchange processes,

$$\begin{aligned} |\nu > \; &= \; Q^\dagger_\nu |\mathrm{SQRPA} >= \{ \sum_{p_1 n_1} (X_1^\nu c^\dagger_{p_1} c^\dagger_{n_1} - Y_1^\nu c_{n_1} c_{p_1}) \\ &+ \sum_{p_1<p_2<p_3, n_1} (X_2^\nu c^\dagger_{p_1} c^\dagger_{p_2} c^\dagger_{p_3} c^\dagger_{n_1} - Y_2^\nu c_{n_1} c_{p_3} c_{p_2} c_{p_1}) \\ &+ \sum_{n_1<n_2<n_3, p_1} (X_3^\nu c^\dagger_{n_1} c^\dagger_{n_2} c^\dagger_{n_3} c^\dagger_{p_1} - Y_3^\nu c_{p_1} c_{n_3} c_{n_2} c_{n_1}) \\ &+ \sum_{p_1<p_2, n_1<n_2} (X_4^\nu c^\dagger_{p_1} c^\dagger_{n_1} c^\dagger_{p_2} c^\dagger_{n_2} \\ &- Y_4^\nu c_{n_2} c_{p_2} c_{n_1} c_{p_1}) \} |\mathrm{SQRPA} > . \end{aligned} \tag{7.1}$$

In this section, the labels on $X$ and $Y$ are $1 = (p_1 n_1)$, $2 = (p_1 p_2 p_3 n_1)$, $3 = (n_1 n_2 n_3 p_1)$, $4 = (p_1 n_1 p_2 n_2)$. The ground state is |SQRPA>, which is discussed in Appendix D.

To derive the second pnQRPA, we insert the above phonon creation operator and appropriate variational operators $c_{p_1} c_{n_1}$, $c^\dagger_{p_1} c^\dagger_{n_1}$, $c^\dagger_{p_1} c^\dagger_{p_1} c^\dagger_{p_3} c^\dagger_{n_1}$, $\cdots$, and $c_{p_2} c_{n_2} c_{p_1} c_{n_1}$ into the equation of motion (Eq. (6.1)). The BCS ground state is used when we calculate the matrix elements in the second pnQRPA. Then the second pnQRPA is obtained with the following matrix form,

$$\begin{pmatrix} A_{11'} & B_{11'} & A_{12'} & & A_{13'} & & & \\ -B^*_{11'} & -A^*_{11'} & & -A^*_{12'} & & -A^*_{13'} & & \\ A_{21'} & & A_{22'} & & A_{23'} & & & \\ & -A^*_{21'} & & -A^*_{22'} & & -A^*_{23'} & & \\ A_{31'} & & A_{32'} & & A_{33'} & & & \\ & -A^*_{31'} & & -A^*_{32'} & & -A^*_{33'} & & \\ & & & & & & A_{44'} & \\ & & & & & & & -A^*_{44'} \end{pmatrix} \begin{pmatrix} X_{1'} \\ Y_{1'} \\ X_{2'} \\ Y_{2'} \\ X_{3'} \\ Y_{3'} \\ X_{4'} \\ Y_{4'} \end{pmatrix} = \hbar\omega \begin{pmatrix} X_1 \\ Y_1 \\ X_2 \\ Y_2 \\ X_3 \\ Y_3 \\ X_4 \\ Y_4 \end{pmatrix} \text{.(7.2}$$

The matrix elements are given by

$$\begin{aligned} A_{11'} &= <\mathrm{SQRPA}|[c_{n_1}c_{p_1},[H,c^\dagger_{p'_1}c^\dagger_{n'_1}]]|\mathrm{SQRPA}> \\ &\approx <\mathrm{BCS}|[c_{n_1}c_{p_1},[H,c^\dagger_{p'_1}c^\dagger_{n'_1}]]|\mathrm{BCS}> \\ &= (E_{p_1}+E_{n_1})\delta_{p_1p'_1}\delta_{n_1n'_1}+(H^{\mathbf{pn}}_{22})_{p_1n_1p'_1n'_1} \end{aligned} \tag{7.3}$$

$$\begin{aligned} B_{11'} &= -<\mathrm{SQRPA}|[c_{n_1}c_{p_1},[H,c_{n'_1}c_{p'_1}]]|\mathrm{SQRPA}> \\ &\approx -<\mathrm{BCS}|[c_{n_1}c_{p_1},[H,c_{n'_1}c_{p'_1}]]|\mathrm{BCS}> \\ &= -(H^{\mathbf{pn}}_{40})_{p_1n_1p'_1n'_1}-(H^{\mathbf{pn}}_{40})_{p'_1n'_1p_1n_1}+(H^{\mathbf{pn}}_{40})_{p'_1n_1p_1n'_1} \\ &\quad +(H^{\mathbf{pn}}_{40})_{p_1n'_1p'_1n_1} \end{aligned} \tag{7.4}$$

$$\begin{aligned} A_{12'} &= <\mathrm{SQRPA}|[c_{n_1}c_{p_1},[H,c^\dagger_{p'_1}c^\dagger_{p'_2}c^\dagger_{p'_3}c^\dagger_{n'_1}]]|\mathrm{SQRPA}> \\ &\simeq <\mathrm{BCS}|[c_{n_1}c_{p_1},[H,c^\dagger_{p'_1}c^\dagger_{p'_2}c^\dagger_{p'_3}c^\dagger_{n'_1}]]|\mathrm{BCS}> \\ &= \delta_{p_1p'_1}\mathcal{A}(p'_2,p'_3)(P^{\mathbf{pn}}_{13})_{p'_2n'_1p'_3n_1}+\delta_{p_1p'_2}\mathcal{A}(p'_1,p'_3)(P^{\mathbf{pn}}_{13})_{p'_3n'_1p'_1n_1} \\ &\quad +\delta_{p_1p'_3}\mathcal{A}(p'_2,p'_1)(P^{\mathbf{pn}}_{13})_{p'_1n'_1p'_2n_1} \\ &\quad (p'_1<p'_2<p'_3) \end{aligned} \tag{7.5}$$

$$\begin{aligned} A_{13'} &= <\mathrm{SQRPA}|[c_{n_1}c_{p_1},[H,c^\dagger_{n'_1}c^\dagger_{n'_2}c^\dagger_{n'_3}c^\dagger_{p'_1}]]|\mathrm{SQRPA}> \\ &\simeq <\mathrm{BCS}|[c_{n_1}c_{p_1},[H,c^\dagger_{n'_1}c^\dagger_{n'_2}c^\dagger_{n'_3}c^\dagger_{p'_1}]]|\mathrm{BCS}> \\ &= \delta_{n_1n'_1}\mathcal{A}(n'_2,n'_3)(N^{\mathbf{pn}}_{13})_{p'_1n'_2p_1n'_3}+\delta_{n_1n'_2}\mathcal{A}(n'_1,n'_3)(N^{\mathbf{pn}}_{13})_{p'_1n'_3p_1n'_1} \\ &\quad +\delta_{n_1n'_3}\mathcal{A}(n'_2,n'_1)(N^{\mathbf{pn}}_{13})_{p'_1n'_1p_1n'_2} \end{aligned}$$

$$(n'_1 < n'_2 < n'_3) \tag{7.6}$$

$$A_{ij} = A^*_{ji} \quad \text{for} \quad i \neq j \tag{7.7}$$

$$\begin{aligned}
A_{22'} &= < \mathrm{SQRPA}|[c_{n_1} c_{p_3} c_{p_2} c_{p_1}, [H, c^\dagger_{p'_1} c^\dagger_{p'_2} c^\dagger_{p'_3} c^\dagger_{n'_1}]]|\mathrm{SQRPA} > \\
&\simeq < \mathrm{BCS}|[c_{n_1} c_{p_3} c_{p_2} c_{p_1}, [H, c^\dagger_{p'_1} c^\dagger_{p'_2} c^\dagger_{p'_3} c^\dagger_{n'_1}]]|\mathrm{BCS} > \\
&= (E_{p_1} + E_{p_2} + E_{p_3} + E_{n_1}) \delta_{p_1 p'_1} \delta_{p_2 p'_2} \delta_{p_3 p'_3} \delta_{n_1 n'_1} + \\
&\quad \delta_{n_1 n'_1} [\delta_{p_1 p'_1} (H^{\mathrm{pp}}_{22})_{p_3 p_2 p'_3 p'_2} + \delta_{p_1 p'_2} (H^{\mathrm{pp}}_{22})_{p_2 p_3 p'_3 p'_1} + \delta_{p_1 p'_3} (H^{\mathrm{pp}}_{22})_{p_3 p_2 p'_2 p'_1} \\
&\quad + \delta_{p_2 p'_1} (H^{\mathrm{pp}}_{22})_{p_1 p_3 p'_3 p'_2} + \delta_{p_2 p'_2} (H^{\mathrm{pp}}_{22})_{p_1 p_3 p'_1 p'_3} + \delta_{p_2 p'_3} (H^{\mathrm{pp}}_{22})_{p_1 p_3 p'_2 p'_1} \\
&\quad + \delta_{p_3 p'_1} (H^{\mathrm{pp}}_{22})_{p_1 p_2 p'_2 p'_3} + \delta_{p_3 p'_2} (H^{\mathrm{pp}}_{22})_{p_1 p_2 p'_3 p'_1} + \delta_{p_3 p'_3} (H^{\mathrm{pp}}_{22})_{p_1 p_2 p'_1 p'_2}] \\
&\quad + \delta_{p_1 p'_1} \delta_{p_2 p'_2} (H^{\mathrm{pn}}_{22})_{p_3 n_1 p'_3 n'_1} + \delta_{p_2 p'_2} \delta_{p_3 p'_3} (H^{\mathrm{pn}}_{22})_{p_1 n_1 p'_1 n'_1} \\
&\quad + \delta_{p_3 p'_3} \delta_{p_1 p'_1} (H^{\mathrm{pn}}_{22})_{p_2 n_1 p'_2 n'_1} - \delta_{p_2 p'_3} \delta_{p_1 p'_1} (H^{\mathrm{pn}}_{22})_{p_3 n_1 p'_2 n'_1} \\
&\quad - \delta_{p_3 p'_2} \delta_{p_1 p'_1} (H^{\mathrm{pn}}_{22})_{p_2 n_1 p'_3 n'_1} - \delta_{p_1 p'_2} \delta_{p_3 p'_3} (H^{\mathrm{pn}}_{22})_{p_2 n_1 p'_1 n'_1} \\
&\quad - \delta_{p_2 p'_1} \delta_{p_3 p'_3} (H^{\mathrm{pn}}_{22})_{p_1 n_1 p'_2 n'_1} + \delta_{p_2 p'_3} \delta_{p_1 p'_2} (H^{\mathrm{pn}}_{22})_{p_3 n_1 p'_1 n'_1} \\
&\quad + \delta_{p_3 p'_2} \delta_{p_2 p'_1} (H^{\mathrm{pn}}_{22})_{p_3 n_1 p'_1 n'_1}
\end{aligned}$$

$$(p_1 < p_2 < p_3, \ p'_1 < p'_2 < p'_3) \tag{7.8}$$

$$\begin{aligned}
A_{33'} &= < \mathrm{SQRPA}|[c_{p_1} c_{n_3} c_{n_2} c_{n_1}, [H, c^\dagger_{n'_1} c^\dagger_{n'_2} c^\dagger_{n'_3} c^\dagger_{p'_1}]]|\mathrm{SQRPA} > \\
&\simeq (\text{exchange p, n label in } (A_{22})\ )
\end{aligned} \tag{7.9}$$

$$\begin{aligned}
A_{44'} &= < \mathrm{SQRPA}|[c_{n_2} c_{p_2} c_{n_1} c_{p_1}, [H, c^\dagger_{p'_1} c^\dagger_{n'_1} c^\dagger_{p'_2} c^\dagger_{n'_2}]]|\mathrm{SQRPA} > \\
&\simeq < \mathrm{BCS}|[c_{n_2} c_{p_2} c_{n_1} c_{p_1}, [H, c^\dagger_{p'_1} c^\dagger_{n'_1} c^\dagger_{p'_2} c^\dagger_{n'_2}]]|\mathrm{BCS} > \\
&= (E_{p_1} + E_{n_1} + E_{p_2} + E_{n_2}) \delta_{p_1 p'_1} \delta_{n_1 n'_1} \delta_{p_2 p'_2} \delta_{n_2 n'_2} \\
&\quad + \delta_{n_1 n'_1} \delta_{n_2 n'_2} (H^{\mathrm{pp}}_{22})_{p_1 p_2 p'_1 p'_2} + \delta_{p_1 p'_1} \delta_{p_2 p'_2} (H^{\mathrm{nn}}_{22})_{n_1 n_2 n'_1 n'_2} \\
&\quad + \delta_{p_1 p'_1} \delta_{n_1 n'_1} (H^{\mathrm{pp}}_{22})_{p_2 n_2 p'_2 n'_2} + \delta_{p_1 p'_1} \delta_{n_2 n'_2} (H^{\mathrm{pp}}_{22})_{p_2 n_1 p'_2 n'_1} \\
&\quad + \delta_{p_2 p'_2} \delta_{n_1 n'_1} (H^{\mathrm{pp}}_{22})_{p_1 n_2 p'_1 n'_2} + \delta_{p_2 p'_2} \delta_{n_2 n'_2} (H^{\mathrm{pp}}_{22})_{p_1 n_1 p'_1 n'_1} \\
&\quad + \delta_{p_1 p'_2} \delta_{n_2 n'_1} (H^{\mathrm{pp}}_{22})_{p_2 n_1 p'_1 n'_2} + \delta_{p_1 p'_2} \delta_{n_1 n'_2} (H^{\mathrm{pp}}_{22})_{p_2 n_2 p'_1 n'_1}
\end{aligned}$$

$$
\begin{aligned}
&+\delta_{p_2p'_1}\delta_{n_2n'_1}(H_{22}^{\mathrm{pp}})_{p_1n_1p'_2n'_2} + \delta_{p_2p'_1}\delta_{n_1n'_2}(H_{22}^{\mathrm{pp}})_{p_1n_2p'_2n'_1} \\
&-\delta_{p_1p'_1}\delta_{n_2n'_1}(H_{22}^{\mathrm{pp}})_{p_2n_1p'_2n'_2} - \delta_{p_1p'_1}\delta_{n_1n'_2}(H_{22}^{\mathrm{pp}})_{p_2n_2p'_2n'_1} \\
&-\delta_{p_1p'_2}\delta_{n_2n'_2}(H_{22}^{\mathrm{pp}})_{p_2n_1p'_1n'_1} - \delta_{p_1p'_2}\delta_{n_1n'_1}(H_{22}^{\mathrm{pp}})_{p_2n_2p'_1n'_2} \\
&-\delta_{p_2p'_1}\delta_{n_2n'_2}(H_{22}^{\mathrm{pp}})_{p_1n_1p'_2n'_1} - \delta_{p_2p'_1}\delta_{n_1n'_1}(H_{22}^{\mathrm{pp}})_{p_1n_2p'_2n'_2} \\
&-\delta_{p_2p'_2}\delta_{n_2n'_1}(H_{22}^{\mathrm{pp}})_{p_1n_1p'_1n'_2} - \delta_{p_2p'_2}\delta_{n_1n'_2}(H_{22}^{\mathrm{pp}})_{p_1n_2p'_2n'_1} \\
&(p_1 < p_2,\ n_1 < n_2,\ p'_1 < p'_2,\ n'_1 < n'_2) \qquad (7.10)
\end{aligned}
$$

The operators associated with the $X_1$, $Y_1$ in Eq. (7.1) describe states in the ($N\pm1$ , $Z\pm1$) nuclei; $X_2$, $Y_2$ describe ($N\pm1$ , $Z\pm1,3$) nuclei; $X_3$, $Y_3$ describe ($N\pm1,3$ , $Z\pm1$) nuclei; and $X_4$, $Y_4$ describe ($N\pm0,2,4$ , $Z\pm0,2,4$) nuclei. Hence, the $X_4$, $Y_4$ amplitudes decouple from the others and cannot describe beta decay states. We will not consider them in further calculations. The closure relation for the second pnQRPA becomes

$$
\begin{aligned}
\sum_{pn}(X_1^{\nu *}X_1^{\nu'} - Y_1^{\nu *}Y_1^{\nu'}) + \sum_{p_1<p_2<p_3,n_1}(X_2^{\nu *}X_2^{\nu'} - Y_2^{\nu *}Y_2^{\nu'}) \\
+ \sum_{n_1<n_2<n_3,p_1}(X_3^{\nu *}X_3^{\nu'} - Y_3^{\nu *}Y_3^{\nu'}) = \delta_{\nu'\nu}. \qquad (7.11)
\end{aligned}
$$

Now we can rewrite Eq. (7.2) projected onto the two quasiparticle subspace,

$$
\begin{pmatrix} \tilde{A}_{11'}(\omega) & B_{11'} \\ -B^*_{11'} & -\tilde{A}^*_{11'}(-\omega) \end{pmatrix} \begin{pmatrix} X_{1'} \\ Y_{1'} \end{pmatrix} = \hbar\omega \begin{pmatrix} X_1 \\ Y_1 \end{pmatrix} \qquad (7.12)
$$

with

$$
\begin{aligned}
\tilde{A}_{11'}(\omega) \;=\; & A_{11'} + \sum_{2,2'} A_{12}[\hbar\omega - A_{22'} - \sum_{3,3'} A_{23}(\hbar\omega - A_{33'})^{-1}A_{3'2'}]^{-1} \\
& [A_{2'1'} + \sum_{3,3'} A_{2'3}(\hbar\omega - A_{33'})^{-1}A_{3'1'}] \\
& + \sum_{3,3'} A_{13}[\hbar\omega - A_{33'} - \sum_{2,2'} A_{32}(\hbar\omega - A_{22'})^{-1}A_{2'3'}]^{-1} \\
& [A_{3'1'} + \sum_{2,2'} A_{3'2}(\hbar\omega - A_{22'})^{-1}A_{2'1'}]. \qquad (7.13)
\end{aligned}
$$

For the one-body charge exchange operator $\hat{O}$, the transition matrix elements between the excited states of the second pnQRPA are

$$\begin{aligned} <\nu|\hat{O}|\mathrm{SQRPA}> &= <\mathrm{SQRPA}|[Q_\nu, \hat{O}]]|\mathrm{SQRPA}> \\ &\simeq <\mathrm{BCS}|[Q_\nu, \hat{F}]]|\mathrm{BCS}> \\ &= (\text{expressions of Eqs. } (3.18-3.19)). \end{aligned} \tag{7.14}$$

Although Eq. (7.14) has the same form as Eqs. (3.18-3.19), the coefficients $X_1$ and $Y_1$ here are obtained by solving Eq. (7.2) or Eq. (7.12) rather than the pnQRPA. Thus, the four quasiparticle excitations and the ground state correlations are included in the coefficients.

## 7.3 Extended Second pnQRPA Equations

The extended second pnQRPA can be obtained by replacing $|\mathrm{BCS}>$ by $|\mathrm{CBCS}>$ in Eqs. (7.3,−,7.10). Here we are interested in the low-lying excitations where the coefficients $X_i$ and $Y_i$ ( $i \geq 2$) are assumed to be small quantities and have the same magnitude of the corrections in the correlated BCS wave function. Then we drop the second-order terms and obtain the following results, (1) the matrix element $A_{11'}$ and $B_{11'}$ in Eqs. (7.3,7.4) have the corrections $\Delta A$ and $\Delta B$, which are given by Eqs. (6.9,6.10) in angular momentum space, (2) other matrix elements have the same forms as Eqs. (7.5 − 7.10).

## 7.4 Summary

We have derived the second pnQRPA equation based on the extension of the phonon operator up to four quasiparticle creation and destruction operators. In the equation, the BCS ground state is still used. We also develop the extended second pnQRPA equation, in which the phonon operators are expanded up to four quasiparticle creation and destruction operators and the correlated BCS ground state is employed to calculated the matrix elements. The numerical evaluation of the second pnQRPA and the extended pnQRPA will provide a formidable challenge and we plan to proceed along the lines developed for the extension of the RPA [Wam 88, Dro 90].

# Chapter 8

# Summary and Conclusions

The nuclear shell model and the pnQRPA equation are very important nuclear structure theories for studying $\beta$ and $\beta\beta$ decays. But the approach of these two models is different. Many or all types of many-body correlations are taken into account in the large- or full-basis shell-model calculations. Thus the full-basis shell model is the *exact* calculation when it is feasible to carry out. The pnQRPA is an approximate model, which includes only some special classes of the correlations. The goals of this thesis consisted of three aspects, (1) study of $\beta$ and the $\beta\beta$ decay of mass $A = 48$ nuclei with the large-basis shell-model calculations, (2) examinations of the validity and accuracy of the pnQRPA for $\beta^+$ and $\beta\beta$ processes, and (3) improvements and extensions of the pnQRPA model.

In Chapter 2, the large-basis shell-model calculations are employed to calculate $\beta^-$ and $\beta^+$ Gamow-Teller spectra of $^{48}$Ca and $^{48}$Ti, and $2\nu\beta\beta$ decay matrix element of $^{48}$Ca. The $B(\mathrm{GT}^-)$ and $B(\mathrm{GT}^+)$ behavior in the energy region (2.5~15.0 MeV) are well described by the effective Gamow-Teller operator $\tilde{\sigma t} = 0.77\sigma t$ and a new effective interaction MSOBEP. With this interaction and effective operator, our shell-model calculation predicts the $2\nu\beta\beta$ decay matrix element of $^{48}$Ca to be $M_{\mathrm{GT}}^{2\nu}$=0.070, giving a half life $T_{1/2}$= $1.9\times10^{19}$yr, which differs by nearly a factor of two from the experimental limit [Bar 70] of $T_{1/2} > 3.6\times10^{19}$ yr. We believe that the most important aspect of these calculations, which cannot be directly tested by the (p,n) and (n,p) experiments, is the amount of strength in the (n,p) $\beta^+$ spectrum above 5 MeV in the excitation. This is because there is a large uncertainty in the amount of Gamow-Teller strength in the background above this energy. Also further refinements of the effective interaction are necessary.

Since the pnQRPA is an approximate model, in Chapter 3 and 4 we have investigated the accuracy of the pnQRPA approach to $\beta^+$ and $\beta\beta$ decays. Comparisons of the pnQRPA and full-basis shell-model calculations have been made. In our study, a self-consistent BCS-pnQRPA have been developed. " Self-consistent " means that the input ingredients in the BCS-pnQRPA are the same as those in the shell model, namely, the bare single particle energies at the closed shell and two-body interaction matrix elements. Therefore there is no free parameter for both models in our comparison. The coherent one-body transition density (COBTD) and coherent transition matrix elements (CTME) are introduced for analysis of the single-particle state contributions in $\beta^+$ decay. Our comparisons have shown the pnQRPA overestimates the total $B(\mathrm{GT}^+)$ and $\beta\beta$ decay matrix elements, and there are large discrepancies in the shapes of the strength distributions between the pnQRPA and shell-model calculations. The COBTD and CTME of the pnQRPA are also in poor agreement with those of the shell-model. Thus we may conclude there must be some correlations which are important to $\beta^+$ and $\beta\beta$ decay but have not been included in the pnQRPA.

Empirical improvements for the pnQRPA, namely, the " hybrid " pnQRPA, which are obtained by using the shell-model occupation probabilities and the shell-model quasiparticle energies in the pnQRPA, are discussed. About 50 % suppressions are found for the total $B(\mathrm{GT}^+)$ strength. The shape of the $B(\mathrm{GT}^+)$ distribution has not been improved but it is more reasonable than that in the pnQRPA with larger $g_{pp}$ values. In Chapter 4, we find the " hybrid " pnQRPA does not work for $\beta\beta$ decay.

The theoretical improvements of the pnQRPA equation start with the introduction of the correlated BCS theory. The quasiparticle interaction dropped in BCS is incorporated by first-order perturbation theory. The extended BCS equation has been derived based on the correlated BCS and has shown improvement over the standard BCS for the occupation probabilities. In our study, only the proton-neutron interaction terms are considered.

We have derived an extended pnQRPA equation, in which the correlated BCS is used to calculate the matrix elements. The equation has the pnQRPA form but the matrix elements include additional first-order correction terms. The equation has been applied to $\beta^+$ decay and gives an additional suppression of about 40 % in the total $B(\mathrm{GT}^+)$. Around 10 % of the sum rule is violated because of dropping the second-order terms. Also the double-beta decay matrix elements are suprressed but not enough to reproduce the shell-model result. The disagreements in the shape of the $\beta^+$ and $\beta\beta$ spectra have not yet been improved compared to the shell-model results. The extended BCS and pnQRPA equations were derived in the J-scheme coupling space.

In Chapter 7, we considered the development of the second pnQRPA equation based on the extension of phonon operator up to four quasiparticle creation and destruction operators. In the equations, the BCS ground state is still used. We also derived an extended second pnQRPA equation, in which not only the phonon operators are expanded up to four quasiparticle creation and destruction operators, but also the correlated BCS ground state is employed to calculate the matrix elements. These equations should provide more accurate methods for studying the transition of one- and/or two-body charge exchange modes. The numerical evaluation of the second pnQRPA and the extended pnQRPA will present a formidable challenge and we plan to proceed along the lines developed for the extension of the RPA.

In Appendix A, the QRPA equations have been derived. In Appendix B, we have discussed the relations between the QRPA and pnQRPA equations. In Appendix C, the second QRPA equation has been derived with the phonon creation expanding to four quasiparticle creation and destruction operators. In Appendix D, the coherent one-body transition density and coherent transition matrix element are discussed in detail. In Appendix E, the BCS and the extended BCS theories are derived in angular momentum uncoupled space. Finally in Appendix F, the spurious states in the BCS and the extended BCS are discussed.

# Appendix A

# QRPA equations

In this appendix, we review the derivation of the QRPA equation from the equation of motion method. In the equation of motion, the excited eigenstates $|\nu>$ are constructed from the phonon creation operator $Q_\nu^\dagger$ which is defined by

$$|\nu >= Q_\nu^\dagger|0>, \quad \text{and} \quad Q_\nu|0>= 0, \quad \text{for all } \nu \tag{A.1}$$

where $|\nu>$ and $|0>$ are the excited eigenstate and the physical ground state. They satisfy the Schrödinger equations,

$$H|\nu >= E_\nu|\nu> \quad \text{and} \quad H|0>= E_0|0> . \tag{A.2}$$

Then one obtains the following equation of motion from the above relations;

$$[H, Q_\nu^\dagger]|0>= (E_\nu - E_0)Q_\nu^\dagger|0> . \tag{A.3}$$

Multiplying from the left with an arbitrary state of the form $<0|\delta Q_\nu$, we get

$$<0|[\delta Q_\nu, [H, Q_\nu^\dagger]]|0>= \hbar\omega <0|[\delta Q_\nu, Q_\nu^\dagger]|0> \tag{A.4}$$

where $\hbar\omega = E_\nu - E_0$.

In order to derive the usual QRPA equation, we assume that the excited states are obtained by creating or destroying two quasiparticles from the QRPA ground state $|\mathrm{QRPA}>$,

$$|\nu>=Q^\dagger_\nu|\mathrm{QRPA}>=\sum_{k<k'}(X^\nu_{kk'}c^\dagger_k c^\dagger_{k'}-Y^\nu_{kk'}c_{k'}c_k)|\mathrm{QRPA}>\,. \tag{A.5}$$

The QRPA ground state is defined by

$$Q_\nu|\mathrm{QRPA}>=0. \tag{A.6}$$

Inserting $Q^\dagger_\nu$ into the Eq. (A.4), and choosing $\delta Q$ to be $c_{k'}c_k$ and $c^\dagger_k c^\dagger_{k'}$, one obtains the QRPA equation

$$\begin{pmatrix} A & B \\ -B^* & -A^* \end{pmatrix}\begin{pmatrix} X \\ Y \end{pmatrix}=\hbar\omega\begin{pmatrix} X \\ Y \end{pmatrix}\,. \tag{A.7}$$

The matrix elements are given by $(k<k', l<l')$

$$\begin{aligned} A_{kk',ll'} &= <\mathrm{QRPA}|[c_{k'}c_k,[H,c^\dagger_l c^\dagger_{l'}]]|\mathrm{QRPA}> \\ &\approx <\mathrm{BCS}|[c_{k'}c_k,[H,c^\dagger_l c^\dagger_{l'}]]|\mathrm{BCS}> \\ &= (E_k+E_{k'})\delta_{kl}\delta_{k'l'}+(H_{22})_{kk'll'} \end{aligned} \tag{A.8}$$

$$\begin{aligned} B_{kk',ll'} &= -<\mathrm{QRPA}|[c_{k'}c_k,[H,c_{l'}c_l]]|\mathrm{QRPA}> \\ &\approx -<\mathrm{BCS}|[c_{k'}c_k,[H,c_{l'}c_l]]|\mathrm{BCS}> \\ &= (H_{40})_{kk'll'}+(H_{40})_{ll'kk'}-(H_{40})_{klk'l'}-(H_{40})_{k'l'kl} \\ &\quad -(H_{40})_{l'kk'l}-(H_{40})_{lk'kl'} \end{aligned} \tag{A.9}$$

where we approximate the QRPA ground state as the BCS state in Eqs. (A.8-A.9).

# Appendix B

# Relation between QRPA and pnQRPA Equations

When we consider Eq. (A.5) including the proton and neutron components, it can be expanded as,

$$\begin{aligned}
Q^{\dagger}_{\nu} &= \sum_{k<k'} (X^{\nu}_{kk'} c^{\dagger}_{k} c^{\dagger}_{k'} - Y^{\nu}_{kk'} c_{k'} c_{k}) \\
&= \sum_{p<p'} (X^{\mathrm{pp}}_{pp'} c^{\dagger}_{p} c^{\dagger}_{p'} - Y^{\mathrm{pp}}_{kk'} c_{p'} c_{p}) + \sum_{n<n'} (X^{\mathrm{nn}}_{nn'} c^{\dagger}_{n} c^{\dagger}_{n'} - Y^{\mathrm{nn}}_{kk'} c_{n'} c_{n}) \\
&\quad + \sum_{pn} (X^{\mathrm{pn}}_{pn} c^{\dagger}_{p} c^{\dagger}_{n} - Y^{\mathrm{pn}}_{kk'} c_{n} c_{p}). \qquad \text{(B.1)}
\end{aligned}$$

Inserting $Q^{\dagger}_{\nu}$ into the Eq. (A.4), and choosing the variational $\delta Q$ to be $c_{p'}c_{p}$, $c^{\dagger}_{p}c^{\dagger}_{p'}$, $c_{n'}c_{n}$, $c^{\dagger}_{n}c^{\dagger}_{n'}$, $c_{n}c_{p}$ and $c^{\dagger}_{p}c^{\dagger}_{n}$, one obtains,

$$\left(\begin{array}{cccccc}
A^{\mathrm{pp}} & B^{\mathrm{pp}} & C & D & & \\
-B^{\mathrm{pp}*} & -A^{\mathrm{pp}*} & -D^{*} & -C^{*} & & \\
F & D & A^{\mathrm{nn}} & B^{\mathrm{nn}} & & \\
-D^{*} & -F^{*} & -B^{\mathrm{nn}*} & -A^{\mathrm{nn}*} & & \\
 & & & & A^{\mathrm{pn}} & B^{\mathrm{pn}} \\
 & & & & -B^{\mathrm{pn}*} & -A^{\mathrm{pn}*}
\end{array}\right)
\begin{pmatrix} X^{\mathrm{pp}} \\ Y^{\mathrm{pp}} \\ X^{\mathrm{nn}} \\ Y^{\mathrm{nn}} \\ X^{\mathrm{pn}} \\ Y^{\mathrm{pn}} \end{pmatrix}
= \hbar\omega
\begin{pmatrix} X^{\mathrm{pp}} \\ Y^{\mathrm{pp}} \\ X^{\mathrm{nn}} \\ Y^{\mathrm{nn}} \\ X^{\mathrm{pn}} \\ Y^{\mathrm{pn}} \end{pmatrix} . \text{(B.2)}$$

The matrix elements $A^{\mathrm{pp}}, B^{\mathrm{pp}}, A^{\mathrm{nn}}$ and $B^{\mathrm{nn}}$ are given by Eqs. (A.8,A.9), and $A^{\mathrm{pn}}$, and $B^{\mathrm{pn}}$ are given by Eqs. (3.11,3.12). The matrix elements $C, D$ and $F$ are expressed

as

$$\begin{aligned} C_{pp',nn'} &= < \mathrm{QRPA}|[c_{p'}c_p,[H,c_n^\dagger c_{n'}^\dagger]]|\mathrm{QRPA} > \\ &\approx < \mathrm{BCS}|[c_{p'}c_p,[H,c_n^\dagger c_{n'}^\dagger]]|\mathrm{BCS} > \\ &= (P_{22}^{\mathrm{pn}})_{pnp'n'} \end{aligned} \tag{B.3}$$

$$\begin{aligned} D_{pp',nn'} &= -< \mathrm{QRPA}|[c_{p'}c_p,[H,c_{n'}c_n]]|\mathrm{QRPA} > \\ &\approx -< \mathrm{BCS}|[c_{p'}c_p,[H,c_{n'}c_n]]|\mathrm{BCS} > \\ &= -(H_{40}^{\mathrm{pn}})_{pnp'n'} - (H_{40}^{\mathrm{pn}})_{p'n'pn} \\ &\quad +(H_{40})_{p'npn'} + (H_{40})_{pn'p'n} \end{aligned} \tag{B.4}$$

$$\begin{aligned} F_{pp',nn'} &= < \mathrm{QRPA}|[c_{n'}c_n,[H,c_p^\dagger c_{p'}^\dagger]]|\mathrm{QRPA} > \\ &\approx < \mathrm{BCS}|[c_{n'}c_n,[H,c_p^\dagger c_{p'}^\dagger]]|\mathrm{BCS} > \\ &= (N_{22}^{\mathrm{pn}})_{pnp'n'}. \end{aligned} \tag{B.5}$$

From Eq. (B.2), we can find the sub-matrix in low-right corner is the pnQRPA equation which is decoupled from the proton-proton and neutron-neutron QRPA matrix located in up-left corner. The reason for the decoupling is that the operators associated with $X^{\mathrm{pp}}$, $Y^{\mathrm{pp}}$ in Eq. (B.1) describe the states in the $(N, Z \pm 0, 2)$ nuclei; and $X^{\mathrm{nn}}$, $Y^{\mathrm{nn}}$ describe the $(N \pm 0, 2, Z)$ nuclei whereas and $X^{\mathrm{pn}}$, $Y^{\mathrm{pn}}$ describe the $(N \pm 1, Z \pm 1)$ nuclei. Hence, the $X^{\mathrm{pn}}, Y^{\mathrm{pn}}$ amplitudes decouple from the others. But $X^{\mathrm{pp}}$, $Y^{\mathrm{pp}}$ and $X^{\mathrm{nn}}$, $Y^{\mathrm{nn}}$ both can describe the $(N, Z)$ nucleus and consequently couple together.

# Appendix C

# Second QRPA Equations

In this Appendix, we will generalize the QRPA to the second QRPA equation. The phonon creation operator is expanded up to four quasiparticle creation and annihilation operators, i.e.,

$$\begin{aligned} |\nu > &= Q^\dagger_\nu |\mathrm{SQRPA} > \\ &= \{\sum_{k<k'} (X_1^\nu c_k^\dagger c_{k'}^\dagger - Y_1^\nu c_{k'} c_k) \\ &\quad + \sum_{k<k'<m<m'} (X_2^\nu c_k^\dagger c_{k'}^\dagger c_m^\dagger c_{m'}^\dagger - Y_2^\nu c_{m'} c_m c_{k'} c_k)\} |\mathrm{SQRPA} > , \end{aligned} \tag{C.1}$$

where we label $1 = (kk')$ and $2 = (kk'mm')$ for simplicity. |SQRPA> is the second QRPA's ground state defined by

$$Q_\nu |\mathrm{SQRPA} >= 0. \tag{C.2}$$

When $Q^\dagger_\nu$ is put in the equation of motion, we obtain the second QRPA equations,

$$\begin{pmatrix} A_{11'} & B_{11'} & A_{12'} & \\ -B^*_{11'} & -A^*_{11'} & & -A^*_{12'} \\ A_{21'} & & A_{22'} & \\ & -A^*_{21'} & & -A^*_{22'} \end{pmatrix} \begin{pmatrix} X_{1'} \\ Y_{1'} \\ X_{2'} \\ Y_{2'} \end{pmatrix} = \hbar\omega \begin{pmatrix} X_1 \\ Y_1 \\ X_2 \\ Y_2 \end{pmatrix} . \tag{C.3}$$

The matrix elements are given by

$$A_{11'} = < \mathrm{SQRPA}|[c_{k'}c_k, [H, c_l^\dagger c_{l'}^\dagger]]|\mathrm{SQRPA} >$$

$$\begin{aligned} &\approx \; <\mathrm{BCS}|[c_{k'}c_k,[H,c_l^\dagger c_{l'}^\dagger]]|\mathrm{BCS}> = (E_k+E_{k'})\delta_{kl}\delta_{k'l'} + (H_{22})_{kk'll'} \\ &\quad (k<k', l<l') \end{aligned} \tag{C.4}$$

$$\begin{aligned} B_{11'} &= -<\mathrm{SQRPA}|[c_{k'}c_k,[H,c_{l'}c_l]]|\mathrm{SQRPA}> \\ &\approx -<\mathrm{BCS}|[c_{k'}c_k,[H,c_{l'}c_l]]|\mathrm{BCS}> \\ &= (H_{40})_{kk'll'} + (H_{40})_{ll'kk'} - (H_{40})_{klk'l'} - (H_{40})_{k'l'kl} \\ &\quad -(H_{40})_{l'kk'l} - (H_{40})_{lk'kl'} \\ &\quad (k<k', l<l') \end{aligned} \tag{C.5}$$

$$\begin{aligned} A_{12'} &= <\mathrm{SQRPA}|[c_{k'}c_k,[H,c_l^\dagger c_{l'}^\dagger c_m^\dagger c_{m'}^\dagger]]|\mathrm{SQRPA}> \\ &\approx <\mathrm{BCS}|[c_{k'}c_k,[H,c_l^\dagger c_{l'}^\dagger c_m^\dagger c_{m'}^\dagger]]|\mathrm{BCS}>) \\ &= \frac{1}{2}\mathcal{A}(k',k)\mathcal{A}(l',l)\mathcal{A}(m',l')\delta_{k'm'}[\mathcal{A}(l',m)(H_{13})_{klm'l'} \\ &\quad +\mathcal{A}(l',l)(H_{13})_{kml'l} + \mathcal{A}(l,m)(H_{13})_{kl'lm}] \\ &\quad (k<k', l<l'<m<m') \end{aligned} \tag{C.6}$$

$$A_{2'1} = A^*_{12'} \tag{C.7}$$

$$\begin{aligned} A_{22'} &= <\mathrm{SQRPA}|[c_{m'}c_m c_{k'}c_k,[H,c_l^\dagger c_{l'}^\dagger c_n^\dagger c_{n'}^\dagger]]|\mathrm{SQRPA}> \\ &\approx <\mathrm{BCS}|[c_{k'}c_k,[H,c_l^\dagger c_{l'}^\dagger c_m^\dagger c_{m'}^\dagger]]|\mathrm{BCS}> \\ &= (E_k+E_{k'}+E_m+E_{m'})\delta_{kl}\delta_{k'l'}\delta_{mn}\delta_{m'n'} + \delta_{kl}\delta_{k'l'}(H_{22})_{mm'nn'} \\ &\quad +\delta_{mn}\delta_{m'n'}(H_{22})_{kk'll'} + \delta_{kn}\delta_{k'n'}(H_{22})_{mm'll'} + \delta_{ln}\delta_{l'n'}(H_{22})_{kk'nn'} \\ &\quad +\mathcal{A}(k',k)\mathcal{A}(l',l)\mathcal{A}(m',m)\mathcal{A}(n',n)\mathcal{A}(l',n')\delta_{k'l'}\delta_{m'n'}(H_{22})_{kmln} \\ &\quad +\mathcal{A}(k',k)\mathcal{A}(l',l)\mathcal{A}(n',n)\delta_{k'l'}\delta_{kn'}(H_{22})_{mm'ln} \\ &\quad +\mathcal{A}(k',k)\mathcal{A}(l',l)\mathcal{A}(m',m)\delta_{k'l'}\delta_{lm'}(H_{22})_{mkn'n} \\ &\quad +\mathcal{A}(k',k)\mathcal{A}(m',m)\mathcal{A}(n',n)\delta_{m'n'}\delta_{kn'}(H_{22})_{kml'l} \\ &\quad +\mathcal{A}(l',l)\mathcal{A}(m',m)\mathcal{A}(n',n)\delta_{l'm'}\delta_{m'n}(H_{22})_{kk'nl} \\ &\quad (k<k'<m<m', l<l'<n<n') \end{aligned} \tag{C.8}$$

where we label $1' = (ll')$ and $2' = (ll'nn')$ and $\mathcal{A}(p,q)$ is the antisymmetrizer of the indices p and q, which is defined by

$$\mathcal{A}(p,q) f_{\ldots p \ldots q \ldots} = f_{\ldots p \ldots q \ldots} - f_{\ldots q \ldots p \ldots}. \tag{C.9}$$

The algebra calculations for operators in the second quantization scheme are performed by a REDUCE code [Hea 88].

# Appendix D

# Coherent One-Body Transition Density

In the second-quantization formalism, the one-body operator can be expressed by

$$F = \sum_{\alpha\beta} < \alpha|F|\beta > a^\dagger_\alpha a_\beta, \tag{D.1}$$

where $|\alpha >$ and $|\beta >$ are the single particle states. The transition matrix element between the initial state $|i >$ and the final state $|f >$ is given by

$$M_{fi} =< f|F|i >= \sum_{\alpha\beta} < \alpha|F|\beta >< f|a^\dagger_\alpha a_\beta|i > . \tag{D.2}$$

$< \alpha|F|\beta >$ is called the single-particle matrix element (SPME) which is only related to the single-particle states $|\alpha >$ and $|\beta >$. $< f|a^\dagger_\alpha a_\beta|i >$ is called the one-body transition density (OBTD), which is the function of the initial and final states as well as the single-particle states $|\alpha >$ and $|\beta >$. Then Eq. (D.2) can be rewritten as

$$M_{fi} = \sum_o \text{SPME}(o)\text{OBTD}(o, f, i) = \sum_o \text{TME}(o, f, i), \tag{D.3}$$

where $o$ represents the single-particle states.

Now we introduce a *coherent state* $|\text{C} >$ which is defined by

$$|\text{C} >= N_\text{C} F|i > , \tag{D.4}$$

where $N_\mathrm{C}$ is the normalization factor which is determined by

$$\begin{aligned} <\mathrm{C}|\mathrm{C}> &= N_\mathrm{C}^2 < i|F^\dagger F|i> \\ &= N_\mathrm{C}^2 \sum_f < i|F^\dagger|f >< f|F|i > . \end{aligned} \tag{D.5}$$

Then we have

$$N_\mathrm{C} = \frac{1}{\sqrt{\sum_f < f|F|i >^2}}. \tag{D.6}$$

The transition matrix element between the coherent state and initial state is

$$\begin{aligned} <\mathrm{C}|F|i> &= N_\mathrm{C} < i|F^\dagger F|i> \\ &= N_\mathrm{C} \sum_f < i|F^\dagger|f >< f|F|i > \\ &= N_\mathrm{C} \sum_{o,f} M_{fi}\mathrm{SPME}(o)\mathrm{OBTD}(o,f,i) \\ &= \sum_o \mathrm{SPME}(o)\mathrm{COBTD}(o,i) \\ &= \sum_o \mathrm{CTME}(o,i). \end{aligned} \tag{D.7}$$

where the COBTD and CTME are the *coherent one-body transition density* and *coherent transition matrix element* which are defined by

$$\begin{aligned} \mathrm{COBTD}(o,i) &= N_\mathrm{C} \sum_f M_{fi}\mathrm{OBTD}(o,f,i) \\ \mathrm{CTME}(o,i) &= \mathrm{SPME}(o)\mathrm{COBTD}(o,f,i). \end{aligned} \tag{D.8}$$

The COBTD and CTME are a function of the single-particle state and initial state. It represents the single-particle state effects in the total transition strength.

# Appendix E

# BCS and Extended BCS in Uncoupled Representation

In this Appendix, we will discuss the formalism of the BCS and the extended BCS in angular momentum uncoupled space. The BCS equations are given by a lot of textbooks [Row 70, Rin 80]. For the proton-neutron system, the quasiproton energies $E_p$, the parameters $v_p^2$ introduced by Bogoliubov transformation and pairing gaps $\Delta_p$ are given by

$$\begin{aligned} E_p &= \sqrt{(\varepsilon_p - \lambda_\pi)^2 + \Delta_p^2}, && \text{(E.1)} \\ v_p^2 &= \frac{1}{2}\Big(1 - \frac{\varepsilon_p - \lambda_\pi}{\sqrt{(\varepsilon_p - \lambda_\pi)^2 + \Delta_p^2}}\Big), && \text{(E.2)} \\ \Delta_p &= -\frac{1}{2}\sum_{p'} u_{p'} v_{p'} V_{p\bar{p},p'\bar{p}'}, && \text{(E.3)} \end{aligned}$$

where $\lambda_\pi$ is the proton Fermi energy, $\varepsilon_p$ and $V_{pp,p'p'}$ are the single proton energy and proton two-body interaction, respectively. The above equations can be solved under the constraint for the total proton number

$$N_\pi = \sum_p < \mathrm{BCS}|a_p^\dagger a|\mathrm{BCS} > , \tag{E.4}$$

which determines the constant $\lambda_\pi$. A similar set of the equations can be solved for neutrons. In the BCS, $v^2$ turns out the physical meaning – the occupation probability.

The derivation of the extended BCS equations starts with introducing the correlated BCS wave function in section 5.3.2, which can be written as

$$|\mathrm{CBCS}>= N(|\mathrm{BCS}> - \sum_{\substack{p_1<p_2\\ n_1<n_2}} \frac{G^{\mathrm{pn}}_{p_1n_1p_2n_2}}{E_{p_1}+E_{n_1}+E_{p_2}+E_{n_2}} c_{p_1}c_{n_1}c_{p_2}c_{n_2}|\mathrm{BCS}>), \quad (\mathrm{E.5})$$

where the restrictions $p_1 < p_2$ and $n_1 < n_2$ are introduced in order to avoid double counting the states. The expression of $G^{\mathrm{pn}}_{p_1n_1p_2n_2}$ is given by

$$\begin{aligned}(G^{\mathrm{pn}})_{p_1n_1p_2n_2} &= V_{p_1n_1p_2n_2}(u_{p_1}u_{n_1}v_{p_2}v_{n_2}+v_{p_1}v_{n_1}u_{p_2}u_{n_2})\\ &\quad -W_{p_1n_1p_2n_2}(v_{p_1}u_{n_1}u_{p_2}v_{n_2}+u_{p_1}v_{n_1}v_{p_2}u_{n_2}),\end{aligned} \quad (\mathrm{E.6})$$

where $W_{p_1n_1p_2n_2}$ is the particle-hole interaction to be equal to $-V_{p_1n_2p_1n_1}$.

The normalization factor $N$ in Eq. (E.5) can be determined by

$$< \mathrm{CBCS}|\mathrm{CBCS} >= 1. \quad (\mathrm{E.7})$$

Then we obtain

$$N^{-2} = 1 + \sum_{\substack{p_1<p_2\\ n_1<n_2}} \{\frac{G^{\mathrm{pn}}_{p_1n_1p_2n_2}}{E_{p_1}+E_{n_1}+E_{p_2}+E_{n_2}}\}^2. \quad (\mathrm{E.8})$$

The occupation probabilities of protons and neutrons are given by

$$\begin{aligned}< \mathrm{CBCS}|a^\dagger_p a_p|\mathrm{CBCS} > &= v_p^2 + (u_p^2 - v_p^2)N^2 \sum_{\substack{p_2\\ n_1<n_2}} (\frac{G_{pn_1p_2n_2}}{E_p+E_{n_1}+E_{p_2}+E_{n_2}})^2\\ < \mathrm{CBCS}|a^\dagger_n a_n|\mathrm{CBCS} > &= v_n^2 + (u_n^2 - v_n^2)N^2 \sum_{\substack{p_1<p_2\\ n_2}} (\frac{G_{p_1np_2n_2}}{E_{p_1}+E_n+E_{p_2}+E_{n_2}})^2.\end{aligned}$$

$$(\mathrm{E.9})$$

The correlated BCS wave function is required to have the correct mean proton and neutron numbers. Thus the constraints are

$$\sum_p < \mathrm{CBCS}|a_p^\dagger a_p|\mathrm{CBCS} >= N_\pi \tag{E.10}$$

$$\sum_n < \mathrm{CBCS}|a_n^\dagger a_n|\mathrm{CBCS} >= N_\nu . \tag{E.11}$$

The set of equations Eq. (E.1,–,E.3,E.5,–, E.11) are called the extended BCS equation. They can be solved iteratively. From Eqs. (E.9), we find that $v^2$ is no longer the occupation probability.

The ground state energy of the correlated BCS is given by

$$E_{\mathrm{corr}} = E_{\mathrm{BCS}} + E^{(1)} + E^{(2)}, \tag{E.12}$$

where

$$E^{(1)} = 0 \tag{E.13}$$

$$E^{(2)} = - \sum_{\substack{p_1 < p_2 \\ n_1 < n_2}} \frac{(G_{p_1 n_1 p_2 n_2})^2}{E_{p_1} + E_{n_1} + E_{p_2} + E_{n_2}} . \tag{E.14}$$

$E_{\mathrm{BCS}}$ is given by Eq. (5.48).

# Appendix F

# Spurious States in the BCS and extended BCS.

In Chapter 5, we constructed the first-order corrections for the BCS ground state. The correlated BCS ground state mixes two-quasiproton two-quasineutron excitations with the quasiparticle vacuum. But these excitations may contain some unphysical states – spurious states, which should be projected out in principle.

Spurious excitations can occur whenever the approximation used breaks the symmetries of the Hamiltonian or violates the conservation laws. Since the BCS violates the particle-number conservation, spurious states may occur when we construct the unperturbed excitations from the BCS ground state in subsect. 5.2.3. For example, if we consider the two-quasiproton excitations, the state

$$\begin{aligned} |\mathrm{sp}_2> &= N_{sp2}(\hat{N}_p - N_\pi)|\mathrm{BCS}> \\ &= -N_{sp2}\sum_p \sqrt{2(2j_p+1)}u_p v_p \mathcal{A}^\dagger_{\mathrm{pp}}(pp,00)|\mathrm{BCS}> \end{aligned} \tag{F.1}$$

is an excitation but it is spurious i.e., if the wave function is the eigenstate of $\hat{N}$, this state does not exist because we have $|\mathrm{sp}_2>= 0$.

The four-quasiparticle (like particle) spurious states were discussed by several authors before[Ott 67, Pal 67, Gmi 68] when they studied the excitations in quasiparticle TDA equation. Their method requires an explicit construction of the most important spurious states to be eliminated. Following this method, we construct the spurious states in the two-quasiproton two-quasineutron doublet configurations, which should be removed when calculating the correlated BCS wave function. The spurious states can be written as

$$|\mathrm{sp}\pi > = N_{sp\pi}(\hat{N}_p - N_\pi)\mathcal{A}^\dagger_{\mathrm{nn}}(n_1 n_1, 00)|\mathrm{BCS}> , \tag{F.2}$$

or

$$|\mathrm{sp}\nu > = N_{sp\nu}(\hat{N}_n - N_\nu)\mathcal{A}^\dagger_{\mathrm{pp}}(p_1 p_1, 00)|\mathrm{BCS}> , \tag{F.3}$$

where $\hat{N}_p$ and $\hat{N}_n$ are the proton and neutron number operators, $N_\pi$ and $N_\nu$ are the proton and neutron mean numbers given by the nuclear system. In fact, the Eqs. (F.2,F.3) are equivalent to each other.

In order to discuss the properties of spurious state and understand the projection procedure, we now consider a special spurious state, it is the combination of the states in Eq. (F.2) or Eq. (F.3).

$$|\mathrm{sp}_4 > = N_{\mathrm{sp}}(\hat{N}_p - N_\pi)(\hat{N}_n - N_\nu)|\mathrm{BCS}> , \tag{F.4}$$

where $N_{\mathrm{sp}}$ is the normalization factor. In the quasiparticle basis, it can be expressed as

$$|\mathrm{sp}_4 > \; = \; N_{\mathrm{sp}} \sum_{pn} \sum_{m_p m_n} (-1)^{j_p+m_p+j_n+m_n} u_p v_p u_n v_n c^\dagger_{j_p m_p} c^\dagger_{j_p -m_p} c^\dagger_{j_n m_n} c^\dagger_{j_n -m_n} |\mathrm{BCS}> . \tag{F.5}$$

$N_{\mathrm{sp}}$ can be determined by

$$< \mathrm{sp}_4 | \mathrm{sp}_4 > = 1, \tag{F.6}$$

so we obtain

$$N_{\mathrm{sp}}^{-2} = 4\sum_{pn}(2j_p+1)(2j_n+1)(u_p v_p u_n v_n)^2. \tag{F.7}$$

$|\mathrm{sp}_4>$ may be expanded in terms of our orthogonal complete basis obtained by Eq. (5.80),

$$\begin{aligned} |\mathrm{sp}_4> &= \sum_{\substack{p_1n_1p_2n_2\\k}} b_k|p_1n_1p_2n_2,k> \\ &= \sum_{\substack{p_1n_1p_2n_2\\k}}\sum_i b_k\alpha_{ki}B^{\dagger}_{J_iJ_i}(p_1n_1p_2n_2,00)|\mathrm{BCS}> . \end{aligned} \tag{F.8}$$

The coefficients $b_k$ are determined by

$$\begin{aligned} b_k &= <p_1n_1p_2n_2,k|\mathrm{sp}_4> \\ &= 4N_{\mathrm{sp}}\sum_i \alpha_{ki}\sqrt{2J_i+1}N_{Bi}u_{p_1}v_{p_1}u_{n_1}v_{n_1}\delta_{p_1p_2}\delta_{n_1n_2}, \end{aligned} \tag{F.9}$$

where

$$<\mathrm{sp}_4|\mathrm{sp}_4>= \sum_{p_1n_1p_2n_2,k} b_k^2 = 1. \tag{F.10}$$

In order to project out this spurious state, we have to use the Gram-Schmidt orthogonalization again. The procedure is as follows. Based on the normalized orthogonal basis $|p_1n_1p_2n_2,k>$, one introduces a new basis by replacing the first vector by $|\mathrm{sp}_4>$. However, the new basis is no longer orthogonal anymore since $<p_1n_1p_2n_2,k|\mathrm{sp}_4>\neq 0$, where $k>1$. We construct, with the Gram-Schmidt orthogonalization procedure, another basis $|\Psi_i>$ which are orthogonal to $|\mathrm{sp}_4>$.

$$|\Psi_1> = |\mathrm{sp}_4> \tag{F.11}$$

$$|\Psi_i> = \sum_{\substack{p_1n_1p_2n_2\\k}} \eta^{(k)}_{p_1n_1p_2n_2}|p_1n_1p_2n_2,k> \quad \text{where } i>1. \tag{F.12}$$

Then we have

$$< \mathrm{sp}_4|\Psi_i >= \delta_{1i}. \tag{F.13}$$

So it is easy to remove the spurious state when we calculate the first-order corrections,

$$|\mathrm{CBCS} >= \mathcal{N}(|\mathrm{BCS} > + {\sum_i}' \frac{< \Psi_i|H_{40}^{\mathrm{pn}}|\mathrm{BCS} >}{E_{\mathrm{BCS}} - E_{\Psi_i}}|\Psi_i > , \tag{F.14}$$

where $\sum_i'$ means the summation does not include $|\mathrm{sp}_4 >$.

# Bibliography

[Ada 88] S. Adachi and E. Lipparini, Nucl. Phys. **A489**, (1988), 445.

[Alb 85] D.E. Alburger, Nucl. Data Sheets **45** (1985), 557.

[Alf 91] W.P. Alford, et. al., Nucl. Phys. **A514**, (1990), 49.

[And 85] B.D. Anderson, et. al. Phys. Rev. C **31**, (1985), 1161.

[Ari 87] A. Arima, K. Shimizu, W. Bentz and H. Hyuga Adv. Nucl. Phys. **18** (1987), 1.

[Avi 91] F.T. Avignone III, et. al, Phys. Lett. **256B**, (1991), 559.

[BAB 85] B.A. Brown, *Nuclear Shell Models*, Editor, M. Vallieres, B.H. Wildenthal, p42, Singapore: World Sci. (1985).

[BAB 88] B.A. Brown, W.A. Richter, R.E. Julies and B.H. Wildenthal, Ann. Phys. **182** (1988), 191.

[Bar 60] M. Baranger, Phys. Rev. **120**, (1960), 957.

[Bar 70] R.K. Bardin, et. al., Nucl. Phys. **A158**, (1970), 337.

[BCS 57] J. Bardeen, L.N. Cooper and J.R. Schrieffer, Phys. Rev. **108**, (1957), 1175.

[Bel 59] S.T. Belyaev, Mat. Fys. Medd. Dan. Vid. Selsk. **31**, (1959) no. 11.

[Ber 82] G.F. Bertsch and I. Hamamoto Phys. Rev. C **26**, (1982), 1323.

[BMP 58] A. Bohr, B.R. Mottelson and D. Pines, Phys. Rev. **110**, (1958), 936.

[Boh 81] A. Bohr and B.R. Mottelson, Phys. Lett. **100B**, (1981), 10.

[Bro 71] G.E. Brown, *Many-Body Problem*, North-Holland, Amsterdam, 1971.

[Bro 79] B.A. Brown and R. Sherr, Nucl. Phys. **A322**, (1979) 61.

[Bro 85] B.A. Brown and B.H. Wildenthal, Atomic Data and Nucl. Data Tables **33**, (1985), 347.

[Bro 88] B.A. Brown and B.H. Wildenthal, Ann. Rev. of Nucl. Part. Sci. **38**, (1988), 29.

[Bru 77] P.J. Brussaard and P.W.M. Glaudemans, *Shell Model Applications in Nuclear Spectroscopy* North-Holland, Amsterdam, 1977.

[Brz 89] B.A. Brown and L. Zhao, *Nuclear weak Process and Nuclear Structure* , Edited by A. M. Morita, et. al. p291, Singapore: World Sci., (1989).

[Brz 90] B.A. Brown and L. Zhao, *Understanding the Variety of Nuclear Excitations* , Edited by A. Covello, p497, Singapore: World Sci., (1990).

[Cha 83] D. Cha, Phys. Rev.**C27**, (1983), 2269.

[Civ 87] O. Civitarese, A. Faessler and T. Tomada, Phys. Lett. **194B**, (1987), 11.

[Civ 91] O. Civitarese, H. Müther, L.D. Skouras and A. Faessler, J. Phys. G: Nucl. Part. Phys. **17**, (1991), 1363.

[Doi 85] M. Doi, T. Kotani and E. Takasugi, Prog. Theor. Phys. suppl. **83**, (1985), 1.

[Dro 90] S. Drozdz, S. Nishizaki, J. Speth and J. Wambach, Phys. Rep **197**, (1990), 1.

[Eji 91] H. Ejiri, et. al., Phys. Lett. **258B**, (1991), 17.

[Ell 87] S.R. Elliott, A.A. Hahn and M.K. Moe Phys. Rev. Lett., **59**, (1987), 2020.

[Eng 88] J. Engel, P. Vogel and M.R. Zirnbauer, Phys. Rev. **C37**, (1988), 731.

[Etc 85] A. Etchegoyen, W.D.M. Rae, N.S. Godwin, W.A. Richter, C.H. Zimmerman, B.A. Brwon, W.E. Ormand and J.S. Winfield, MSU-NSCL report #524 (1985).

[Fet 71] A.L. Fetter and J.D. Walecka, *Quantum Theory of Many-Particle System* , McGraw-Hill, 1971.

[Gmi 68] M. Gmitro, A. Rimini, J. Sawicki and T. Weber Phys. Rew. **173**, (1968), 964.

[Goo 70] A.L. Goodman, G.L. Struble, J. Bar-Touv and A. Goswami, Phys. Rew. **C2**, (1970), 380.

[Goo 79] A.L. Goodman, Adv. Nucl. Phys. **11**, (1979), 263.

[Goo 81] C.D. Goodman, et. al. Phys. Lett. **107B**, (1981), 406.

[Gro 86] K. Grotz and H.V. Klapdor, Nucl. Phys. **A460**, (1986), 395.

[Hal 67] J.A. Halbeib and R.A. Sorensen, Nucl. Phys. **A98**, (1967), 542.

[Hax 84] W.C. Haxton and G.J. Stephenson, Prog. Part. Nucl. Phys. **12**, (1984), 409.

[Hea 88] A.C. Hearn, L.R. Seward and G.P. Duggan, " REDUCE User's Guide, Version 3.3 ", Rand, 1988.

[Iac 87] F. Iachello and I. Talmi, Rev. Mod. Phys. **59**, (1987), 339.

[Kle 85] Kleinheinz, et. al., Phys. Rev. Lett. **55**, (1985), 2664.

[Kuo 68] T.T.S. Kuo and G.E. Brown Nucl. Phys. **A114**, (1968), 241.

[Lan 64] A.M. Lane, *Nuclear Theory*, Benjamin, New York, 1964.

[Lan 91] *Computational Nuclear Physics* I *Nuclear Structure*, Editors, K. Langanke, J.A. Maruhn and S.E. Koonin, Springer-Verlag, (1991).

[Lau 88] B. Lauritzen, Nucl. Phys. **A489**, (1988), 237.

[Law 80] R.D. Lawson, *Theory of the Nuclear Shell Model*, Clarendon Press, Oxford, (1980).

[May 55] M.G. Mayer and J.H.D. Jensen, *Elementary Theory of Nuclear Structure*, New York, Wiley, (1955).

[McG 70] J.B. McGrory, B.H. Wildenthal and E.C. Halbert Phys. Rev. C **2**, (1970), 186.

[McG 81] J.B. McGrory, and B.H. Wildenthal Phys. Lett. **103B**, (1981), 173.

[Mut 84] K. Muto and H. Horie, Phys. Lett. **138B**, (1984), 9.

[Mut 88] K. Muto and H.V. Klapdor, in *Neutrinos* Editor, H.V. Klapdor (Springer-Verlag, 1988)

[Mut 89] K. Muto, E. Bender and H.V. Klapdor, Z. Phys. **A333**, (1989), 125; K. Muto, E. Bender and H.V. Klapdor, Z. Phys. **A334**, (1989), 177; K. Muto, E. Bender and H.V. Klapdor, Z. Phys. **A334**, (1989), 187.

[Mut 91] K. Muto, E. Bender and H.V. Klapdor, Z. Phys. **A339**, (1991), 435.

[Oga 89] K. Ogawa and H.Horie, in *Nuclear Weak Process and Nuclear Structure* Editor, M.Morita, H. Ejiri, H. Ohtsubo and T. Sato. ( World Scientific, Singapore, 1989), 308.

[Ott 67] P.L. Ottaviani, M. Savoia, J. Sawicki and A. Tomasini, Phys. Rev. **153** (1967), 1138.

[Pal 67] M.K. Pal, Y.K. Gambhir and R. Raj, Phys. Rev. **155**, (1967), 1144.

[Ric 91] W.A. Richter, M.G.V.D. Merwe, R.E. Julies and B.A. Brown, Nucl. Phys. **A523**, (1991), 325.

[Rin 80] P. Ring and P. Schuck, *The Nuclear Many-Body Problem* , Springer-Verlag, New York, (1980).

[Ros 88] S. P. Rosen, Comments Nucl. Part. Phys. **18**, (1988), 31.

[Row 68] D.J. Rowe, Rev. Mod. Phys. **40**, (1968), 153.

[Row 70] D.J. Rowe, *Nuclear Collective Motion*, Methuen, London, (1970).

[Sko 83] L.D. Skouras and J.D. Vergados, Phys. Rev. C **28**, (1983), 2122.

[Sub 88] J. Suhonen, A. Faessler, T. Taigel, and T. Tomoda, Phys. Lett. **202B**, (1988), 174; J. Suhonen, T. Taigel, and A. Faessler, Nucl. Phys. **A486**, (1988), 91.

[Tak 84] K. Takayanagi, K. Shimizu and A. Arima, Nucl. Phys. **A444**, (1984), 436.

[Tak 88] K. Takayanagi, K. Shimizu and A. Arima, Nucl. Phys. **A477**, (1988), 205.

[Tow 87] I.S. Towner Phys. Rep. **155**, No. 5, (1987), 263.

[Tsu 84] T.Tsuboi, K. Muto and H. Horie, Phys. Lett. **143B** (1984), 293.

[Tur 91] A.L. Turkevich, T.E. Economou and G.A. Cowan, Phys. Rev. lett., **67**, (1991), 3211.

[Ver 86] J.D. Vergados, Phys. Rep. **133**, (1986), 1.

[Vol 86] P. Vogel and M.R. Zirnbaur, Phys. Rev. Lett. **57** (1986), 3148.

[War 85] E.K. Warburton, Phys. Rev. C **31**, (1985), 1896.

[Wap 71] A.H. Wapstra and N.B. Gove, Nucl. Data Table **9**, (1971), 265.

[Wap 85] A.H. Wapstra and G. Audi, Nucl. Phys. **A432**, (1985), 1.

[Wil 84] B.H. Wildenthal, Prog. Part. Nucl. Phys. **11**, (1984), 5.

[Wam 88] J. Wambach, Rep. Prog. Phys. **51**, (1988),989.

[Yan 83] C. Yannouleas, M.Dworecka and Griffin, Nucl. Phys. **A397**, (1983), 239.

[Yee 88] K. Yee, J. Engel and P. Vogel, Phys. Rev. C **38**, (1988), 2971.

[Zam 82] L. Zamick and N. Auerbach, Phys. Rev. C **26**, (1982), 2185.

[Zha 92] L. Zhao and A. Sustich, Ann. Phys., **213**, (1992), 378.

MICHIGAN STATE UNIV. LIBRARIES
31293010554396